NATIONAL ADVISORY COMMITTEE
FOR AERONAUTICS

TECHNICAL NOTE 4135

INFLUENCE OF SOLID-BODY ROTATION ON

SCREEN-PRODUCED TURBULENCE

By Stephen C. Traugott

The Johns Hopkins University

NACA

Washington

August 1958

NATIONAL ADVISORY COMMITTEE FOR AERONAUTICS

TECHNICAL NOTE 4135

INFLUENCE OF SOLID-BODY ROTATION ON

SCREEN-PRODUCED TURBULENCE

By Stephen C. Traugott

SUMMARY

The influence of solid-body rotation on a screen-produced turbulence in a flow between concentric, rotating cylinders has been investigated. Radial distributions of the three components of turbulence intensity and the three turbulent shear stresses were measured at a fixed distance downstream of the screen both with and without rotation. An energy balance is made for the three intensities from measured decay and dissipation terms.

In addition, the change of the axial and peripheral mean velocity profiles with distance along the axis of rotation is presented.

INTRODUCTION

Although the bulk of theoretical work on turbulence has been restricted to homogeneous isotropic turbulence, there have appeared in recent years a number of investigations on turbulent shear flows characterized by the presence of mean velocity gradients. The ordinary types of shear flows that have been investigated, for example, channel (ref. 1), pipe (ref. 2), wake (ref. 3), boundary layer (refs. 4 to 6), and jet (ref. 7), have one thing in common: The principal mean rate of strain is either exactly or approximately equal to the rotation, that is, one-half the vorticity, of the mean flow. A somewhat unusual experiment on a turbulent flow with uniform mean rate of strain but with no mean vorticity was recently reported by Townsend (ref. 8). The present investigation deals with the other extreme case, namely a turbulent flow with uniform mean vorticity but with no mean rate of strain. Such a flow was obtained by a solid-body rotation of the mean flow between two concentric circular walls, the walls also rotating like a rigid body about their common axis. An approximately uniform mean axial velocity served as a carrier. The turbulence was created by letting the flow pass through a series of screens, a customary method for generating turbulence except that in

this investigation the screens were attached rigidly to the tunnel walls
and therefore also rotate with the walls.

Even without the influence of viscosity and turbulence, the solid-
body rotation of an ideal fluid has received considerable attention.
(See a recent survey in ref. 9.) Taylor (ref. 10) showed that all small
steady motions relative to the rotating fluid must be two-dimensional in
the sense that any two fluid particles originally in a line parallel to
the axis of rotation must remain so. This work was extended recently by
Long (ref. 11). Morgan (ref. 12) considered the same problem without
the restriction that the motion be steady. For the case of small forced
oscillations that vary sinusoidally with time, he found that the differ-
ential equations describing these oscillations are of elliptic type for
$\sigma > 2\omega$ and of hyperbolic type for $\sigma < 2\omega$, where σ is the frequency
of oscillation and ω is the angular speed of rotation. He speculated
therefore that, for $\sigma = 2\omega$, the oscillation may grow to very large ampli-
tudes. It was also found in the same reference that the ratio of ampli-
tudes of the radial velocity to the tangential velocity is $\sigma/2\omega$; thus,
for large values of ω compared with values of σ, the radial component
of the oscillations is suppressed, and the motion again appears to be
two-dimensional. Stewartson (ref. 13) treated a weak source in a rotating
fluid; the very peculiar result was obtained that the output of the source
spreads axially but not radially, again a two-dimensional effect.

An important feature of many flows encountered in practice (e.g.,
the flow in a turbomachine) is the fact that the streamlines may be
curved, often quite strongly, introducing a pressure gradient in the
direction perpendicular to the main flow direction. It is of great
interest to know something of the effect that this curvature may have
on the turbulence characteristics. One such investigation is reported
in reference 14, where the effect of curvature on a fully developed
channel flow is studied. It is clear that the curvature of the stream-
lines alone is not sufficient to determine uniquely the characteristics
of turbulence; the velocity distribution also must be considered. In
the present investigation a solid-body rotation was therefore chosen for
the simplicity of constant mean vorticity and zero laminar shearing
stress.

SYMBOLS

A	coefficient in relation $\dfrac{\lambda}{M} = \dfrac{A}{\sqrt{\dfrac{\overline{v}M}{\nu}}}$
a	radius of inner cylinder, 2.766 in.
b	radius of outer cylinder, 5.344 in.
C	constant of integration
d	channel width
E	mean voltage across hot wire
e	fluctuating voltage across hot wire, dE
$F_{\overline{v^2}}(K_1)$	fraction of turbulent energy $\overline{v^2}$ associated with K_1, cm^3/sec^2
g.	strength of disturbance defined in appendix B, $v_0/\omega r_0$
I	mean hot-wire heating current
I_0	hot-wire heating current extrapolated to zero velocity
K_1	one-dimensional wave number in direction of mean flow, cm^{-1}
L_s	integral scale of turbulence in direction of flow
M	mesh length, that is, distance between mesh wires (reciprocal of mesh number), in.
N	signal from hot wire defined in appendix A
n	coordinate measured perpendicular to streamwise direction on stream surface
P	mean static pressure
p	instantaneous pressure fluctuation

$$q = \sqrt{\overline{v_r^2} + \overline{v_\theta^2} + \overline{v_z^2}}$$

R	hot-wire resistance with heating
R_o	hot-wire resistance with no heating
Re	Reynolds number, $V_o(b - a)/\nu$
R_{xy}	correlation coefficient, $\overline{v_x v_y}/\tilde{v}_x \tilde{v}_y$
R_λ	turbulence Reynolds number, $\tilde{v}\lambda/\nu$
r	radial cylindrical coordinate
r_i	radius of inner wall of plane curved channel
r_o	radius of outer wall of plane curved channel
S	slope of hot-wire calibration curve
s	coordinate measured along streamwise direction
U	component of mean velocity parallel to surface
V	mean velocity component, direction indicated by subscripts r, θ, z, n, and s
V_o	mean throughflow velocity (V_z averaged over flow area)
V_p	mean velocity component perpendicular to hot-wire axis
v	instantaneous velocity fluctuation, direction indicated by subscripts r, θ, z, s, n, x, and y
$\tilde{v}$	root-mean-square value of velocity fluctuation v
X	coefficient in the hot-wire response equation, $\dfrac{\sin \beta \cos \beta \sin \alpha}{1 - \sin^2\alpha \, \sin^2\beta}$
x,y,z	Cartesian coordinates

γ coefficient in the hot-wire response equation,
$$\frac{\sin \alpha \cos \alpha \sin^2\beta}{1 - \sin^2\alpha \sin^2\beta}$$

z coordinate along axis of rotation; also axial distance from farthest downstream 20-mesh screen

α angle of turning of hot-wire probe, measured in plane perpendicular to probe axis

β angle between hot-wire axis and radial direction

δ boundary-layer thickness

ξ axial distance from farthest downstream 4-mesh screen

η exponent in relation $I^2 = S\sqrt{V_s(\cos \alpha)^\eta} + I_o^2$

θ peripheral cylindrical coordinate

λ microscale of turbulence, $\lambda_{v_z,z}^2 = \dfrac{\overline{v_z^2}}{\overline{\left(\dfrac{\partial v_z}{\partial z}\right)^2}}$, $\lambda_{v_\theta,z}^2 = \dfrac{\overline{2v_\theta^2}}{\overline{\left(\dfrac{\partial v_\theta}{\partial z}\right)^2}}$, and so forth

μ viscosity

ν kinematic viscosity

ρ density

σ frequency of forced oscillations

τ_l laminar shearing stress

τ_t turbulent shearing stress

ϕ flow angle, measured from the axial direction

ω angular velocity of rotation

WIND TUNNEL

The rotating wind tunnel was designed to produce a radially uniform axial velocity and solid-body peripheral velocity distribution, axially symmetric to prevent further complications. These combined requirements suggested the idea of using rotating screens.

It is known that a flow, approaching with some angle to the normal to a screen, will be turned by the screen toward that normal so that downstream of the screen the velocity component parallel to the plane of the screen will be smaller than the corresponding component upstream of the screen. For a large number of screens, the parallel component of the approaching flow will be substantially reduced in the flow behind, this component vanishing in the limit of infinitely many screens. If the screens are rotated about a normal axis the flow behind them will also rotate like a solid body. Further, if the pressure-drop coefficient of the screens depends on the normal component of velocity only, as it does for approach angles of up to 45° (ref. 15), nonuniformities in axial velocity will be diminished by the screens as well as peripheral nonuniformities.

To avoid the excessively large number of screens that would be necessary to induce rotation by this method alone, an impeller with approximately axial vanes at discharge was employed here to create a prerotation. This impeller was followed by a system of screens rigidly attached to it and thus rotating with it. These acted to reduce both nonuniformities in axial velocity and departures from solid-body rotation. They also acted to suppress peripheral variations caused by the wakes of the vanes.

The impeller was a modified version of a previously existing mixed-flow runner (fig. 1). By machining, a vane system resulted whose outer surface was cylindrical and 10.688 inches in diameter, but whose hub varied in diameter from $2\frac{3}{8}$ inches at the inlet to 5.532 inches at the outlet. Five screens, spaced 1/4 inch apart, were attached to the hub in a single unit just downstream of the trailing edge of the vanes. They were 20-mesh screens, of 0.01-inch-diameter wire, resulting in a solidity of 0.360 and a pressure drop coefficient of approximately 1.0 for each screen for the throughflow velocity of 42.3 fps that has been used in these experiments. The screen Reynolds number based on rod diameter and throughflow velocity is 207. As will be described, two additional turbulence-producing 4-mesh screens were later installed 8 inches and $13\frac{3}{4}$ inches, respectively, downstream from the last 20-mesh screen. The Reynolds number of these screens is 975.

Since the impeller alone will not produce a sufficient throughflow, a 3.75-horsepower axial blower is used to supply air to it at the rate of 4,000 cu ft/min through a settling chamber. A 20-mesh screen is located just before the impeller entrance. An adjustable bleed is provided between blower and impeller to make up for blower characteristics unfavorable for this particular application. With the speeds of the blower and impeller separately controlled, variation in the ratio of peripheral to axial velocity is possible.

Downstream of the impeller and screens, two coaxial cylinders form the inner and outer walls of the tunnel; the inner wall is rigidly attached to the hub of the impeller, the outer wall, rigidly attached to its shroud.

The inner wall of the test section is formed by the outside surface of a piece of aluminum pipe 6 feet in length, with an outside diameter of 5.532 inches, supported by two bearings on a shaft extending through the inside of the pipe on which is also supported the impeller on its own two bearings. Both pipe and impeller rotate as a unit when the pipe is driven by a belt from the rear with a variable-speed direct-current motor.

The outer wall of the test section consists of sections of various lengths of a cylindrical plastic tube having an inside diameter of 10.688 inches and a wall thickness of 1/2 inch, supported from the outside on separate bearings. The ratio of inner to outer diameter of the test section is thus 5.532 inches to 10.688 inches or 0.518. The distance between inner and outer walls is 2.578 inches. The length of this outer wall is adjustable by fitting together a different number of sections. As mentioned, the outer wall is rigidly attached to the impeller and thus also rotates with it.

With impeller, screens, inner wall, and outer wall all rotating together as a unit, a special arrangement is necessary to introduce measuring probes into the flow. The scheme used is as follows: A stationary section of the outer wall is fitted to the downstream end of the tunnel. The measuring probe enters radially through a hole in this piece as close to the sealed joint between the rotating and stationary sections as possible. Thus the outer wall at the traversing station is not in rotation, but it is felt that the resulting sudden change in peripheral velocity is limited to a region very close to the wall.

An assembly drawing of the wind tunnel is shown in figure 2. Figure 3 shows in more detail the traversing section.

The flow leaving the screens will undergo considerable change as it proceeds downstream. Thus, in contrast to investigations on fully developed flow, several traverses are necessary at various distances from the

screens. This is accomplished by varying the length of the outer wall
by fitting together the proper number of rotating sections and then
adding the stationary traversing section at the end.

Two general views of the tunnel are shown in figures 4 and 5, looking
downstream and upstream, respectively.

INSTRUMENTATION

The instruments used for all mean flow measurements were a shielded
total head probe (Kiel probe), a Pitot static tube, and a claw direction-
finding probe. These instruments were mounted on a micrometer traversing
apparatus to allow for radial traversing between inner and outer walls.
Attached to this traversing apparatus was also a protractor, and with a
pointer attached to the stem of the probe, angles may be read to within
1/2°.

The same constant-current hot-wire set described in reference 14
was used for turbulence measurements. (A complete description of the
equipment is given in ref. 16.) Tungsten wires 0.0003 inch in diameter
and about 0.03 inch long have been employed. The bare tungsten wire
was copper plated to enable soldering to the probe. The wire was com-
pensated through a manually controlled resistance-capacitance network
using the square-wave method. The time constant ranged from 0.7 to
1.0 millisecond. The mean-square values of the turbulent quantities
were measured through a vacuum thermocouple unit. Time derivatives of
the fluctuating quantities were measured with an electronic differentiator.
All three components of the turbulence intensity, as well as the three
turbulent shear stresses, were measured by a single inclined wire. The
technique employed is more fully described in appendix A. In addition,
an X-wire was used to measure the spectrum of radial fluctuations. All
spectra measurements were made on a Hewlett-Packard wave analyzer.

ANALYTICAL CONSIDERATIONS

With the assumption of axial symmetry, the Reynolds equations in
the cylindrical coordinate system are

$$V_r \frac{\partial V_r}{\partial r} + V_z \frac{\partial V_r}{\partial z} - \frac{V_\theta^2}{r} = -\frac{1}{\rho}\frac{\partial P}{\partial r} - \frac{1}{r}\frac{\partial}{\partial r}\left(r\overline{v_r^2}\right) + \frac{\overline{v_\theta^2}}{r} -$$

$$\frac{\partial}{\partial z}\left(\overline{v_r v_z}\right) + \nu\left(\nabla^2 V_r - \frac{V_r}{r^2}\right) \qquad (1)$$

$$V_r \frac{\partial V_\theta}{\partial r} + V_z \frac{\partial V_\theta}{\partial z} + \frac{V_r V_\theta}{r} = - \frac{1}{r^2} \frac{\partial}{\partial r}\left(r^2\overline{v_r v_\theta}\right) - \frac{\partial}{\partial z}\left(\overline{v_\theta v_z}\right) + \nu\left(\nabla^2 V_\theta - \frac{V_\theta}{r^2}\right) \quad (2)$$

$$V_r \frac{\partial V_z}{\partial r} + V_z \frac{\partial V_z}{\partial z} = - \frac{1}{\rho} \frac{\partial P}{\partial z} - \frac{1}{r} \frac{\partial}{\partial r}\left(r\overline{v_r v_z}\right) - \frac{\partial}{\partial z}\left(\overline{v_z^2}\right) + \nu\left(\nabla^2 V_z\right) \quad (3)$$

where

$$\nabla^2 = \frac{\partial^2}{\partial r^2} + \frac{\partial}{r\, \partial r} + \frac{\partial^2}{\partial z^2}$$

The equation of continuity for incompressible, axially symmetrical flows is

$$\frac{\partial r V_r}{r\, \partial r} + \frac{\partial V_z}{\partial z} = 0 \quad (4)$$

As mentioned previously, the region of flow to be investigated is the free-stream region in which V_z is practically constant with the radius. (This excludes the boundary layers in which V_z drops rapidly to zero at the inner and outer walls.) In this region of interest, it was found that V_z increases only slightly with z. The continuity equation then gives an estimate of V_r. The experiments indicate that V_r is smaller than the turbulence intensities but is still of the same order of magnitude as the latter. For this reason the terms involving V_r should, in general, be retained for this type of flow in equations (1) to (3). However, the terms involving viscosity ν in these equations as well as the term $V_r \frac{\partial V_z}{\partial r}$ in equation (3) can be neglected for the region under investigation. (Naturally none of these terms can be neglected in the boundary layers near the two walls.)

Although every quantity in equations (1) to (3) has been measured in this investigation, it seems futile to try to balance these equations by experimental data. For example, in equation (1) the two terms V_θ^2/r

and $\dfrac{1}{\rho}\dfrac{\partial P}{\partial r}$ are of a larger order of magnitude when compared with the rest
of the terms so that any experimental error in these two terms would com-
pletely overshadow the others. It appears that no useful purpose can be
served by balancing Reynolds equations except perhaps as a check of
measurements.

Among the turbulence quantities to be studied under the influence
of a gross rotation, the most interesting quantity appears to be $\overline{V_r V_\theta}$.
Idealize the situation a little more and imagine the following case:
Let the wind tunnel with the inner and outer walls rotating (as a unit)
at a constant angular speed ω be filled with turbulent flows whose mean
velocity at the initial instant $t = 0$ is purely tangential and is such
that $V_\theta = \omega r$ and hence there is no slipping at the walls. The question
is what will be the V_θ distribution at later instants. The appropriate
equation describing this idealized case is, corresponding to equation (2)
but taking into consideration that possibly $\dfrac{\partial V_\theta}{\partial t} \neq 0$ although $V_r =$
$V_z = \dfrac{\partial}{\partial z} = 0$,

$$\rho \frac{\partial V_\theta}{\partial t} = \frac{1}{r^2}\frac{\partial}{\partial r}\left[r^2\left(\tau_t + \tau_l\right)\right] \tag{5}$$

where for turbulent shear stress

$$\tau_t = -\rho\overline{V_r V_\theta}$$

and for laminar shear stress

$$\tau_l = \mu r \frac{\partial}{\partial r}\left(\frac{V_\theta}{r}\right)$$

It is known that eventually, as the turbulence dies out, the flow becomes
laminar and, under the condition of rotating walls, the V_θ distribution
of the fluid must again be that of solid-body rotation, that is, $V_\theta = \omega r$.
It is plausible therefore to assume that, between $t = 0$ and $t = \infty$,
V_θ remains always ωr. With this assumption,

$$\frac{\partial}{\partial r}\left[r^2\left(\tau_t + \tau_l\right)\right] = 0$$

so that either

$$\tau_t + \tau_l = 0$$

or

$$\tau_t + \tau_l = \frac{c}{r^2}.$$

The latter possibility must however be ruled out, since it would impose a nonzero value for τ_l at the walls where τ_t vanishes (τ_l is zero everywhere for $V_\theta = \alpha r$).

The statement that $\overline{v_r v_\theta}$ is likely to be zero for solid-body rotation of the mean flow would have been so obvious as to become trivial if it were not for the fact that such a conclusion apparently contradicts the prediction by the well-known momentum transport theory or turbulent shear flows. As pointed out by Taylor (ref. 17), this theory gives for shear flow along circular paths

$$\tau_t = \rho K \frac{d}{r\ dr}(rV_\theta) \tag{6}$$

where ρK is the eddy viscosity and rV_θ is the angular momentum. This is analogous to unidirectional shear flows for which $\tau_t = \rho K \frac{\partial U}{\partial y}$. The basis for equation (6) is, of course, the conservation of angular momentum of fluid elements in circular flows, which is analogous to the conservation of linear momentum in unidirectional flows. According to equation (6), the turbulent shear stress $\tau_t = -\rho \overline{v_r v_\theta}$ for solid-body rotation of mean flow would be a positive constant and equal to $2\rho K \omega$ everywhere.

Now the shortcomings of momentum transport theory are, of course, well known. The assumption, for example, that the masses of fluid which transport the momentum from one layer to another move about without losing their identities and without the influence of viscosity and fluctuating pressure gradients is not true. Nevertheless predictions by this theory on turbulent shearing stress in unidirectional shear flows are at least

qualitatively correct, although quantitatively inexact. The fact that in solid-body rotation this theory appears to run into difficulty even in a qualitative way is somewhat puzzling.

Dr. Hsuan Yeh is responsible for the following application of the momentum transport theory which makes the theory predict a zero turbulent shearing stress for a solid-body rotation type of mean flow. This correction is based on taking into consideration the mean pressure gradient normal to the flow, a quantity existing prominently in curved mean flows but not in straight mean flows. The other simplifying assumptions of the transport theory are retained. The detail of such a development is given in appendix B. The conclusions can be stated briefly as follows. If at any instant a fluid element possesses an excess velocity, either in v_r or in v_θ or both, it will then oscillate around an oval path relative to the mean flow. The frequency of oscillation, irrespective of the magnitude and direction of the initial disturbance, is always 2ω. This confirms the speculation by Morgan (ref. 12, see "Introduction") that 2ω might be the resonance frequency of forced oscillations; this value is indeed the natural frequency of the system. Furthermore, the amplitude of v_r is equal to that of v_θ for any kind of initial disturbance. This again seems to confirm Morgan's result for $\sigma = 2\omega$. However, unlike Morgan's assumption, the fluctuating velocities v_r and v_θ do not vary sinusoidally with time, although the departure from a sinusoidal function is not very great. Another interesting fact is that the magnitudes of v_r and v_θ at subsequent times do not bear a simple proportion to the magnitude of the initial disturbance. Finally, such a simplified analysis shows that when a fluid element moves out with a positive value of v_r, for example, then there is equal chance of its possessing either a positive or a negative value of v_θ, so that the correlation $\overline{v_r v_\theta}$ is zero.

The equations governing the six components of Reynolds stress tensor (three component intensities and three shear correlations) and the total turbulent energy, in cylindrical coordinates, were derived in reference 18. These equations, after simplification by the assumption of axial symmetry, are reproduced as follows:

$$\frac{1}{2}\left(V_r \frac{\partial \overline{v_r^2}}{\partial r} + V_z \frac{\partial \overline{v_r^2}}{\partial z}\right) - \overline{v_r v_\theta}\frac{2V_\theta}{r} + \overline{v_r^2}\frac{\partial V_r}{\partial r} + \overline{v_r v_z}\frac{\partial V_r}{\partial z} =$$

$$-\frac{1}{\rho}\overline{v_r \frac{\partial p}{\partial r}} - \frac{1}{2}\left(\frac{1}{r}\frac{\partial}{\partial r}\overline{r v_r^3} + \frac{\partial}{\partial z}\overline{v_z v_r^2} - 2\frac{\overline{v_r v_\theta^2}}{r}\right) -$$

$$\nu\left[\overline{\left(\frac{\partial v_r}{\partial r}\right)^2} + \overline{\left(\frac{\partial v_r}{\partial z}\right)^2} + \overline{\left(\frac{\partial v_r}{r\,\partial\theta}\right)^2} + \frac{\overline{v_r^2}}{r^2} + 2\frac{\overline{v_r}}{r}\frac{\partial v_\theta}{r\,\partial\theta}\right] \tag{7}$$

$$\frac{1}{2}\left(V_r \overline{\frac{\partial v_\theta^2}{\partial r}} + V_z \overline{\frac{\partial v_\theta^2}{\partial z}}\right) + \overline{v_r v_\theta}\,\frac{1}{r}\frac{\partial}{\partial r}(rV_\theta) + \overline{v_z v_\theta}\,\frac{\partial V_\theta}{\partial z} + \overline{v_\theta^2}\,\frac{V_r}{r} =$$

$$-\frac{1}{\rho}\,\overline{v_\theta\,\frac{\partial p}{r\,\partial\theta}} - \frac{1}{2}\left(\frac{1}{r}\frac{\partial}{\partial r}\,\overline{rv_r v_\theta^2} + \frac{\partial}{\partial z}\,\overline{v_z v_\theta^2} + 2\,\overline{\frac{v_r v_\theta^2}{r}}\right) -$$

$$\nu\left[\overline{\left(\frac{\partial v_\theta}{\partial r}\right)^2} + \overline{\left(\frac{\partial v_\theta}{\partial z}\right)^2} + \overline{\left(\frac{\partial v_\theta}{r\,\partial\theta}\right)^2} + \overline{\frac{v_\theta^2}{r^2}} - 2\,\overline{\frac{v_\theta}{r}\frac{\partial v_r}{r\,\partial\theta}}\right] \tag{8}$$

$$\frac{1}{2}\left(V_r \overline{\frac{\partial v_z^2}{\partial r}} + V_z \overline{\frac{\partial v_z^2}{\partial z}}\right) + \overline{v_r v_z}\,\frac{\partial v_z}{\partial r} + \overline{v_z^2}\,\frac{\partial v_z}{\partial z} = -\frac{1}{\rho}\,\overline{v_z\,\frac{\partial p}{\partial z}} -$$

$$\frac{1}{2}\left(\frac{1}{r}\frac{\partial}{\partial r}\,\overline{rv_r v_z^2} + \frac{\partial}{\partial z}\,\overline{v_z^3}\right) - \nu\left[\overline{\left(\frac{\partial v_z}{\partial r}\right)^2} + \overline{\left(\frac{\partial v_z}{\partial z}\right)^2} + \overline{\left(\frac{\partial v_z}{r\,\partial\theta}\right)^2}\right] \tag{9}$$

$$\frac{1}{2}\left(V_r \overline{\frac{\partial q^2}{\partial r}} + V_z \overline{\frac{\partial q^2}{\partial z}}\right) + \overline{v_\theta^2}\,\frac{V_r}{r} + \overline{v_r^2}\,\frac{\partial V_r}{\partial r} + \overline{v_z^2}\,\frac{\partial V_z}{\partial z} + \overline{v_z v_\theta}\,\frac{\partial V_\theta}{\partial z} +$$

$$\overline{v_z v_r}\left(\frac{\partial V_z}{\partial r} + \frac{\partial V_r}{\partial z}\right) + \overline{v_r v_\theta}\,r\,\frac{\partial}{\partial r}\overline{\left(\frac{V_\theta}{r}\right)} = -\left[\frac{1}{r}\frac{\partial}{\partial r}\,\overline{rv_r\left(\frac{q^2}{2} + \frac{p}{\rho}\right)} +\right.$$

$$\frac{\partial}{\partial z}\,\overline{v_z\left(\frac{q^2}{2} + \frac{p}{\rho}\right)}\left.\right] - \nu\left[\overline{\frac{\partial u_i}{\partial x_j}\frac{\partial u_i}{\partial x_j}} + \overline{\frac{v_\theta^2 + v_r^2}{r^2}} - 2\left(\overline{\frac{v_\theta}{r}\frac{\partial v_r}{r\,\partial\theta}} - \overline{\frac{v_r}{r}\frac{\partial v_\theta}{r\,\partial\theta}}\right)\right] \tag{10}$$

$$\frac{1}{2}\left(V_r\ \overline{\frac{\partial v_r v_\theta}{\partial r}}\ +\ V_z\ \overline{\frac{\partial v_r v_\theta}{\partial z}}\right)\ +\ \frac{1}{2}\left[\overline{v_r v_\theta}\left(\frac{\partial V_r}{\partial r}\ +\ \frac{V_r}{r}\right)\ +\ \overline{v_\theta{}^2}\left(-2\ \frac{V_\theta}{r}\right)\ +\right.$$

$$\left.\overline{v_z v_\theta}\ \frac{\partial V_r}{\partial z}\ +\ \overline{v_r{}^2}\ \frac{\partial}{r}\ \frac{\partial}{\partial r}(rV_\theta)\ +\ \overline{v_r v_z}\ \frac{\partial V_\theta}{\partial z}\right]\ =\ -\ \frac{1}{2\rho}\left(\overline{v_\theta\ \frac{\partial p}{\partial r}}\ +\ \overline{v_r\ \frac{\partial p}{r\ \partial \theta}}\right)\ -$$

$$\frac{1}{2}\left(\frac{1}{r^2}\ \frac{\partial}{\partial r}\ r^2\overline{v_r{}^2 v_\theta}\ -\ \overline{\frac{v_\theta{}^3}{r}}\ +\ \frac{\partial}{\partial z}\ \overline{v_z v_r v_\theta}\right)\ -\ \nu\left(\overline{\frac{\partial v_\theta}{\partial z}\ \frac{\partial v_r}{\partial z}}\ +\ \overline{\frac{\partial v_\theta}{r\ \partial \theta}\ \frac{\partial v_r}{r\ \partial \theta}}\ +\right.$$

$$\left.\overline{\frac{\partial v_\theta}{\partial r}\ \frac{\partial v_r}{\partial r}}\ +\ \overline{\frac{v_r v_\theta}{r^2}}\right) \tag{11}$$

$$\frac{1}{2}\left(V_r\ \overline{\frac{\partial v_z v_\theta}{\partial r}}\ +\ V_z\ \overline{\frac{\partial v_z v_\theta}{\partial z}}\right)\ +\ \frac{1}{2}\left[\overline{v_r v_z}\ \frac{1}{r}\ \frac{\partial}{\partial r}(rV_\theta)\ +\ \overline{v_z v_\theta}\ \frac{V_r}{r}\ +\right.$$

$$\left.\overline{v_z v_\theta}\ \frac{\partial V_z}{\partial z}\ +\ \overline{v_z{}^2}\ \frac{\partial V_\theta}{\partial z}\ +\ \overline{v_r v_\theta}\ \frac{\partial V_z}{\partial r}\right]\ =\ -\ \frac{1}{2\rho}\left(\overline{v_\theta\ \frac{\partial p}{\partial z}}\ +\ \overline{v_z\ \frac{\partial p}{r\ \partial \theta}}\right)\ -$$

$$\frac{1}{2}\left(\frac{1}{r^2}\ \frac{\partial}{\partial r}\ r^2\overline{v_r v_\theta v_z}\ +\ \frac{\partial}{\partial z}\ \overline{v_z{}^2 v_\theta}\right)\ -\ \nu\left(\overline{\frac{\partial v_\theta}{\partial z}\ \frac{\partial v_z}{\partial z}}\ +\ \overline{\frac{\partial v_\theta}{r\ \partial \theta}\ \frac{\partial v_z}{r\ \partial \theta}}\ +\right.$$

$$\left.\overline{\frac{\partial v_\theta}{\partial r}\ \frac{\partial v_z}{\partial r}}\ +\ \overline{\frac{v_z v_\theta}{2r^2}}\ -\ \overline{\frac{v_z}{r}\ \frac{\partial v_r}{r\ \partial \theta}}\right) \tag{12}$$

$$\frac{1}{2}\left(V_r\ \overline{\frac{\partial v_r v_z}{\partial r}} + V_z\ \overline{\frac{\partial v_r v_z}{\partial z}}\right) + \frac{1}{2}\left[\overline{v_r v_z}\left(\frac{\partial V_r}{\partial r} + \frac{\partial V_z}{\partial z}\right) + \overline{v_z v_\theta}\left(-\frac{2V_\theta}{r}\right) + \right.$$

$$\left. \overline{v_z^2}\ \frac{\partial V_r}{\partial z} + \overline{v_r^2}\ \frac{\partial V_z}{\partial r}\right] = -\frac{1}{2\rho}\left(\overline{v_z\ \frac{\partial p}{\partial r}} + \overline{v_r\ \frac{\partial p}{\partial z}}\right) - \frac{1}{2}\left(\frac{1}{r}\ \frac{\partial}{\partial r}\ \overline{rv_r^2 v_z} - \right.$$

$$\frac{\overline{v_z v_\theta^2}}{r} + \frac{\partial}{\partial z}\ \overline{v_r v_z^2}\right) - \nu\left(\overline{\frac{\partial v_z}{\partial z}\frac{\partial v_r}{\partial z}} + \overline{\frac{\partial v_z}{r\ \partial\theta}\frac{\partial v_r}{r\ \partial\theta}} + \overline{\frac{\partial v_z}{\partial r}\frac{\partial v_r}{\partial r}} + \right.$$

$$\left. \frac{\overline{v_r v_z}}{2r^2} + \overline{\frac{v_z}{r}\frac{\partial v_\theta}{r\ \partial\theta}}\right) \qquad\qquad (13)$$

In any one of these equations, the interpretation of the groups of terms, from left to right, is as follows: (1) The convective rate of change of some turbulent quantity; (2) the production of that quantity from the mean velocity (a positive production is associated with a negative value for this term); (3) the increase or decrease of the quantity due to the fluctuating pressure velocity correlation. This usually serves to feed the smaller intensity component at the expense of the larger (refs. 19 to 21), as will be more fully discussed later; (4) the increase or decrease due to turbulent diffusion; (5) the change due to the action of viscosity. This term is a combination of the rate of dissipation of turbulent energy to heat and the rate at which viscous forces are doing work on a fluid element (see ref. 22). This term is obtained by a transformation in each equation of the type

$$\nu\left(\overline{v_i \nabla^2 v_j} + \overline{v_j \nabla^2 v_i}\right) = \nu \nabla^2 \overline{v_i v_j} - 2\nu\ \overline{\frac{\partial v_i}{\partial x_k}\frac{\partial v_j}{\partial x_k}}$$

The second derivative of the fluctuating quantity is neglected because it is small compared with the other terms except in the region very close to the wall.

The most direct influence of the rotation would seem to be in the production terms, where the peripheral mean velocity appears. The way the various turbulent quantities are changed by rotation from the values without rotation would depend therefore on this distribution. Since the turbulence problem is nonlinear, the mean peripheral velocity of course depends in turn on the turbulent quantities. The system of equations presented so far is indeterminate. As an equation is derived for each of the unknown fluctuating quantities, new unknowns appear. The theoretical motivation of deriving such a chain of sets of equations seems to be the hope that eventually the new unknowns generated may be evaluated by some plausible physical assumption to which the system is not sensitive and the process stopped. Meanwhile, the equations have served as a guide in interpreting experimental work. In the next sections the determination of the mean velocity field and the measurement of some of the various turbulent quantities encountered will be presented.

The following speculation by Dr. Hsuan Yeh on the conditions for similarity to exist in a turbulence field under gross rotation is of interest. For the idealized case in which $V_r = 0$, $V_\theta = \omega r$, and V_z is constant everywhere, the equations can be reduced considerably. Since V_z now serves merely as a carrier, the magnitude of V_z cannot influence the problem. With respect to a coordinate system moving with a velocity V_z, equation (7), for example, appears as follows:

$$\frac{\partial \overline{v_r^2}}{\partial t} - 2\omega \overline{v_r v_\theta} = -\frac{\overline{v_r}}{\rho}\frac{\partial p}{\partial r} - \frac{1}{2}\frac{1}{r}\frac{\partial}{\partial r}\,\overline{r v_r^3} + \frac{\overline{v_r v_\theta^2}}{r} -$$

$$\nu\left[\overline{\left(\frac{\partial v_r}{\partial r}\right)^2} + \overline{\left(\frac{\partial v_r}{\partial z}\right)^2} + \overline{\left(\frac{\partial v_r}{r\,\partial \theta}\right)^2} + \frac{\overline{v_r^2}}{r^2} + 2\,\overline{\frac{v_r}{r}\frac{\partial v_\theta}{r\,\partial \theta}}\right]$$

The last term is proportional to $\nu\dfrac{\tilde{v}^2}{\lambda^2}$ where $\tilde{v}$ is a typical turbulence intensity and λ is a typical turbulence microscale. This equation can be made dimensionless by dividing each term by $\omega\tilde{v}^2$. In the resulting equation there appears two dimensionless parameters $\tilde{v}/\omega r$ and $\nu/\omega\lambda^2$. Physically the first parameter is the ratio of the Coriolis forces due to turbulence to the centrifugal force from the gross rotation of the mean motion. On account of the fact that the dissipation term $\nu\dfrac{\tilde{v}^2}{\lambda^2}$ is proportional to $\tilde{v}^3/l$ where l is a typical length of the energy-containing eddies (ref. 23), the second parameter can also be written

as $\tilde{v}/\omega l$ and therefore represents the ratio of the Coriolis forces due to turbulence to the centrifugal force due to mean rotation of the large eddies.

Since only one rotational speed and one type of turbulence were fully investigated in this work, no conclusions can be drawn as to the influence of a continuous variation of these two parameters.

<div align="center">PRELIMINARY MEASUREMENTS</div>

In order to isolate the effect of rotation on the flow field, it was necessary to investigate the flow both with and without rotation. As previously described, a prerotation is induced in the flow before it enters the rotating screens by a rotating impeller. Due to the twist of its blades this impeller when it is not rotating blocks the flow coming from the main blower; it must therefore either be modified or removed for tests without rotation.

Initially, the latter arrangement was used. A series of radial rods of the same spacing and thickness as the impeller vanes was mounted on a dummy hub in an attempt to give similar conditions upstream of the system of 20-mesh screens. These screens were then attached to the hub in the same way they had been mounted on the impeller.

A number of traverses were made at various axial positions both with and without rotation, using the dummy hub in the latter case. The speed of rotation of the tunnel was 1,560 rpm (corresponding to maximum rated speed of the driving motor), giving a peripheral velocity of 37.7 fps and 72.8 fps to the inner and outer walls, respectively. A throughflow of 19.3 cu ft/sec was used both with and without rotation, corresponding to an average throughflow velocity of 42.3 fps. This value was arbitrarily chosen to give a ratio of peripheral to axial velocity of nearly unity near the inner wall. The Reynolds number based on this velocity and half the distance between inner and outer wall is 26,700.

The results of these measurements are shown in figures 6, 7, and 8, where axial velocities without rotation, axial velocities with rotation, and peripheral velocities, respectively, are shown at various axial stations. The axial distance z is measured from the farthest downstream 20-mesh screen. (It should be noted that the 4-mesh turbulence-producing grids mentioned in the section "Wind Tunnel" were not yet installed.) The axial velocities are made dimensionless with the average throughflow velocity, the peripheral with the peripheral velocity of the outer wall.

In figure 8, the striking lack of change of the peripheral velocity with distance along the axis should be noted. Although the peripheral velocity is not strictly one of solid-body rotation, it nevertheless has

changed very little when compared with the changes that have occurred in the axial velocity profile in the same distance downstream.

Turning to the axial velocity profiles as a function of distance downstream both with and without rotation as shown in figures 6 and 7, it is interesting to compare the thickness of the boundary layers on both inside and outside walls for these profiles. The boundary-layer thickness is here defined as that distance from the wall at which the velocity distribution given by the power law which best fits the observed data is equal to the free-stream value. Results are given in figure 9. It is seen that without rotation the boundary layer on the outer cylinder is thicker than that on the inner. For fully developed laminar flow in an annular space the maximum velocity occurs closer to the inner wall than to the outer wall (see ref. 24). To satisfy this condition the boundary layer on the outer wall in a laminar flow that is not fully developed will have to grow faster than that on the inner wall. It is interesting to note that the same trend still holds for turbulent flow.

With rotation, the very interesting effect is seen that the boundary layer on the inner wall grows faster than it did before, while the opposite is true for the boundary layer on the outer wall. A detailed analysis of boundary-layer growth must include measurements very close to the wall. This is beyond the scope of the present report, since the emphasis is on the region between the boundary layers.

A profile of turbulence intensity $\tilde{v}_z/V_z$ at the farthest downstream station without rotation is shown in figure 10. As would be expected, at a given distance from the wall a larger turbulence level exists near the outer wall than near the inner, since the boundary layer near the outer wall is thicker.

From the velocity profiles just presented, one may estimate the order of magnitudes of the following terms in Reynolds equations (1) to (3):

$$V_r \frac{\partial V_r}{\partial r} \qquad\qquad V_z \frac{\partial V_r}{\partial z} \qquad\qquad \frac{V_\theta^2}{r}$$

$$0(0.0001) \qquad\qquad 0(0.0001) \qquad\qquad 0(1)$$

$$V_r \frac{\partial V_\theta}{\partial r} \qquad\qquad V_z \frac{\partial V_\theta}{\partial z} \qquad\qquad \frac{V_r V_\theta}{r}$$

$$0(0.01) \qquad\qquad 0(0.01) \qquad\qquad 0(0.01)$$

$$V_r \frac{\partial V_z}{\partial r} \qquad\qquad V_z \frac{\partial V_z}{\partial z}$$

$$0(0.001) \qquad\qquad 0(0.01)$$

ESTABLISHMENT OF SIMILAR UPSTREAM CONDITIONS

The measurements and results described in the previous section were obtained, in the case of nonrotating flow, with the impeller removed from the system and replaced by the dummy hub and rods described. This was intended to give the same conditions upstream of the screens both with and without rotation. The effectiveness of this device cannot rigorously be established without a direct comparison to nonrotating flow produced with the impeller left in place.

It was found that if the impeller is rotated at a low speed, a flow with no peripheral velocity is obtained behind it. This is so because the trailing edge of the impeller vanes is not axial but rather at an angle of about 20° to the axis of rotation. The flow is deflected toward the axis by the 20-mesh screens behind the impeller but not enough to make it axial. A slight rotation (about 160 rpm) then eliminates the remaining peripheral component. At this low speed of rotation, however, the inlet vane angles are not correct. An upstream extension was therefore attached to each moving blade, tangent to it at its leading edge and designed to meet the inlet flow at the proper angle. To reduce secondary flows between impeller vanes, a series of four flat concentric rings was attached to the vanes by cutting slots chordwise into the trailing edge of the vanes and fitting the rings into these slots. These rings, 1/2 inch wide and coaxial with the axis of rotation, extend 1/4 inch upstream and 1/4 inch downstream of the vane trailing edge. The 20-mesh screens were reattached. A mean velocity profile was then obtained for slow rotation at $\dfrac{z}{b - a} = 1.1$, corresponding to the farthest upstream profile shown in figure 6. At this station, comparison of the profiles with slowly rotating impeller and with dummy hub and rods showed them to be almost identical.

Preliminary turbulence intensity measurements in the mean flow direction showed the turbulence level also to be about the same with the two different methods of producing purely axial flow. Thus the data taken with the dummy hub with its radial rods shown in figure 6 are believed to offer a good comparison with the flow in rotation.

With slow rotation the axial turbulence intensity component at $\dfrac{z}{b - a} = 3.2$, a traversing station fairly close to the screens, varied in peripheral direction from 1.8 to 2.2 percent of the mean velocity with the impeller in place. These variations were traced to wakes from the impeller vanes passing through the four 20-mesh screens. At this distance from the screen, which corresponds to about 150-mesh lengths, the

turbulence created by these screens has therefore decayed to such a small value that nonuniformities passing through the screen become significant. In order to avoid these axially asymmetric blade wakes one could go farther downstream until they have died out, but one then approaches the flow region where the axial velocity is no longer uniform. It was decided to install additional large-mesh screening some distance downstream of the 20-mesh screens. A large-mesh screen will create turbulence of a larger scale which allows more time to decay. At a given station, the turbulence level will then be higher, and if the peripheral variations in the turbulence upstream of the screen remain the same, such variations downstream of the screen will be proportionately lower. The position of the screen will be a compromise: If it is too far downstream the boundary layers are too thick, too far upstream the wakes become stronger.

Various arrangements of 4-mesh, 0.047-inch-diameter wire (Solidity = 0.340) screens were tried. The best arrangement turned out to be the following: one 4-mesh screen 160 mesh lengths (referred to the fine screen) behind the last of the 20-mesh screens followed by another 4-mesh screen 23 meshes (referred to the coarse screen) farther downstream. The traversing station closest to this screen is 17.5 mesh lengths away.

(This station will henceforth be identified by $\dfrac{\xi}{M} = 17.5$ where ξ is

the axial distance measured from the last 4-mesh screen (in contrast to z which is measured from the farthest downstream 20-mesh screen). All further radial traverses were made at this station. In terms of the distance between inside and outside walls, this station corresponds to

$\dfrac{z}{b - a} = 7.1$. Peripheral variations at this station were only ±2.5 percent of the turbulence level. Measurements taken at this station are presented in the following section.

EXPERIMENTAL RESULTS

Mean Velocities

Axial velocity profiles with and without rotation, 17.5 mesh lengths downstream of the last 4-mesh screen, are shown in figure 11. The through-flow velocity is the same as that for the preliminary experiments, but with rotation the angular velocity has been increased from 1,560 to 2,000 rpm to maximize the effects of the rotation within the limits of the equipment. It can be seen that the presence of the two additional

screens has made the axial velocity more uniform compared with the previous profiles shown in figures 6 and 7. As before, the rotation seems to have decreased the boundary layer on the outside wall, which without rotation is thicker on the outer wall than on the inner. The peripheral velocity is shown in figure 12, where for comparison the previous profile is shown as a solid line. Due to the higher speed of rotation and the two extra screens, the peripheral velocity distribution is much closer to solid-body rotation than it was before. Figure 12 shows that there is still a small relative peripheral velocity between fluid and screen.

<div style="text-align: center">Turbulence Intensity and Shearing Stresses</div>

The method used in measuring the various fluctuating quantities is described fully in appendix A. The essential point is that with this method the three components of the intensity as well as the three shear stresses are measured at one time. Results of these measurements follow:

Figure 13 shows the radial, tangential, and axial turbulence intensity, without rotation, made dimensionless with the local mean velocity. As would be expected for a grid-produced turbulence with no mean velocity gradients, the intensities are fairly uniform in the region excluding the boundary layers, with $\tilde{v}_r/V_z$ and $\tilde{v}_\theta/V_z$ about the same, both less than $\tilde{v}_z/V_z$. Again, because of the thicker outer boundary layer, the intensity near the outer wall is larger than that near the inner wall, at the same distance from the walls. The three shear correlation coefficients for purely axial flow are shown in figure 14. Since there are no mean velocity gradients in this case except for those near the wall, one would expect no shear stresses other than those near the wall. Figure 14 shows that this is indeed the case.

For experiments with rotation, two sets of results are presented. One set is in a s,n,r coordinate system, with s in the mean velocity direction, n perpendicular to it in the stream surface, and r radial. The other set of results is in the usual cylindrical coordinate system. The conversion from one to the other is given in appendix A.

With rotation, figure 15 shows the three components of the turbulence intensity in s,n,r coordinates (made dimensionless with the local mean velocity). It is to be noted that, except near the outer wall, $\tilde{v}_s/V_s$ and $\tilde{v}_n/V_s$ are nearly the same. The radial fluctuation intensity is much less. Shear correlation coefficients in the same coordinates are

given in figure 16; although there is considerable scatter of the data
it appears that the coefficients are no longer zero.

The same results in r,θ,z coordinates are shown in the next two
illustrations. The intensities are given in figure 17 and were made
dimensionless with the axial component of the mean velocity. Since the
axial velocity is nearly the same both with and without rotation, the
results as plotted can be directly compared with the intensities pre-
viously given for purely axial flow. The rotation has not appreciably
changed the axial fluctuations, but the radial fluctuations have been
markedly decreased and the peripheral, increased. The shear correlation
coefficients are shown in figure 18. The coefficients R_{rz} and $R_{z\theta}$
still appear to be zero, the same as they are with no rotation. How-
ever, the rotation is seen to have produced a slightly positive value
for $R_{r\theta}$ over the entire flow area. Since in the peripheral Reynolds
equation, equation (2), the term $\dfrac{\partial}{\partial r}\left(r^2\overline{v_r v_\theta}\right)$ appears, the variation of

$\overline{v_r v_\theta}$ is shown as $\left(\dfrac{r}{b-a}\right)^2 \dfrac{\overline{v_r v_\theta}}{V_o{}^2}$ in figure 19, with V_o again the

average throughflow velocity.

A more direct comparison of the turbulence intensities with and
without rotation is given in figures 20, 21, and 22.

Integral Scales

The integral scale in the direction of the mean velocity is defined
as

$$L_S = \int_0^\infty R_S \; dS$$

where R_S is the correlation between simultaneous measurements of v_S
at two points separated by the distance s, measured in the mean flow
direction. From the ratio of the compensated to uncompensated signal
from a hot wire placed normal to the flow, L_S may be determined approxi-
mately (see, for instance, ref. 1). Results for L_S/M, with M the mesh
size of the screen, are shown in figure 23 both with and without rotation.

As a comparison, reference 26 shows $\frac{L_s}{M} = 0.22$ for the same ratio of distance to mesh size behind a single 1-mesh screen at 32.8 fps.

Microscales

The microscales of turbulence are here defined in the following way:

$$\lambda_{v_z,z}^2 = \frac{\overline{v_z^2}}{\overline{\left(\frac{\partial v_z}{\partial z}\right)^2}} \qquad \lambda_{v_z,r}^2 = \frac{\overline{2v_z^2}}{\overline{\left(\frac{\partial v_z}{\partial r}\right)^2}} \qquad \lambda_{v_z,\theta}^2 = \frac{\overline{2v_\theta^2}}{\overline{\left(\frac{\partial v_z}{r\,\partial \theta}\right)^2}}$$

$$\lambda_{v_\theta,z}^2 = \frac{\overline{2v_\theta^2}}{\overline{\left(\frac{\partial v_\theta}{\partial z}\right)^2}} \qquad \cdot\ \cdot\ \cdot\ \cdot\ \cdot\ \cdot\ \cdot \qquad \cdot\ \cdot\ \cdot\ \cdot\ \cdot\ \cdot$$

$$\lambda_{v_r,z}^2 = \frac{\overline{2v_r^2}}{\overline{\left(\frac{\partial v_r}{\partial z}\right)^2}} \qquad \cdot\ \cdot\ \cdot\ \cdot\ \cdot\ \cdot\ \cdot\ \cdot \qquad \cdot\ \cdot\ \cdot\ \cdot\ \cdot\ \cdot\ \cdot$$

The mean-square derivatives appearing above can be related, in homogeneous turbulence, to the various correlations of the particular velocity component at a point with the same component at another point removed from it in the proper direction. (See, for instance, ref. 1.) In isotropic turbulence all these microscales are the same, but this is not true otherwise. The measurement of two-point correlations was not made in the present work. However, by Taylor's hypothesis, ds may be replaced by $-V_s$ dt, where ds is in the mean flow direction and V_s is the mean velocity. Hence, a direct measurement of the time derivative

may be used to calculate microscales, but only those involving derivatives in the mean flow direction.

For flow with no rotation, only one radial station was measured at $\frac{r - a}{b - a} = 0.5$, halfway between the two walls. Since the turbulence level was found to be fairly uniform in the region away from the boundary layers, it was not considered necessary to take a complete radial traverse. It was found that, in this region,

$$\frac{\lambda_{v_z, z}}{M} = 0.17$$

$$\frac{\lambda_{v_\theta, z}}{M} = \frac{\lambda_{v_r, z}}{M} = 0.19$$

For the rotating case, since only the derivatives involving the streamwise direction s can be measured by time differentiation, scales in the streamwise direction are given in figure 24. To express these scales in the more meaningful cylindrical coordinate system, it becomes necessary to make certain assumptions based on isotropic relationships. The details of such transformation of coordinates are given in appendix A. With these assumptions, $\frac{\lambda_{v_z, z}}{M}$, $\frac{\lambda_{v_\theta, z}}{M}$, and $\frac{\lambda_{v_r, z}}{M}$ were calculated. They are shown in figure 25. The values without rotation in the region excluding the boundary layer are indicated in the same figure by dashed lines.

Turbulence Decay

Since the flow is not fully developed, it is important to know how the turbulence is changing with distance along the axis. All of the measurements reported so far in this section have been made at a fixed distance from the farthest downstream screen, at $\frac{\xi}{M} = 17.5$. With suitable modifications in the traversing apparatus to allow movement in the axial direction, axial traverses were made over a distance of about

10 mesh lengths at the midstream position without rotation and at several radii with rotation.

Without rotation, measurements of $\tilde{v}_z/V_z$ agreed very well with some screen decay data by Corrsin (ref. 26). Since $\dfrac{\tilde{v}_\theta}{V_z} \approx \dfrac{\tilde{v}_r}{V_z}$ at $\dfrac{\xi}{M} = 17.5$ was found also to be in agreement with this reference, the variation of these latter quantities in the axial direction was taken from there. Figure 26 shows the inverse of the turbulence levels plotted against distance from the screen, again made dimensionless with the mesh size.

As is described in appendix A, the method of measurement of the turbulence employed herein makes use of the signals from a single hot wire oriented in various positions with respect to the mean velocity. In each position, it is sensitive to one or more of the turbulent intensities and shear stresses; by an algebraic manipulation of the signals for the various positions the desired quantities are obtained. It was found that with rotation of the flow the wire signals as a function of axial distance could be collapsed into a single curve, regardless of radius or wire position. This implies that for the range of axial distance considered, the ratio of any one intensity component to another remains constant, within the accuracy of measurement. Making use of this fact, decay curves with rotation are shown for the three intensities at the midstream position in figure 27. For any other radial position, the curves are shifted in such a way as to go through the previously measured values at that position, at $\dfrac{\xi}{M} = 17.5$. It can be seen that the effect of rotation has been to lessen the decay, for all components, with the strongest effect on the radial component.

Spectrum[1]

The spectra of $v_r{}^2$, $v_\theta{}^2$, and $v_z{}^2$ with rotation are shown in figure 28, all taken at one point $\left(\dfrac{r - a}{b - a} = 0.2, \; \dfrac{\xi}{M} = 17.5 \right)$. The abscissa of these curves is the one-dimensional wave number K_1, oriented along the direction of the mean velocity. In figure 29 the $v_r{}^2$ spectra at two radial positions, $\dfrac{r - a}{b - a} = 0.2$ and 0.8, are compared.

---

[1]Spectral measurements were made by Dr. Hsuan Yeh.

DISCUSSION

General Considerations

The left-hand sides of equations (7) to (13) for turbulence inten-
sity and shear stress components become, respectively, when simplified
by $V_\theta = \omega r$ in the present problem,

$$\frac{1}{2} V_z \frac{\partial \overline{v_r^2}}{\partial z} - \overline{v_r v_\theta} 2\omega$$

$$\frac{1}{2} V_z \frac{\partial \overline{v_\theta^2}}{\partial z} + \overline{v_r v_\theta} 2\omega$$

$$\frac{1}{2} V_z \frac{\partial \overline{v_z^2}}{\partial z}$$

$$\frac{1}{2} V_z \frac{\partial \overline{q^2}}{\partial z}$$

$$\frac{1}{2} V_z \frac{\partial \overline{v_r v_\theta}}{\partial z} - \left(\overline{v_\theta^2} - \overline{v_r^2}\right)\omega$$

$$\frac{1}{2} V_z \frac{\partial \overline{v_\theta v_z}}{\partial z} + \overline{v_r v_z}\omega$$

$$\frac{1}{2} V_z \frac{\partial \overline{v_r v_z}}{\partial z} - \overline{v_\theta v_z}\omega$$

The statement on orders of magnitude (given in the section "Prelim-
inary Measurements") for the various mean velocity terms has been used

to eliminate those terms that would otherwise appear. The terms on the right-hand sides of equations (7) to (13) remain the same and are not repeated here.

In the simplified left-hand-side expressions just given, the second term stands for the production of the quantity whose rate of change is given by the first term. In the present case, this first term is found to be negative for the first three equations, corresponding to a decay of turbulence. A negative sign for the second term implies a positive production, and vice versa. For example, in the first expression, if $\overline{v_r v_\theta} < 0$, $\partial \overline{v_r^2}/\partial z$ would be decreased by the shear stress acting on the mean velocity. If $\overline{v_r v_\theta} > 0$, $\partial \overline{v_r^2}/\partial z$ would be increased. A positive production of course does not necessarily mean a larger value of $\overline{v_r^2}$ compared with no production since the pressure and triple velocity correlation terms also enter into the energy balance.

The influence of rotation is directly apparent in the production terms; with $\omega = 0$ all these terms vanish. However, all the terms on the right-hand side of equations (7) to (13) will probably also be different with and without rotation.

Flow without rotation.- In considering flow without rotation, all production terms vanish, and the turbulence decay is given then by the combined influence of the viscous terms, pressure correlations, and triple velocity correlations. At any point the values of the turbulence intensities depend on this decay and on the manner of production at the screen. Immediately downstream of the screen, velocity gradients exist in the flow due to the wire wakes. There are both $\partial V_z/r\,\partial\theta$ and $\partial V_z/\partial r$ terms, alternating in sign on either side of a wire wake. (It would be more natural in the nonrotating case to use Cartesian coordinates, with x,y instead of r,θ. The cylindrical coordinates are retained, however, for comparison with the rotating case.)

Very close to the screen, the left-hand sides of equations (7) to (9) and (11) to (13) become for turbulence intensities:

$$\frac{1}{2} V_z \frac{\partial \overline{v_r^2}}{\partial z}$$

$$\frac{1}{2} V_z \frac{\partial \overline{v_\theta^2}}{\partial z}$$

$$\frac{1}{2} V_z \frac{\overline{\partial v_z^2}}{\partial z} + \overline{v_\theta v_z} \frac{\partial V_z}{r\, \partial \theta} + \overline{v_r v_z} \frac{\partial V_z}{\partial r}$$

and for turbulent shear stresses:

$$\frac{1}{2} V_z \frac{\overline{\partial v_r v_\theta}}{\partial z}$$

$$\frac{1}{2} V_z \frac{\overline{\partial v_\theta v_z}}{\partial z} + \frac{\overline{v_\theta^2}}{2} \frac{\partial V_z}{r\, \partial \theta} + \frac{\overline{v_r v_\theta}}{2} \frac{\partial V_z}{\partial r}$$

$$\frac{1}{2} V_z \frac{\overline{\partial v_r v_z}}{\partial z} + \frac{\overline{v_r^2}}{2} \frac{\partial V_z}{\partial r} + \frac{\overline{v_r v_\theta}}{2} \frac{\partial V_z}{r\, \partial \theta}$$

Assume that, in the shear equations only, the production term alone is important in the determination of the value of the quantity being produced. By this assumption, since there is no production of $\overline{v_r v_\theta}$, this quantity vanishes. In the last two shear-stress equations, it follows from the same assumption that when $\dfrac{\partial V_z}{r\, \partial \theta} > 0$ then $\overline{v_\theta v_z} < 0$ and when $\dfrac{\partial V_z}{r\, \partial \theta} < 0$ then $\overline{v_\theta v_z} > 0$. It also follows that when $\dfrac{\partial V_z}{\partial r} > 0$ then $\overline{v_r v_z} < 0$ and when $\dfrac{\partial V_z}{\partial r} < 0$ then $\overline{v_r v_z} > 0$.

Thus the quantities $\overline{v_\theta v_z}\, \partial V_z / r\, \partial \theta$ and $\overline{v_r v_z}\, \partial V_z / \partial r$ are negative throughout the entire region immediately behind the screen. Considering now the intensity equations, there is no direct production of $\overline{v_\theta^2}$ and $\overline{v_r^2}$ but always a direction production for $\overline{v_z^2}$. It is known that some distance behind the screen the turbulence will become nearly isotropic. Since there is direct production from the mean velocity only of $\overline{v_z^2}$, the other two components must receive their energy from the pressure velocity correlation (see, e.g., refs. 19 to 21). Thus the assumption made above for the shear equations that the production term alone

determines the value of the quantity being produced cannot be valid for the intensity equations.

The physical picture is then a direct production of $\overline{v_z^2}$, with about equal feeding of $\overline{v_\theta^2}$ and $\overline{v_r^2}$ by the pressure velocity correlations. Some distance behind the screen when the wakes have died out there is no longer any direct production since the velocity gradients in V_z have vanished; the terms $\overline{v_r v_z}$ and $\overline{v_\theta v_z}$ therefore vanish, while $\overline{v_z^2}$, $\overline{v_\theta^2}$, and $\overline{v_r^2}$ decay, with $\overline{v_z^2}$ larger than $\overline{v_\theta^2} \approx \overline{v_r^2}$ but decaying faster due to energy loss by pressure fluctuations which feed $\overline{v_\theta^2}$ and $\overline{v_r^2}$.

Flow with rotation.- A similar reasoning is now applied to the case when rotation is imposed on the flow field. Far enough downstream so that the wire wakes have disappeared, the only production terms are those given in the section "General Considerations."

Within the limits of the previous assumption it is seen that in the last two equations the production of $\overline{v_\theta v_z}$ necessitates a nonzero value of $\overline{v_r v_z}$, while the production of $\overline{v_r v_z}$ necessitates a nonzero value of $\overline{v_\theta v_z}$. Thus $\overline{v_r v_z}$ is necessary to produce $\overline{v_\theta v_z}$ which is necessary to produce $\overline{v_r v_z}$ and if $\overline{v_r v_z}$ is zero it must remain so. The same is true for $\overline{v_\theta v_z}$. Furthermore, the system is such that if in the $\overline{v_\theta v_z}$ equation, $\overline{v_r v_z} > 0$, the production of $\overline{v_\theta v_z}$ is negative, and $\overline{v_\theta v_z} < 0$. Then in the $\overline{v_r v_z}$ equation the production of $\overline{v_r v_z}$ is negative so that $\overline{v_r v_z}$ decreases. Arguing from the production terms alone, the last two equations are such that neither $\overline{v_\theta v_z}$ nor $\overline{v_r v_z}$ could be produced directly from the rotation.

The equation for $\overline{v_r v_\theta}$, however, involves the turbulent intensities in the production term. It is seen that if $\overline{v_r^2} > \overline{v_\theta^2}$ then $\overline{v_r v_\theta} < 0$ and if $\overline{v_r^2} < \overline{v_\theta^2}$ then $\overline{v_r v_\theta} > 0$.

Thus if $\overline{v_r^2} > \overline{v_\theta^2}$, $\overline{v_\theta^2}$ is produced from the rotation by the turbulence-intensity equation, while $\overline{v_r^2}$ is diminished. Similarly, if $\overline{v_\theta^2} > \overline{v_r^2}$, $\overline{v_\theta^2}$ is diminished while $\overline{v_r^2}$ is produced. When $\overline{v_r^2} = \overline{v_\theta^2}$, there will be no production of $\overline{v_r v_\theta}$ and thus no effect of

rotation on the production of either $\overline{v_r{}^2}$ or $\overline{v_\theta{}^2}$. Hence the production terms act in such a way as to keep $\overline{v_r{}^2} \approx \overline{v_\theta{}^2}$, even with rotation. The actual values of $\overline{v_r{}^2}$ and $\overline{v_\theta{}^2}$, of course, will depend on the more indirect effects of rotation on the remaining terms in the first three equations.

Close to the screen, the production of turbulence is not affected by the rotation if there is no relative motion between screen and fluid, that is if both are in solid-body rotation. If there is relative motion, however, similar reasoning as before shows a positive production of $\overline{v_\theta{}^2}$ due to the term $\overline{v_z v_\theta}\, \dfrac{\partial V_\theta}{\partial z}$, which is found to be always of one sign.

The physical picture, then, for solid-body rotation is a direct production at the screen of $\overline{v_z{}^2}$, with subsequent direct production or diminishing of $\overline{v_r{}^2}$ and $\overline{v_\theta{}^2}$, depending on the values of $\overline{v_r{}^2}$ and $\overline{v_\theta{}^2}$, in such a way as to keep them about equal. If there is relative motion between fluid and screen there will be an additional production of $\overline{v_\theta{}^2}$ at the screen. The turbulence then decays under the influence of viscous dissipation and energy transfer between components by the pressure velocity correlations; both quantities are presumably also influenced by the rotation.

Energy Balance

In considering the energy balance it will be recalled that, at the one axial station considered, the experiments showed the following results over most of the flow field, excluding the boundary layers:

Without rotation,

$$\overline{v_z{}^2} > \overline{v_r{}^2} \approx \overline{v_\theta{}^2}$$

$$\overline{v_r v_z} = \overline{v_\theta v_z} = \overline{v_r v_\theta} = 0$$

with rotation,

$$\overline{v_z{}^2} \approx \overline{v_\theta{}^2} > \overline{v_r{}^2}$$

$$\overline{v_r v_z} = \overline{v_\theta v_z} = 0, \quad \overline{v_r v_\theta} > 0$$

The result that $\overline{v_r v_\theta} > 0$ is entirely consistent with the finding of $\overline{v_\theta{}^2} > \overline{v_r{}^2}$ by the preceding considerations. Since measurements of the microscales and turbulence decay were made in addition to the measurements of the quantities above, it is possible to substitute these measured quantities into the three turbulence-intensity equations (7) to (9).

For the purposes of calculation, the turbulence-intensity equations were made dimensionless by multiplying each term of these equations by $M/V_o{}^3$. In calculating the dissipation term, the following assumptions, which are strictly valid only for isotropic turbulence, were used:

$$\overline{\left(\frac{\partial v_\theta}{\partial z}\right)^2} = 2\overline{\left(\frac{\partial v_\theta}{r\,\partial\theta}\right)^2} = \overline{\left(\frac{\partial v_\theta}{\partial r}\right)^2}$$

$$\overline{\left(\frac{\partial v_r}{\partial z}\right)^2} = 2\overline{\left(\frac{\partial v_r}{\partial r}\right)^2} = \overline{\left(\frac{\partial v_r}{r\,\partial\theta}\right)^2}$$

$$\overline{\left(\frac{\partial v_z}{\partial z}\right)^2} = \frac{1}{2}\overline{\left(\frac{\partial v_z}{r\,\partial\theta}\right)^2} = \frac{1}{2}\overline{\left(\frac{\partial v_z}{\partial r}\right)^2}$$

An assumption of this type is necessary because only derivatives in the flow direction were measured. Furthermore, since neither the triple velocity nor the pressure velocity correlation terms are measured, they will be considered together. Substituting the measured values into the energy equations for the case of no rotation, it was found that, at $\frac{\xi}{M} = 17.5$ and $\frac{r - a}{b - a} = 0.5$, (without rotation, the energy balance is made only at the

midstream position, since conditions were previously found to be radially uniform except near the wall):

	Decay term	Production term	Pressure velocity and triple velocity correlations	Viscous term
v_r	3.6×10^{-5}	0	-0.3×10^{-5}	3.9×10^{-5}
v_θ	3.6×10^{-5}	0	-0.3×10^{-5}	3.9×10^{-5}
v_z	6.4×10^{-5}	0	0.6×10^{-5}	5.8×10^{-5}
q	13.6×10^{-5}	0	0	13.6×10^{-5}

The exact balancing of the total energy equation is not a coincidence. Measured values of the derivative terms consistently gave λ too large and a dissipation which was too small to balance this equation. This discrepancy, amounting to a factor of about 2.0, could be due to the assumption of isotropy used in their calculation. For lack of a better procedure, all measured values of λ were adjusted by the same amount in such a way as to balance the total energy equation for the case of no rotation.

A result consistent with the previous considerations is obtained. The unknown pressure-velocity-correlation and triple-velocity-correlation term is obtained by difference; when positive it represents a loss of energy and when negative, a gain. Thus $\overline{v_r^2}$ and $\overline{v_\theta^2}$ are seen to be gaining energy at the expense of $\overline{v_z^2}$ due to the influence of this effect.

The same procedure when applied at several radial positions in the rotating flow at the same station, $\frac{\xi}{M} = 17.5$, gives the results shown in figures 30 to 33 for the three intensity components and the total energy. In each case, the relative gain and loss due to the various terms necessary to make up the measured decay are shown. The viscous term, combining dissipation and viscous work, is denoted by DVW. The pressure velocity and triple velocity term, considered together and denoted by PTC, is again obtained by difference.

The balance on total energy shows over the center region a larger loss due to viscous action than the decay, which implies a gain due to the term obtained by difference. Near the walls the opposite is true. This implies a flow of total energy from both walls to the center. The same considerations hold for the energy balance on $\overline{v_z^2}$. Similarly, for both $\overline{v_\theta^2}$ and $\overline{v_r^2}$, a comparison of the decay term with the viscous term shows the former to be less in the center, implying an inward flow of energy. The picture is made more complicated by the production term $\overline{2v_r v_\theta \omega}$, which for $\overline{v_r v_\theta} > 0$ gives a gain by direct production for $\overline{v_r^2}$ and a loss for $\overline{v_\theta^2}$. This must be made up by the pressure and triple correlation term, which therefore gives a gain for $\overline{v_\theta^2}$ and a loss for $\overline{v_r^2}$. It will be recalled that this term, without rotation, acted as a gain for both $\overline{v_r^2}$ and $\overline{v_\theta^2}$.

It is interesting to compare the coefficients A both with and without rotation. These coefficients are defined in the following way:

$$\frac{\lambda_{v_z,z}}{M} = \frac{A_z}{\sqrt{\dfrac{M\tilde{v}_z}{\nu}}}$$

$$\frac{\lambda_{v_r,z}}{M} = \frac{A_r}{\sqrt{\dfrac{M\tilde{v}_r}{\nu}}}$$

$$\frac{\lambda_{v_\theta,z}}{M} = \frac{A_\theta}{\sqrt{\dfrac{M\tilde{v}_\theta}{\nu}}}$$

For a given value of $\tilde{v}$, an increase in A implies an increase in λ and therefore a decrease in viscous dissipation and work. Figure 34 shows the distributions of A_z, A_r, and A_θ calculated from the

measured intensities and time derivatives. It can be seen that A_z and A_θ are about the same, with A_r considerably less over the entire range.

Thus, the relative loss of energy by viscous action is larger for $\overline{v_r{}^2}$ than for the other two components.

A tentative physical picture for the effect of rotation is then as follows: The rotation increases the loss through viscous action for the radial fluctuations relative to the peripheral and axial fluctuations. A shear stress $\overline{v_r v_\theta}$ is produced by the difference of $\overline{v_\theta{}^2}$ and $\overline{v_r{}^2}$ in such a way as to restore their equality by direct production from the mean peripheral velocity. Because of this, the pressure velocity and triple velocity correlations, which without rotation fed $\overline{v_r{}^2}$ and $\overline{v_\theta{}^2}$ from $\overline{v_z{}^2}$, now feed $\overline{v_\theta{}^2}$ at the expense of $\overline{v_r{}^2}$.

It is interesting to note that solid-body rotation causes an increased loss of energy by viscous action for the radial velocity fluctuations compared with the radial and peripheral fluctuations. It will be recalled that in the Introduction reference was made to investigations of small motions relative to solid-body rotation. There it is found that the radial velocity component is suppressed by the rotation, but this is an effect associated with potential (Coriolis and centrifugal) forces and not with viscosity.

It should be pointed out that the considerations above are beclouded by the following facts:

(1) The turbulence-producing screen has a peripheral velocity relative to the fluid since the fluid is not quite in solid-body rotation at the screen. This implies a larger $\overline{v_\theta{}^2}$ production than would be due to purely solid-body rotation, as previously mentioned.

(2) Due to the presence of the walls and axial velocity boundary layers, there is a flow of turbulent energy inward from the walls.

(3) Because only time derivatives were measured, the viscous terms of the energy equations are calculated with the assumption of isotropic relations between the derivatives of any one velocity component with respect to different directions. This assumption is usually verified for sufficiently high values (of the order 100) of R_λ, defined as

$$R_\lambda = \frac{\tilde{v}\lambda}{\nu}$$

For the different intensity components, the values of R_λ obtained in this investigation are shown in figure 35, with and without rotation. It is seen that they are comparatively low, casting some doubt on the validity of the assumption of isotropic relations between viscous terms.

Production of Turbulent Shear Stresses

The assumption that in the turbulent-shear-stress equations only the production term is important in the qualitative determination of these stresses will now be further examined.

It will be recalled that in any one of these equations it was assumed that a positive production would give a positive shear stress, negative production, a negative shear stress, and no production would lead to vanishing of the shear stress. For unidirectional shear flows this assumption is certainly true.

Take the case of fully developed flow through a two-dimensional straight channel, where x is the direction of mean flow and y is the distance from the wall. For this case, the production terms of the shear-stress equations are as follows:

For $\overline{v_x v_z}$: $\qquad\qquad\qquad \dfrac{\overline{v_y v_z}}{2} \dfrac{\partial V_x}{\partial y}$

For $\overline{v_x v_y}$: $\qquad\qquad\qquad \dfrac{\overline{v_y^2}}{2} \dfrac{\partial V_x}{\partial y}$

For $\overline{v_y v_z}$: $\qquad\qquad\qquad\qquad 0$

Again a negative sign of these terms implies a positive production. Now since there is no production of $\overline{v_y v_z}$, $\overline{v_y v_z}$ vanishes. There is then no production of $\overline{v_x v_z}$, which also vanishes. Since $\overline{v_y^2}$ is always > 0, there will be a production of negative $\overline{v_x v_y}$ when $\partial V_x / \partial y$ is positive, and vice versa. Hence $\overline{v_x v_y}$ is negative in the region where $\partial V_x / \partial y$ is positive, and vice versa. At the center of the channel $\dfrac{\partial V_x}{\partial y} = 0$, there is no production of $\overline{v_x v_y}$ and $\overline{v_x v_y}$ will be zero there. Thus the assumption is in complete agreement with the experimental fact and also with the well-known momentum transfer theory.

The case of fully developed flow in a two-dimensional curved channel is considered next. An investigation of this flow configuration is reported in reference 14. Using cylindrical coordinates, let the θ

direction be in the direction of mean flow and r, the radial direction
(i.e., the direction across the channel). The production terms of the
shear-stress equations are as follows:

For $\overline{v_\theta v_z}$:

$$\frac{\overline{v_r v_z}}{2}\left(\frac{\partial V_\theta}{\partial r} + \frac{V_\theta}{r}\right)$$

For $\overline{v_r v_\theta}$:

$$\frac{\overline{v_r^2}}{2}\frac{\partial V_\theta}{\partial r} + \left(\frac{\overline{v_r^2}}{2} - \overline{v_\theta^2}\right)\frac{V_\theta}{r}$$

For $\overline{v_r v_z}$:

$$-\overline{v_\theta v_z}\,\frac{V_\theta}{r}$$

For a very large radius of curvature, the terms involving V_θ/r
become small, and in the limit of zero curvature the production terms
are the same as in the straight channel except for the change of nota-
tion from y to r and from x to θ. The influence of curvature is
thus represented by the terms involving V_θ/r. For a fully developed
flow, $\overline{v_r v_z}$ vanishes (this can be shown from the Reynolds equations,
see ref. 14); then, since there is no production of $\overline{v_\theta v_z}$, it also is

zero. Close to the wall, $\left|\dfrac{\partial V_\theta}{\partial r}\right| \gg \dfrac{V_\theta}{r}$, and the first term alone produces

a negative shear $\overline{v_r v_\theta}$ on the inner wall and a positive term $\overline{v_r v_\theta}$ on
the outer, by the assumptions made herein. The influence of curvature

on $\overline{v_r v_\theta}$ is seen to depend on the term $\left(\dfrac{\overline{v_r^2}}{2} - \overline{v_\theta^2}\right)\dfrac{V_\theta}{r}$. If $\overline{v_\theta^2} > \dfrac{\overline{v_r^2}}{2}$

over the entire flow, this term will cause an additional production of
positive $\overline{v_r v_\theta}$ everywhere. Thus the $\overline{v_r v_\theta}$ shear-stress distribution
would shift in the direction of positive $\overline{v_r v_\theta}$ over the entire channel
under the influence of a mild curvature. Measured $\overline{v_r v_\theta}$ distributions
obtained in such a curved channel are reproduced in figure 36; the results
were taken from references 14 and 16. For this flow, $\overline{v_\theta^2}$ does exceed
$\overline{v_r^2}/2$, and a shift of $\overline{v_r v_\theta}$ in the proper direction is in fact observed.

A physical interpretation of the influence of curvature was first
suggested by Rayleigh (ref. 27) in the following way: It may be assumed
that for flow with curvature a displaced fluid element conserves its

angular momentum. Then a positive radial displacement of a fluid element is associated with a velocity defect if the mean peripheral velocity decreases more slowly with radius than $1/r$. The radial motion of the element is retarded since the radial pressure gradient existing in the mean flow exceeds the centrifugal force acting on the fluid element. On the other hand, if the mean peripheral velocity decreases with radius faster than $1/r$, any radial displacement would be increased by the action of the radial pressure gradient. Thus radial motion is suppressed on the inner wall of the curved channel and increased on the outer, resulting in an increase of $\overline{v_r v_\theta}$ on the outside and a decrease on the inside.

As is shown in the "Introduction" and appendix B, such simple reasoning requires an extension in the case of solid-body rotation. The modified theory still assumes the conservation of angular momentum (which is, of course, not exactly true) but traces through the complete history of a displaced particle. The theory then predicts that $\overline{v_r v_\theta} = 0$ for solid-body rotation. This still does not explain the experimental fact that $\overline{v_r v_\theta}$ is slightly on the positive side. A simple physical interpretation of the positive value of $\overline{v_r v_\theta}$ found in solid-body rotation might be as follows: For a fluid element a positive value of v_θ corresponds to a small motion relative to the rotation in the direction of rotation. This would be associated with a Coriolis force acting radially outward, causing a $v_r > 0$. Thus $\overline{v_r v_\theta} > 0$. Similarly, a small negative peripheral velocity relative to the rotation would give rise to a negative value of v_r, again giving $\overline{v_r v_\theta} > 0$. Thus a peripheral fluctuation causes a positive value of $\overline{v_r v_\theta}$. Similar reasoning shows that a radial fluctuation causes, again due to the action of Coriolis forces, a negative value of $\overline{v_r v_\theta}$. If the peripheral fluctuations are larger, as they are here, the former effect predominates to give a resultant positive value of $\overline{v_r v_\theta}$.

CONCLUDING REMARKS

A peripheral velocity distribution like that of a rotating solid body imposed on the turbulence produced by screens is found to undergo very little change with distance along the axis of rotation. Experimental measurements of the turbulent shear correlation between radial and peripheral fluctuations 17.5 mesh lengths from the farthest downstream screen give a small positive value for this quantity over the major portion of the flow field. The other shear correlations are found to vanish. It is believed that the nonvanishing of this shear correlation is due to

the fact that the flow is not fully developed, although the exact mechanism is not clear.

Consideration of the qualitative nature of the turbulent shear stresses, based on the production term in the equations for these stresses, leads to results in agreement with the experimental findings. Such considerations also lead to results in agreement with experiment for the influence of curvature on a fully developed channel flow.

The influence of rotation on the intensity of the fluctuations 17.5 mesh lengths from the screen is as follows: The radial fluctuation intensity is suppressed, the peripheral intensity is increased, and the axial intensity is not largely affected by the rotation. The turbulent energy balance for these intensities indicates a larger loss of energy by dissipation and viscous work for the radial intensity than for the other two, with a gain by production from the mean velocity for the radial fluctuations, and a loss by production for the peripheral fluctuations. The action of the pressure velocity and triple velocity correlations, which without rotation serve to increase the radial and peripheral fluctuations at the expense of the axial, is, with rotation, to increase the peripheral fluctuations at the expense of the radial. These results are obtained under the assumption of certain isotropic relations for the viscous terms of the energy equations.

The influence of rotation on the various mean-square derivatives of the turbulent fluctuations which make up this viscous term should be investigated further; this would serve to check the validity of the assumption just mentioned and to aid in the interpretation of the result that radial fluctuations experience a relatively larger energy loss through viscosity than do the peripheral and axial fluctuations.

It would also be extremely interesting to study the flow considered herein after it has become fully developed. The measured lack of change of the peripheral velocity profile with axial distance indicates that the length of tunnel necessary to achieve this would probably not be larger than that necessary to achieve fully developed flow without rotation. The complications introduced by changing conditions along the axis would then be eliminated to make a more detailed analysis possible.

The Johns Hopkins University,
     Baltimore, Md., October 8, 1956.

APPENDIX A

METHOD OF MEASUREMENTS

Response of a Hot Wire

The response of an electrically heated fine wire (the hot wire) in a steady flow of airstream is found experimentally to obey the following approximate relation when all quantities have reached an equilibrium state with time:

$$I^2\left(\frac{R}{R - R_o}\right) = A\sqrt{V_p} + B \tag{A1}$$

where

I   wire heating current

R_o wire resistance with no heating

R   wire resistance (with heating) at operating condition

V_p velocity component perpendicular to axis of wire

A,B   constants for a given wire and surrounding medium, to be determined experimentally

In practice, $\dfrac{R}{R - R_o}$ is fixed by the experimenter. In the present investigation $\dfrac{R}{R - R_o}$ is chosen to be 3.0 at all times, corresponding to $\dfrac{R - R_o}{R_o}$, the overheat ratio, of 0.5. For a fixed value of $\dfrac{R}{R - R_o}$, it is convenient to rewrite equation (A1) in the following form:

$$I^2 - I_o^2 = S\sqrt{V_p} \tag{A2}$$

The two constants I_o^2 and S are determined experimentally by measuring I^2 over a suitable range of V_p in a calibrating airstream. The term I_o^2 has the significance of being the extrapolated value of I^2 at zero V_p. It is clear that the constants I_o and S are related to A and B by $I_o^2 = B\left(\dfrac{R - R_o}{R}\right)$ and $S = A\left(\dfrac{R - R_o}{R}\right)$.

If velocity fluctuations exist in the airstream, the wire tempera-
ture and therefore its resistance will also fluctuate with time. In
constant-current operation, I = Constant, the resistance fluctuation dR
is measured as a voltage fluctuation dE. Differentiating both sides of
the steady-state equation (A1), in which R and V_p are the variables,
gives

$$-\frac{dV_p}{V_p} = \frac{2}{\frac{R}{R_o} - 1} \frac{I^2}{I^2 - I_o^2} \frac{dE}{E}$$

In practice, since I does vary slightly, one may have to take its
variations into account also, resulting in the extra factor called the
"degeneracy" or

$$-\frac{dV_p}{V_p} = \frac{2}{\frac{R}{R_o} - 1} \frac{I^2}{I^2 - I_o^2} \left[\frac{1 + 2\left(\frac{R - R_o}{R_o}\right)\frac{E}{E_B}}{1 - \frac{E}{E_B}}\right] \frac{dE}{E} \qquad (A3)$$

where E_B is the supply voltage to the Wheatstone bridge in which the
wire is placed. These equations are valid if the fluctuation occurs
very slowly (quasi-steady condition) or if the effect of the finite heat
capacity of an actual wire has been electronically compensated. The pro-
cedure so far is quite standard; see, for instance, Kovasznay (ref. 28).
By taking the root mean square of equation (A3), the root-mean-square
value of the velocity fluctuation is obtained in terms of the root-mean-
square value of the voltage fluctuation, which is obtained experimentally.

Response of Hot Wire to Three-Dimensional

Velocity Fluctuations

Consider the general case when the axis of the hot wire is arbitrarily
oriented with respect to the mean velocity direction. To anticipate such
applications in this investigation, it is considered that the mean veloc-
ity V_s is in the θ,z plane, making an angle ϕ with the z-direction.
Let the direction of V_s be denoted by subscript s and the direction
normal to V_s by subscript n, the s,n plane being coincident to the
θ,z plane (fig. 37(a)). The stem or holder of the hot wire is always along
the direction of r. The orientation of the hot wire itself is determined
by the two angles α and β (fig. 37(b)). The angle α is in the
s,n plane and the angle β is between the wire and its stem or the radial
direction.

Equations (A1) or (A2) assume that the steady response of the wire varies with the sine of the angle between the wire and the mean-velocity V_s direction; that is, only the component of V_s perpendicular to the wire is effective in cooling it. (The validity of this assumption is subject to verification by calibration.) In this case, the velocity perpendicular to the wire is $V_p = V_s \sin \gamma$ (see fig. 37(b)). Expressed in terms of the angles α and β, it is

$$V_p = V_s \sqrt{1 - \sin^2\alpha \, \sin^2\beta} \qquad (A4)$$

Let the unit vectors along the directions s, n, and r be $\vec{U}_s$, $\vec{U}_n$, and $\vec{U}_r$, respectively. Then, the unit vector $\vec{U}_{oA}$ along the direction of the wire is

$$\vec{U}_{oA} = \sin\alpha \sin\beta \vec{U}_s + \cos\beta \vec{U}_r + \cos\alpha \sin\beta \vec{U}_n$$

Hence the unit vector along the direction of $\vec{V}_p$ can be expressed by

$$\frac{\vec{V}_p}{V_p} = \frac{\vec{V} - \vec{V}\vec{U}_{oA}}{V_p}$$

$$= \sqrt{1 - \sin^2\alpha \, \sin^2\beta}\, \vec{U}_s - \frac{\sin\alpha \sin\beta \cos\beta}{\sqrt{1 - \sin^2\alpha \, \sin^2\beta}}\, \vec{U}_r - \frac{\sin\alpha \cos\alpha \sin^2\beta}{\sqrt{1 - \sin^2\alpha \, \sin^2\beta}}\, \vec{U}_n$$

$$(A5)$$

where use has been made of the fact that $\vec{V}_s = V_s\vec{U}_s$. For <u>small</u> velocity fluctuations v_s, v_n, and v_r, only their components along the direction of $\vec{V}_p$ have any influence in changing the magnitude of total V_p and hence in cooling the wire. The total fluctuation of V_p (due to v_s, v_r, and v_n) as a ratio of itself can be obtained from equations (A4) and (A5) as

$$\frac{dV_p}{V_p} = \frac{v_s}{V_s} - X \frac{v_r}{V_s} - Y \frac{v_n}{V_s} \qquad (A6)$$

where

$$X \equiv \frac{\sin \alpha \sin \beta \cos \beta}{1 - \sin^2\alpha \sin^2\beta}$$

$$Y \equiv \frac{\sin \alpha \cos \alpha \sin^2\beta}{1 - \sin^2\alpha \sin^2\beta}$$

Equation (A6) supplies the value for $\frac{dV_p}{V_p}$ of equation (A3). As a check, it is seen that for $\alpha = 0$ or $\beta = 0$, the wire is sensitive only to v_s, in agreement with the customary considerations. For $\beta = 90^\circ$, $X = 0$ and $Y = \tan \alpha$, and for $\alpha = 90^\circ$, $X = \tan \beta$ and $Y = 0$. Both facts are well known in hot-wire anemometry.

Substituting equation (A6) into equation (A3), squaring and averaging over time, gives

$$\frac{\overline{v_s^2}}{V_s^2} + X^2 \frac{\overline{v_r^2}}{V_s^2} + Y^2 \frac{\overline{v_n^2}}{V_s^2} - 2X \frac{\overline{v_s v_r}}{V_s^2} - 2Y \frac{\overline{v_s v_n}}{V_s^2} + 2XY \frac{\overline{v_r v_n}}{V_s^2} =$$

$$\left[\frac{2}{\frac{R}{R_o} - 1} \frac{I^2}{I^2 - I_o^2} \frac{1 + 2\left(\frac{R - R_o}{R_o}\right)\frac{E}{E_B}}{1 - \frac{E}{E_B}} \right]^2 \frac{\overline{dE^2}}{E^2} \qquad (A7)$$

It is seen that all six components of the turbulent stress tensor appear, three components of intensity and three shear correlations.

Application

Since the measuring probes used herein are inserted radially through the wall of the tunnel, it is quite simple to make use of the previous three-dimensional response in the following way: A hot-wire probe is made with one support longer than the other; the wire fastened to them then assumes just the position shown in figure 37(b). The angle β is fixed once the probe is made. Turning the probe stem about its axis has the effect of varying α and therefore X and Y. Since there are six turbulence quantities to be determined, the wire voltage in six positions will be necessary. Two of these were chosen as the positions given by $\alpha = 0$ and $\alpha = -90^\circ$. The other four are taken as symmetrical about the plane formed by the two cross-component fluctuations. Looking radially inwards along the probe stem, the scheme is as follows (fig. 37(c)):

The two F positions are for $\alpha = 0$ and should give the same response, namely, $\overline{v_s^2}/V_s^2$. At the position A the wire is in the r,s plane, with its shorter support at the upstream side. This is necessary to avoid the wake of this support hitting the wire. The other positions are then as shown in figure 37(c).

Let the right-hand side of equation (A7) be defined as N; that is,

$$N \equiv \left(\frac{2}{\dfrac{R}{R_0} - 1} \; \frac{I^2}{I^2 - I_0^2} \; \frac{1 + 2 \dfrac{R - R_0}{R_0} \dfrac{E}{E_B}}{1 - \dfrac{E}{E_B}} \right)^2 \frac{\overline{dE^2}}{E^2}$$

The following system then results:

$$\frac{\overline{v_s^2}}{V_s^2} + X^2 \frac{\overline{v_r^2}}{V_s^2} + Y^2 \frac{\overline{v_n^2}}{V_s^2} + 2X \frac{\overline{v_s v_r}}{V_s^2} - 2Y \frac{\overline{v_s v_n}}{V_s^2} - 2XY \frac{\overline{v_r v_n}}{V_s^2} = N_B$$

$$\frac{\overline{v_s^2}}{V_s^2} + X^2 \frac{\overline{v_r^2}}{V_s^2} + Y^2 \frac{\overline{v_n^2}}{V_s^2} + 2X \frac{\overline{v_s v_r}}{V_s^2} + 2Y \frac{\overline{v_s v_n}}{V_s^2} + 2XY \frac{\overline{v_r v_n}}{V_s^2} = N_C$$

$$\frac{\overline{v_s^2}}{V_s^2} + X^2 \frac{\overline{v_r^2}}{V_s^2} + Y^2 \frac{\overline{v_n^2}}{V_s^2} - 2X \frac{\overline{v_s v_r}}{V_s^2} - 2Y \frac{\overline{v_s v_n}}{V_s^2} + 2XY \frac{\overline{v_r v_n}}{V_s^2} = N_D$$

$$\frac{\overline{v_s^2}}{V_s^2} + X^2 \frac{\overline{v_r^2}}{V_s^2} + Y^2 \frac{\overline{v_n^2}}{V_s^2} - 2X \frac{\overline{v_s v_r}}{V_s^2} + 2Y \frac{\overline{v_s v_n}}{V_s^2} - 2XY \frac{\overline{v_r v_n}}{V_s^2} = N_E$$

$$\frac{\overline{v_s^2}}{V_s^2} + \tan^2\beta \frac{\overline{v_r^2}}{V_s^2} \qquad + 2 \tan \beta \frac{\overline{v_s v_r}}{v_s^2} \qquad = N_A$$

$$\frac{\overline{v_s^2}}{V_s^2} \qquad = N_F$$

Since the coefficients in the first four equations are the same except for their sign, this system is easily solved. It is found that

$$\frac{\overline{v_r v_n}}{V_s{}^2} = \frac{1}{8XY}\left(N_C + N_D - N_B - N_E\right)$$

$$\frac{\overline{v_r v_s}}{V_s{}^2} = \frac{1}{8X}\left(N_B + N_C - N_D - N_E\right)$$

$$\frac{\overline{v_s v_n}}{V_s{}^2} = \frac{1}{8Y}\left(N_C + N_E - N_B - N_D\right)$$

$$\frac{\overline{v_s{}^2}}{V_s{}^2} = N_F$$

$$\frac{\overline{v_r{}^2}}{V_s{}^2} = \frac{1}{\tan\beta}\left[\frac{N_A - N_F}{\tan\beta} - \frac{1}{X}\left(\frac{N_B + N_C - N_E - N_D}{4}\right)\right]$$

$$\frac{\overline{v_n{}^2}}{V_s{}^2} = \frac{1}{Y^2}\left(\frac{N_B + N_C + N_D + N_E}{4} - N_F\right) - \left(\frac{X}{Y}\right)^2 \frac{\overline{v_r{}^2}}{V_s{}^2}$$

It can be seen from these equations that the presence of turbulent shear stresses will be evidenced by an asymmetry of the values of N about the F positions. Considering N as a function of α, N would be a minimum at the two F positions, if all shear stresses are zero and hence $N_B = N_C = N_D = N_E$. The increase of N with α is then the same amount on both sides of the F positions. If the shear stresses are not zero, this is no longer true, and N will not be symmetrical about F. The mean voltage or the wire heating current will still be symmetrical about F regardless of the turbulent quantities, except for the influence of such extraneous factors as possible effects of wire supports, uneven plating of the wire, or curvature of the wire. An illustration of how heating current I and root-mean-square fluctuating voltage vary with angular position is shown in figure 38. These data were taken in the rotating tunnel, at $\dfrac{r - a}{b - a} = 0.35$ and $-\dfrac{\xi}{M} = 17.5$.

Calibration

In the usual application of hot-wire anemometry a wire calibration is necessary to determine I_o^2, the extrapolated value of I^2 at zero velocity, since this quantity enters in the calculation of N. All other quantities that appear in the expression for N are measured directly or preset.

In the present case, it is necessary to know X and Y as well as N to calculate the turbulent quantities. The terms X and Y are functions of α and β, with α determined by the angle through which the probe has been turned about its axis and easily measured with a protractor arrangement. This leaves β and I_o^2 to be found by calibration. This is done in the following way.

The wire is placed in a calibrating airstream, whose velocity can be varied, with its axis perpendicular to the velocity (position F). A series of points is obtained in the usual way by varying the velocity and measuring the wire current. The wire is then turned to position A, which implies that the velocity is decreased by $\cos \beta$ if the cosine response is valid. A further series of points is then taken. The angle β is determined as that angle which gives a straight line for all the points on a plot of I^2 against $\sqrt{V_s \cos \beta}$. An example of this procedure is shown in figure 39. It should be noted that the ability to make all such points fall on a straight line is an indirect verification of the cosine response to angle. With β known, X and Y can then be calculated for this particular probe for any value of α.

It can be seen from figure 38 that a considerable variation of heating current is produced by the turning of the wire. Now if only the component of velocity perpendicular to the wire axis is effective in cooling, as is indicated by figure 39, it is immaterial whether a calibration curve is generated by variations in velocity or variations in wire orientation. If β is known, the perpendicular velocity component, called V_p, may be calculated for any value of α. Then the variation of I^2 with α can be translated to a variation of I^2 with $\sqrt{V_p}$, which should be linear. If the data of figure 38, for instance, are taken and plotted in this way, a straight line does indeed result. It is thus possible, once β is determined by a separate calibration as described, to calculate I_o^2 without further calibrations from the data obtained during an actual experiment.

An expression for I_o^2 as a function of heating current for the various positions can be derived. The equations for the calibration curve are

$$I_F{}^2 = S\sqrt{V_s} + I_o{}^2$$

$$I_B{}^2 = I_C{}^2 = I_D{}^2 = I_E{}^2 = S\sqrt{V_s}\left(1 - \sin^2\alpha \, \sin^2\beta\right)^{1/4} + I_o{}^2$$

$$I_A{}^2 = S\sqrt{V_s}\left(1 - \sin^2\beta\right)^{1/4} + I_o{}^2$$

The subscripts refer to the various positions of the wire as previously described. The slope of the calibration curve is denoted by S. From these equations, it is found that

$$I_o{}^2 = I_F{}^2 - \frac{I_F{}^2 - I_{B,C,D,E}^2}{1 - \left(1 - \sin^2\alpha \, \sin^2\beta\right)^{1/4}}$$

$$= I_F{}^2 - \frac{I_F{}^2 - I_A{}^2}{1 - \sqrt{\cos\beta}}$$

Since differences of measured quantities are involved, the accuracy in determining $I_o{}^2$ from these expressions is not too good unless the values of I^2 are very accurate. In practice it is recommended to plot a calibration curve from a number of points taken at various values of α and to determine $I_o{}^2$ from this curve.

A further check was made for the validity of the cosine law in the following way.

If $\beta = 90°$, that is, with a probe whose wire supports are of equal length, and if the response to angle α is not $\cos\alpha$ but $(\cos\alpha)^\eta$, then

$$I_F{}^2 = S\sqrt{V_s} + I_o{}^2$$

$$I_{B1}{}^2 = S\sqrt{V_s}\cos\alpha_1{}^{\eta/2} + I_o{}^2$$

$$I_{B2}{}^2 = S\sqrt{V_s}\cos\alpha_2{}^{\eta/2} + I_o{}^2$$

where $I_{B1}{}^2$ and $I_{B2}{}^2$ correspond to angles α_1 and α_2.

From these expressions,

$$\frac{I_F{}^2 - I_{B1}{}^2}{I_F{}^2 - I_{B2}{}^2} = \frac{1 - (\cos \alpha_1)^{\eta/2}}{1 - (\cos \alpha_2)^{\eta/2}} \equiv G$$

or

$$\frac{\log_e \left[\dfrac{G - 1}{G - \left(\dfrac{\cos \alpha_1}{\cos \alpha_2}\right)^{\eta/2}} \right]}{\log_e (\cos \alpha_1)} = \frac{\eta}{2}$$

can be derived.

If η is unity, a plot of $\dfrac{G - 1}{G - \sqrt{\dfrac{\cos \alpha_1}{\cos \alpha_2}}}$ against $\cos \alpha_2$ on log-

arithmic coordinates should yield a straight line of slope 0.5. From a number of measurements of I^2 as a function of α for a wire with $\beta = 90^\circ$ the data shown in figure 40 were plotted. Agreement with the line of slope 0.5 seems good.

Change of Coordinates From r,s,n to r,θ,z System

Once all six components of the Reynolds stress tensor in the r,s,n system are obtained, it is a relatively simple matter to find these components in the cylindrical r,θ,z system on account of the relations

$$v_\theta = v_s \sin \phi + v_n \cos \phi$$

$$v_z = v_s \cos \phi - v_n \sin \phi$$

Hence,

$$\frac{\overline{v_\theta^2}}{V_s^2} = \cos^2\phi \, \frac{\overline{v_n^2}}{V_s^2} + \sin^2\phi \, \frac{\overline{v_s^2}}{V_s^2} + 2\sin\phi\cos\phi \, \frac{\overline{v_s v_n}}{V_s^2}$$

$$\frac{\overline{v_z^2}}{V_s^2} = \sin^2\phi \, \frac{\overline{v_n^2}}{V_s^2} + \cos^2\phi \, \frac{\overline{v_s^2}}{V_s^2} - 2\sin\phi\cos\phi \, \frac{\overline{v_s v_n}}{V_s^2}$$

$$\frac{\overline{v_r^2}}{V_s^2} = \frac{\overline{v_r^2}}{V_s^2}$$

$$\frac{\overline{v_\theta v_z}}{V_s^2} = \sin\phi\cos\phi \left(\frac{\overline{v_s^2}}{V_s^2} - \frac{\overline{v_n^2}}{V_s^2} \right) + \left(\cos^2\phi - \sin^2\phi \right) \frac{\overline{v_s v_n}}{V_s^2}$$

$$\frac{\overline{v_r v_\theta}}{V_s^2} = \cos\phi \, \frac{\overline{v_r v_n}}{V_s^2} + \sin\phi \, \frac{\overline{v_r v_s}}{V_s^2}$$

$$\frac{\overline{v_r v_z}}{V_s^2} = -\sin\phi \, \frac{\overline{v_r v_n}}{V_s^2} + \cos\phi \, \frac{\overline{v_r v_s}}{V_s^2}$$

Measurement of Derivatives of Velocity Fluctuations

For the measurement of the viscous terms in the turbulent energy equation it was necessary to measure not only the fluctuating voltage signals from the hot wire but also their time derivatives. Using the Taylor hypothesis for interchanging time derivatives and space derivatives equation (A7) becomes for the wire signal passing through a differentiator

$$\overline{\left(\frac{\partial v_s}{\partial s}\right)^2} + X^2 \overline{\left(\frac{\partial v_r}{\partial s}\right)^2} + Y^2 \overline{\left(\frac{\partial v_n}{\partial s}\right)^2} - 2X \overline{\frac{\partial v_s}{\partial s}\frac{\partial v_r}{\partial s}} - 2Y \overline{\frac{\partial v_s}{\partial s}\frac{\partial v_n}{\partial s}} + 2XY \overline{\frac{\partial v_r}{\partial s}\frac{\partial v_n}{\partial s}} =$$

$$\left[\frac{2}{\frac{R}{R_o} - 1} \frac{I^2}{I^2 - I_o^2} \frac{1 + 2\left(\frac{R - R_o}{R_o}\right)\frac{E}{E_B}}{1 - \frac{E}{E_B}} \right]^2 \frac{\overline{\left(\frac{de}{dt}\right)^2}}{E^2} \equiv N'$$

where $e = dE$ is the voltage fluctuation.

In isotropic turbulence the last three terms on the left are zero. A careful check based on the symmetry of the signal N' with angle α shows that in the flow of this investigation, terms of that type were either zero or too small to be measured both with and without rotation. Assuming that these terms are zero, the previous procedure is then considerably simplified, since there are now only three unknowns and therefore measurements at only three positions of the wire are necessary. In particular, the above equation becomes

$$\overline{\left(\frac{\partial v_s}{\partial s}\right)^2} + X^2\overline{\left(\frac{\partial v_r}{\partial s}\right)^2} + Y^2\overline{\left(\frac{\partial v_n}{\partial s}\right)^2} = N'$$

The transformation from r,s,n coordinates to r,θ,z coordinates involves derivatives with respect to both s and n but the derivatives with respect to n were not measured. To circumvent this difficulty, it is assumed here that the isotropic relations

$$\overline{\left(\frac{\partial v_s}{\partial s}\right)^2} = \frac{1}{2}\overline{\left(\frac{\partial v_s}{\partial n}\right)^2} = \frac{1}{2}\overline{\left(\frac{\partial v_s}{\partial r}\right)^2}$$

hold for any one component, though this is not necessarily true for different components; that is,

$$\overline{\left(\frac{\partial v_s}{\partial s}\right)^2} \neq \frac{1}{2}\overline{\left(\frac{\partial v_n}{\partial s}\right)^2} \neq \frac{1}{2}\overline{\left(\frac{\partial v_r}{\partial s}\right)^2}$$

Furthermore, the following isotropic relations are also assumed:

$$\overline{\frac{\partial v_s}{\partial s}\frac{\partial v_s}{\partial n}} = \overline{\frac{\partial v_n}{\partial s}\frac{\partial v_n}{\partial n}} = \overline{\frac{\partial v_s}{\partial s}\frac{\partial v_n}{\partial s}} = \overline{\frac{\partial v_s}{\partial n}\frac{\partial v_n}{\partial n}} = 0$$

$$\overline{\frac{\partial v_s}{\partial s}\frac{\partial v_n}{\partial n}} = \overline{\frac{\partial v_s}{\partial n}\frac{\partial v_n}{\partial s}} = \frac{1}{4}\left[\overline{\left(\frac{\partial v_s}{\partial s}\right)^2} + \overline{\left(\frac{\partial v_n}{\partial n}\right)^2}\right]$$

With these assumptions, it is found that

$$\overline{\left(\frac{\partial v_z}{\partial z}\right)^2} = \cos^2\!\phi\overline{\left(\frac{\partial v_s}{\partial s}\right)^2} + \frac{\sin^2\phi}{2}\overline{\left(\frac{\partial v_n}{\partial s}\right)^2}$$

$$\overline{\left(\frac{\partial v_z}{r \, \partial \theta}\right)^2} = 2 \cos^2\phi \overline{\left(\frac{\partial v_s}{\partial s}\right)^2} + \sin^2\phi \overline{\left(\frac{\partial v_n}{\partial s}\right)^2}$$

$$\overline{\left(\frac{\partial v_\theta}{\partial z}\right)^2} = 2 \sin^2\phi \overline{\left(\frac{\partial v_s}{\partial s}\right)^2} + \cos^2\phi \overline{\left(\frac{\partial v_n}{\partial s}\right)^2}$$

$$\overline{\left(\frac{\partial v_\theta}{r \, \partial \theta}\right)^2} = \sin^2\phi \overline{\left(\frac{\partial v_s}{\partial s}\right)^2} + \frac{\cos^2\phi}{2} \overline{\left(\frac{\partial v_n}{\partial s}\right)^2}$$

It is seen that because of the assumption made above the isotropic relations still exist for any component in the new coordinates

$$\overline{\left(\frac{\partial v_z}{\partial z}\right)^2} = \frac{1}{2} \overline{\left(\frac{\partial v_z}{r \, \partial \theta}\right)^2}$$

$$\overline{\left(\frac{\partial v_r}{\partial z}\right)^2} = \overline{\left(\frac{\partial v_r}{r \, \partial \theta}\right)^2}$$

$$\overline{\left(\frac{\partial v_\theta}{\partial z}\right)^2} = 2 \overline{\left(\frac{\partial v_\theta}{r \, \partial \theta}\right)^2}$$

These relationships can only be verified by two-wire correlation measurements, which were not made in the present work.

The increase of wire signal with increasing deviation of the wire from a position perpendicular to the mean velocity offers an interesting possibility to check roughly for isotropy in any turbulence field. All shear stresses then vanish and the three intensity components are all the same.

Equation (A7) becomes

$$\frac{\overline{v_s^2}}{V_s^2}\left(1 + X^2 + Y^2\right) = N$$

Since

$$\frac{\overline{v_s^2}}{V_s^2} = N_F$$

the following relation is obtained:

$$1 + X^2 + Y^2 = \frac{N}{N_F}$$

Expanding X and Y in terms of α and β gives

$$1 + \frac{\sin^2\alpha \ \sin^2\beta \left(\cos^2\alpha + \cos^2\beta\right)}{\left(1 - \sin^2\alpha \ \sin^2\beta\right)^2} = \frac{N}{N_F} \qquad (A8)$$

If $\beta = 90^\circ$,

$$1 + \tan^2\alpha = \frac{N}{N_F} \qquad (A9)$$

Following a similar procedure for the differentiated signal gives

$$1 + \frac{2 \ \sin^2\alpha \ \sin^2\beta \left(\cos^2\alpha + \cos^2\beta\right)}{\left(1 - \sin^2\alpha \ \sin^2\beta\right)^2} = \frac{N'}{N_F'} \qquad (A10)$$

If $\beta = 90^\circ$,

$$1 + 2 \tan^2\alpha = \frac{N'}{N_F'} \qquad (A11)$$

In any one of these cases, the ratio $\frac{N}{N_F}$ or $\frac{N'}{N_F'}$ may be plotted
as a function of α, if β is known. The actually measured ratios as
a function of α would indicate isotropy if they follow the relations (A8)
to (A11). As an example, some data taken in the rotating wind tunnel are
shown in figure 41, together with equation (A8) calculated for $\beta = 62.2^\circ$
associated with that particular wire. The nonisotropy of the flow is
quite apparent. For comparison, equation (A9) (for $\beta = 90^\circ$) is also
shown. It is seen that for $\beta < 90^\circ$ the increase of N with α is less
than for $\beta = 90^\circ$; the reason is physically quite obvious since for small
values of β the wire will remain nearly perpendicular to the mean veloc-
ity direction for any value of α.

Accuracy of Measurement

As was previously shown, the determination of the intensities and shear stresses involves sums and differences of the measured quantity N corresponding to several angular positions of the wire.

Due to inherent inaccuracies involved in the method of measurement, the percentage of accuracy in turbulence level in the mean flow direction is believed to be no better than ± 5 percent. This uncertainty is reflected in the calculations of shear and cross components of intensity; furthermore, it will depend on α, since errors become critical when the signals to be subtracted are very nearly equal. From the response of a wire to a turning angle, such as is shown in figure 41, the following estimate of accuracy is made for various values of α for each of the quantities to be calculated:

α, deg	$\dfrac{\Delta \tilde{v}_r/V}{\tilde{v}_r/V}$, percent	α, deg	$\dfrac{\Delta \tilde{v}_n/V}{\tilde{v}_n/V}$, percent	α, deg	ΔR_{sn}	ΔR_{rs}	ΔR_{nr}
25	± 25			20	± 0.08	± 0.22	
35	± 15	30	± 22	30	$\pm .08$	$\pm .15$	± 0.29
45	± 10	40	± 14	40	$\pm .08$	$\pm .12$	$\pm .15$
50	± 9	45	± 11	45	$\pm .08$	$\pm .11$	$\pm .14$
60	± 7	60	± 7	60	$\pm .08$	$\pm .09$	$\pm .11$

The table presents the largest possible errors, including inaccuracies in N, as well as errors in the determination of the angle. The poor accuracy is mainly due to the fact that the change of N with changing α is less for $\beta < 90^\circ$ than for $\beta = 90^\circ$. Here it is necessary to use $\beta < 90^\circ$ in order to find the shear correlation between the two cross-component fluctuations. A penalty is then paid in accuracy of measurement.

APPENDIX B

MOTION OF A PERTURBED ELEMENT IN A ROTATING FLUID

By Hsuan Yeh

Consider a main flow field consisting of a solid-body rotation, that is, $V_\theta = \omega r$. At a certain instant, say $t = 0$, imagine a fluid element at radius r_0 possessing a perturbation velocity in the form of an excess <u>tangential</u> velocity v_0 (hence the total velocity of this particle is $\omega r_0 + v_0$ at $t = 0$). The tangential and radial perturbing velocities (i.e., velocities relative to the mean rotation) at any subsequent time will be denoted by v_θ and v_r, respectively.

If it is assumed that the pressure fluctuation and viscosity exert no influence on the subsequent motion of the fluid element and that the angular momentum of the element is thereby conserved, the total tangential velocity of this particle at any subsequent radius r will be $(\omega r_0 + v_0) r_0 / r$. The centrifugal acceleration is therefore $(\omega r_0 + v_0)^2 r_0^2 / r^3$. However, the pressure gradient of the main flow is such that a centripetal force of $\omega^2 r$ is imposed at any radius r. Hence the net radial acceleration of the fluid particle at any radius r is

$$\frac{dv_r}{dt} = \frac{(\omega r_0 + v_0)^2 r_0^2}{r^3} - \omega^2 r \tag{B1}$$

It is also possible to derive the same equation based on the fact that the total radial acceleration is, in this case, the sum of the Coriolis acceleration and the centrifugal acceleration, both due to the <u>relative</u> (i.e., perturbed) tangential velocity v_θ. (The centrifugal acceleration due to the main flow V_θ is balanced by the pressure gradient.) Hence,

$$\frac{dv_r}{dt} = 2\omega v_\theta + \frac{v_\theta^2}{r}$$

But

$$v_\theta = \frac{(\omega r_0 + v_0) r_0}{r} - \omega r \tag{B2}$$

This again leads to equation (B1).

Using the familiar substitution

$$\frac{dv_r}{dt} = \frac{d}{dr}\left(\frac{v_r^2}{2}\right)$$

equation (B1) can be integrated to become

$$v_r^2 = -\frac{(\omega r_0 + v_0)^2 r_0^2}{r^2} - \omega^2 r^2 + C$$

The integration constant C can be evaluated by the condition that $v_r = 0$ at $t = 0$ and $r = r_0$. After a slight rearrangement, the result is

$$\left(\frac{v_r}{\omega r_0}\right)^2 = \left(1 + \frac{v_0}{\omega r_0}\right)^2\left(1 - \frac{r_0^2}{r^2}\right) + \left(1 - \frac{r^2}{r_0^2}\right) \tag{B3}$$

Substituting dr/dt for v_r, further integration yields the following relation between r and t:

$$\frac{r}{r_0} = \sqrt{1 + \frac{g(2 + g)}{2}(1 - \cos 2\omega t)} \tag{B4}$$

where $g \equiv \dfrac{v_0}{\omega r_0}$ is a dimensionless ratio representing the strength of initial disturbance. From this the radial as well as the perturbation tangential velocities can be obtained as functions of time as follows:

$$\frac{v_r}{\omega r_0} = \frac{\dfrac{g(2 + g)}{2}\sin 2\omega t}{\sqrt{1 + \dfrac{g(2 + g)}{2}(1 - \cos 2\omega t)}} \tag{B5}$$

$$\frac{v_\theta}{\omega r_0} = \frac{g - \dfrac{g(2 + g)}{2}(1 - \cos 2\omega t)}{\sqrt{1 + \dfrac{g(2 + g)}{2}(1 - \cos 2\omega t)}} \tag{B6}$$

These functions are plotted in figure 42 for $g = 0.01$, 0.05, and 0.10. It is noted that their values do not follow a simple proportion to the initial disturbance g.

From this simple analysis the following remarks can be made:

(1) Although the analysis was made for a purely tangential perturbation at $t = 0$, the relative velocity subsequently goes through all possible combinations of $\frac{v_r}{v_\theta}$. Hence the same analysis covers all possible kinds of initial perturbations, the only difference being a shift of the origin $t = 0$.

(2) No matter what the initial disturbance is, the subsequent (relative) motion of a fluid particle is oscillatory, with a circular frequency of 2ω. The maximum radial distance of travel through a complete oscillation is gr_0.

(3) The maximum value of v_r occurs at $\frac{r}{r_0} = \sqrt{1 + g}$, at which point v_θ is zero. Furthermore, $(v_r)_{max} = (v_\theta)_{max}$.

(4) The time-averaged value of the product $v_r v_\theta$ is zero.

REFERENCES

1. Laufer, John: Investigation of Turbulent Flow in a Two-Dimensional Channel. NACA Rep. 1053, 1951. (Supersedes NACA TN 2123.)

2. Laufer, J.: The Structure of Turbulence in Fully Developed Pipe Flow. NACA Rep. 1174, 1954. (Supersedes NACA TN 2954.)

3. Townsend, A. A.: Measurements in the Turbulent Wake of a Cylinder. Proc. Roy. Soc. (London), ser. A, vol. 190, no. 1023, Sept. 9, 1947, pp. 551-561.

4. Schubauer, G. B., and Klebanoff, P. S.: Investigation of Separation of the Turbulent Boundary Layer. NACA Rep. 1030, 1951. (Supersedes NACA TN 2133.)

5. Townsend, A. A.: The Structure of the Turbulent Boundary Layer. Proc. Cambridge Phil. Soc., vol. 47, pt. 2, Apr. 1951, pp. 375-395.

6. Klebanoff, P. S.: Characteristics of Turbulence in a Boundary Layer With Zero Pressure Gradient. NACA Rep. 1247, 1955. (Supersedes NACA TN 3178.)

7. Corrsin, Stanley, and Uberoi, Mahinder S.: Spectra and Diffusion in a Round Turbulent Jet. NACA Rep. 1040, 1951. (Supersedes NACA TN 2124.)

8. Townsend, A. A.: The Uniform Distortion of Homogeneous Turbulence. Quarterly Jour. Mech. and Appl. Math., vol. VII, pt. I, Mar. 1954, pp. 104-127.

9. Squire, H. B.: Rotating Fluids. Surveys in Mechanics, G. K. Batchelor and R. M. Davies, eds., Cambridge Univ. Press, 1956, pp. 139-161.

10. Taylor, G. I.: Experiments With Rotating Fluids. Proc. Roy. Soc. (London), ser. A, vol. 100, 1921, p. 114.

11. Long, Robert R.: A Diffusion Phenomenon in Rotating and Stratified Fluids. Tech. Rep. No. 2, (Contract N-onr-248(31)), The Johns Hopkins Univ., Dept. Civ. Eng., Dec. 1953.

12. Morgan, G. W.: A Study of Motions in a Rotating Liquid. Proc. Roy. Soc. (London), ser. A, vol. 206, no. 1084, Mar. 22, 1951, pp. 108-130.

13. Stewartson, K.: A Weak Spherical Source in a Rotating Fluid. Quarterly Jour. Mech. and Appl. Math., vol. VI, pt. 1, Mar. 1953, pp. 45-49.

14. Eskinazi, Salamon, and Yeh, Hsuan: An Investigation on Fully Developed Turbulent Flows in a Curved Channel. Jour. Aero. Sci., vol. 23, no. 1, Jan. 1956, pp. 23-34.

15. Schubauer, G. B., Spangenberg, W. G., and Klebanoff, P. S.: Aerodynamic Characteristics of Damping Screens. NACA TN 2001, 1950.

16. Eskinazi, Salamon: An Investigation of Fully Developed Turbulent Flow in a Curved Channel. Tech. Rep. No. I-20, (Contract Nonr 248 (33)), The Johns Hopkins Univ., Inst. for Cooperative Res., Dept. Mech. Eng., Aug. 12, 1954.

17. Taylor, G. I.: Distribution of Velocity and Temperature Between Concentric Rotating Cylinders. Proc. Roy. Soc. (London), ser. A, vol. 151, no. 874, Oct. 1, 1935, pp. 491-512.

18. Wislicenus, George F., and Yeh, Hsuan: A Program of Research in the Field of Turbulent Flow in Ducts, in a Space of Revolution, and in Turbomachinery. Tech. Rep. no. I-8, (Contract Nonr 248 (33)), The Johns Hopkins Univ., Inst. for Cooperative Res., Dept. Mech. Eng., Dec. 1952.

19. Batchelor, G. K.: The Theory of Axisymmetric Turbulence. Proc. Roy. Soc. (London), ser. A., vol. 186, 1946.

20. Rotta, J.: Statistische Theorie nichthomogener Turbulenz. Mitt. 1. Zeitschr. f. Phys., Bd. 129, 1951, pp. 547-574.

21. Rotta, J.: Statistische Theorie nichthomogener Turbulenz. Mitt. 2. Zeitschr. f. Phys., Bd. 131, 1951, pp. 51-77.

22. Corrsin, Stanley: Interpretation of the Viscous Terms in the Turbulent Energy Equation. Jour. Aero. Sci. (Readers' Forum), vol. 20, no. 12, Dec. 1953, pp. 853-854.

23. Batchelor, G. K.: The Theory of Homogeneous Turbulence. Cambridge Univ. Press, 1953, p. 103.

24. Lamb, Horace: Hydrodynamics. Reprint of sixth ed. (first Am. ed.), Dover Publications, 1945, p. 586.

25. Traugott, Stephen C.: The Influence of Solid Body Rotation in Turbulent Flow Between Concentric Cylinders. Ph. D. Thesis, The Johns Hopkins Univ., 1956.

26. Corrsin, Stanley: Decay of Turbulence Behind Three Similar Grids.
    A. E. Thesis, C. I. T., 1942.

27. Rayleigh, J. W. S.: On the Dynamics of Revolving Fluids. Proc.
    Roy. Soc. (London), ser. A, vol. 93, 1917, pp. 148-1954.

28. Kovasznay, Laszlo: Calibration and Measurement in Turbulence
    Research by the Hot-Wire Method. NACA TM 1130, 1947.
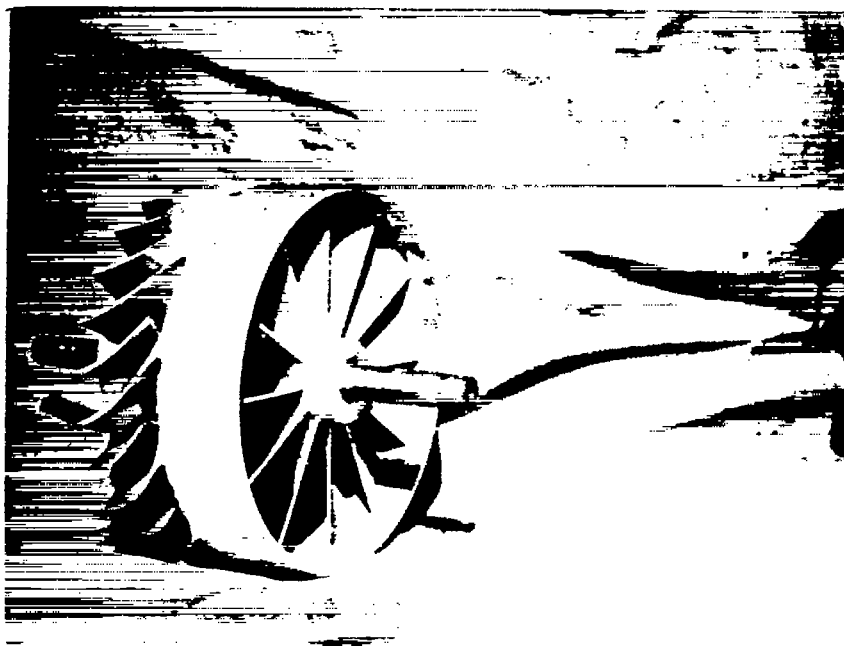
L-57-4342

Figure 1.- View of impeller.

ⓐ BLOWER	ⓔ OUTER WALL
ⓑ BLEED	ⓕ INNER WALL
ⓒ SETTLING CHAMBER	ⓖ STATIONARY SECTION OF OUTER WALL
ⓓ IMPELLER	ⓗ DRIVING MOTOR
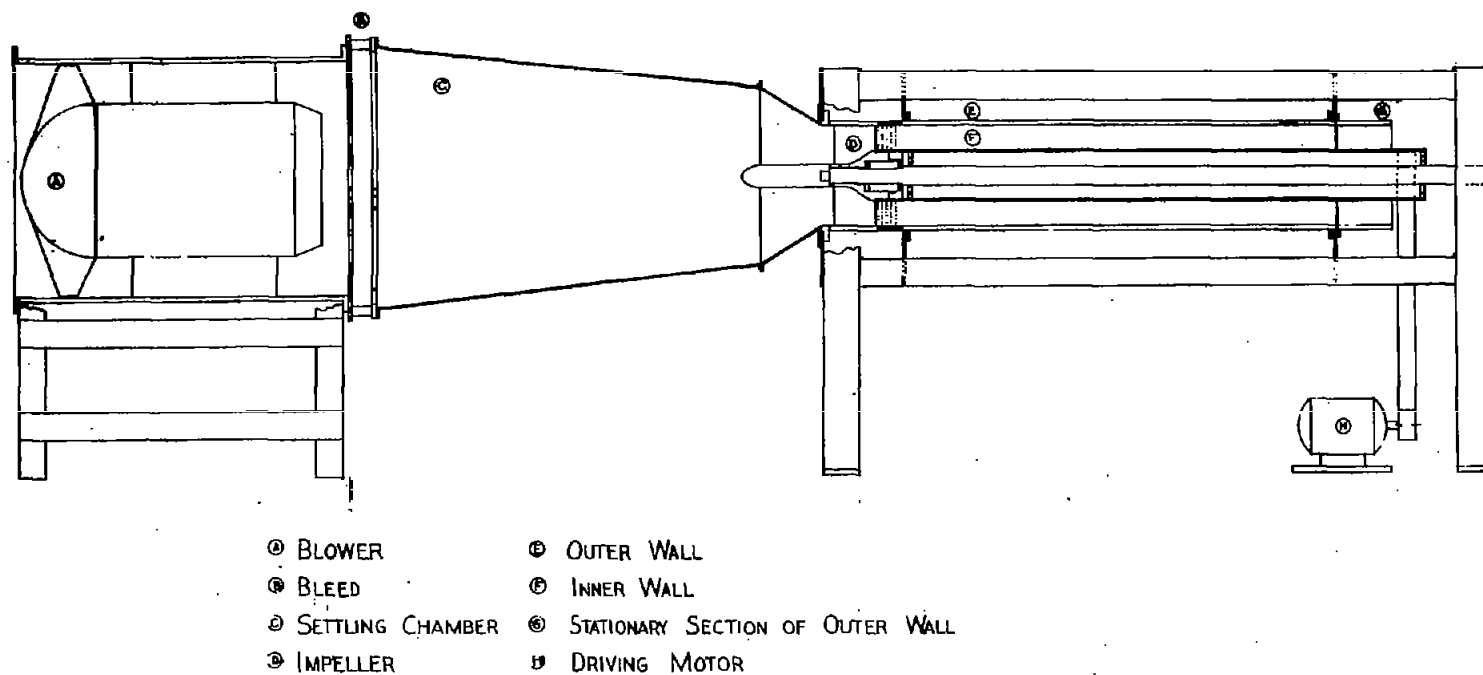
Figure 2.- Assembly drawing of wind tunnel.

Rotating

Stationary
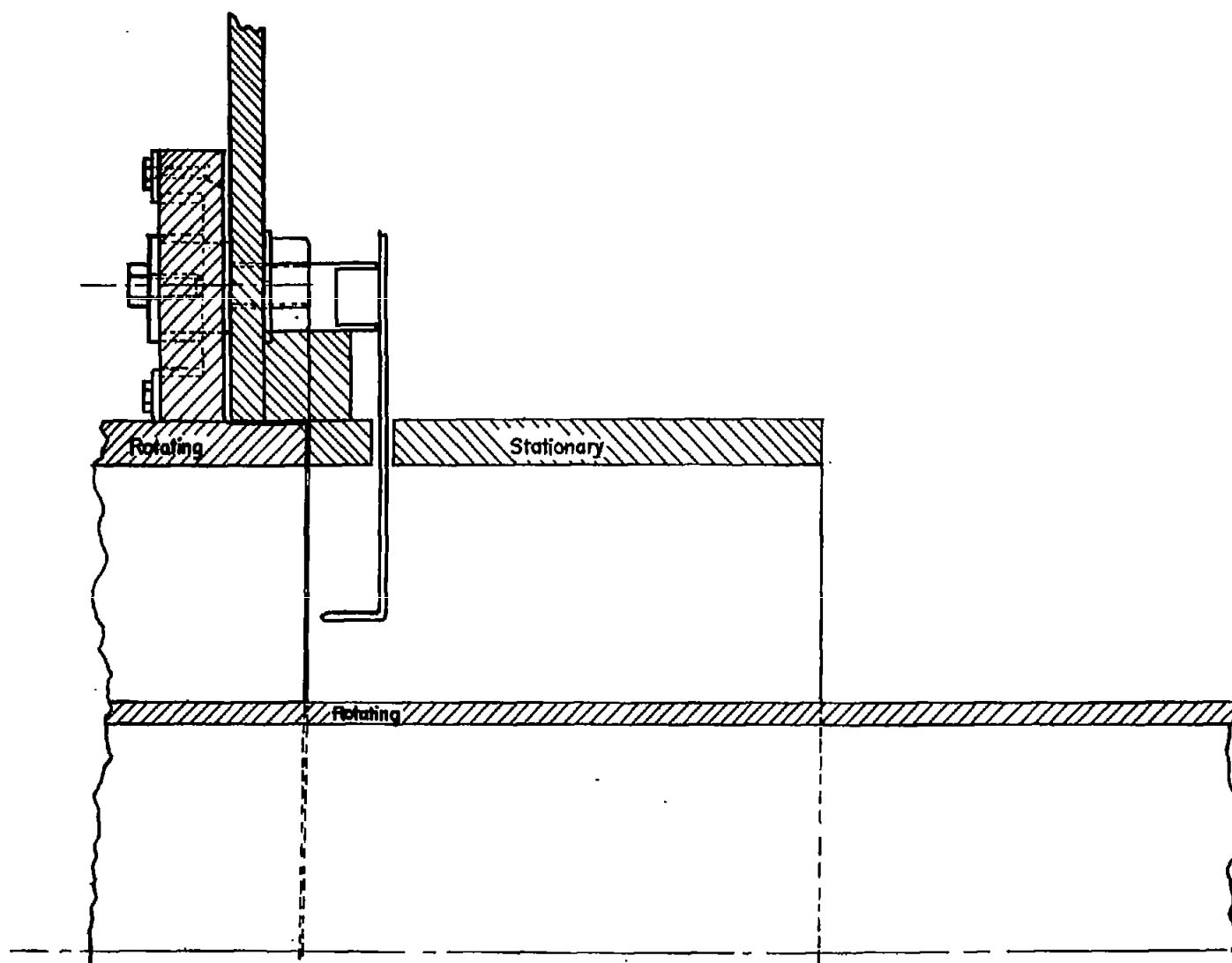
Rotating

Figure 3.- Detail of traversing section.
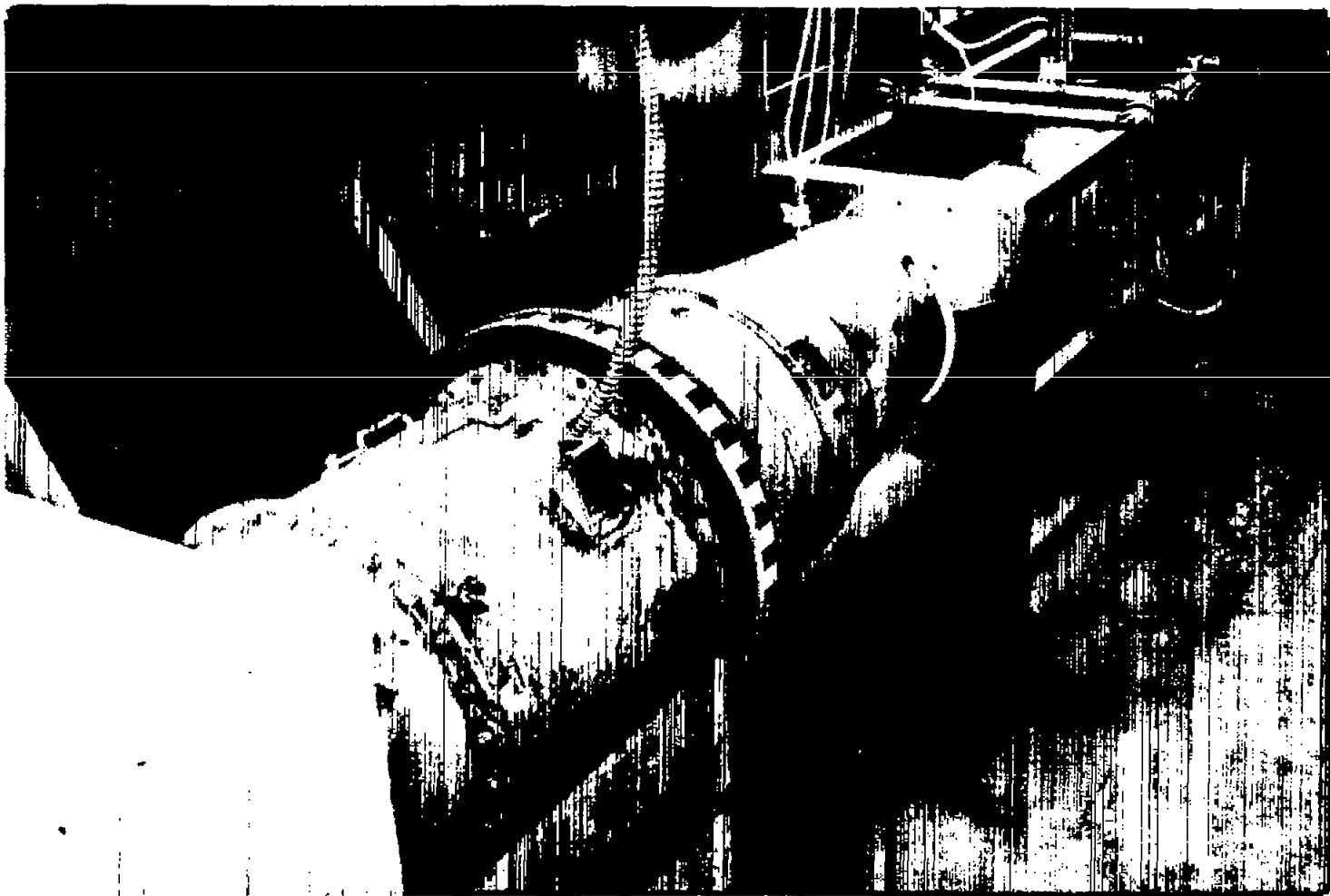
L-57-4343

Figure 4.- View of tunnel, looking downstream.
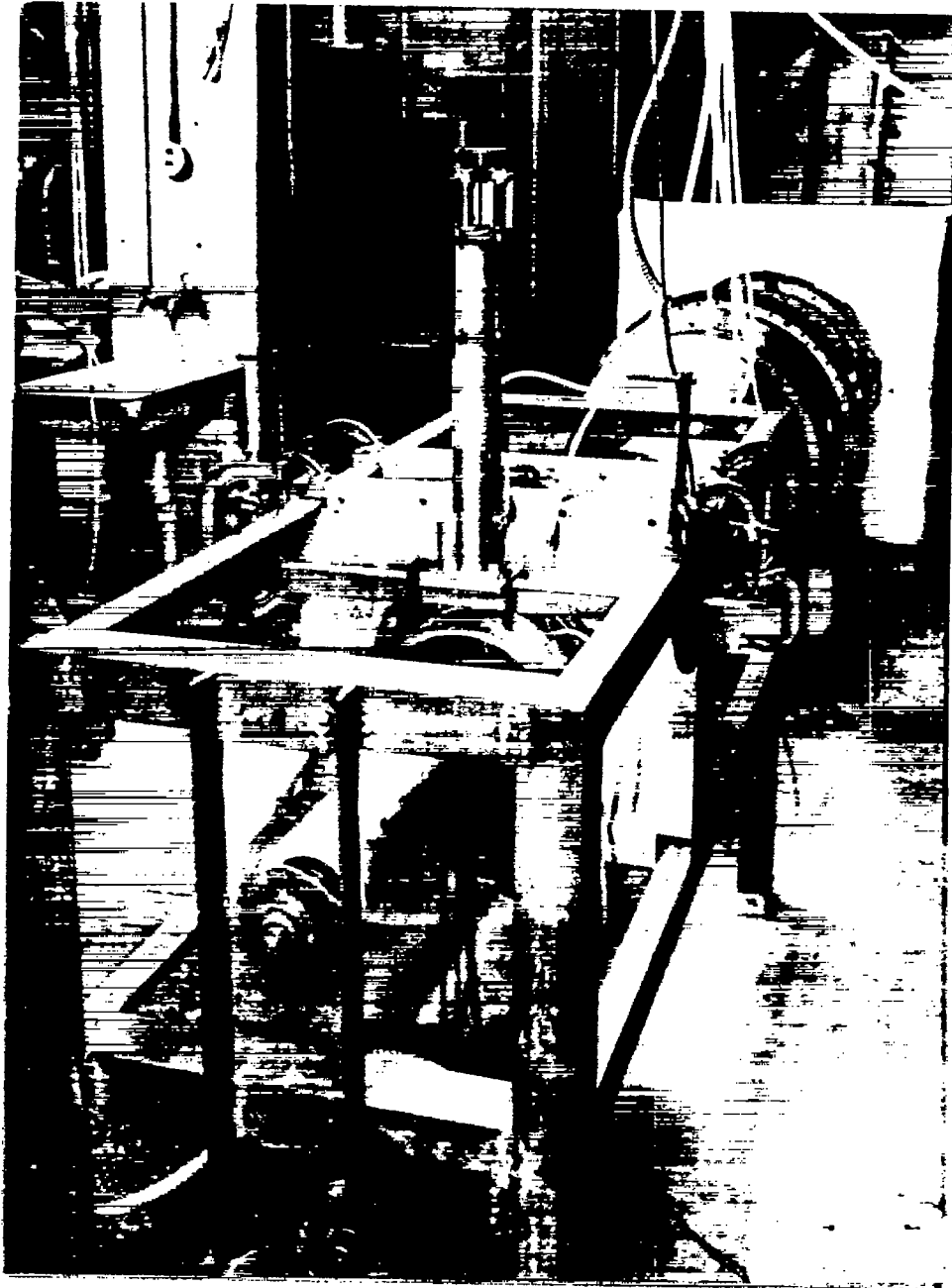
L-57-4344

Figure 5.- View of tunnel, looking upstream.
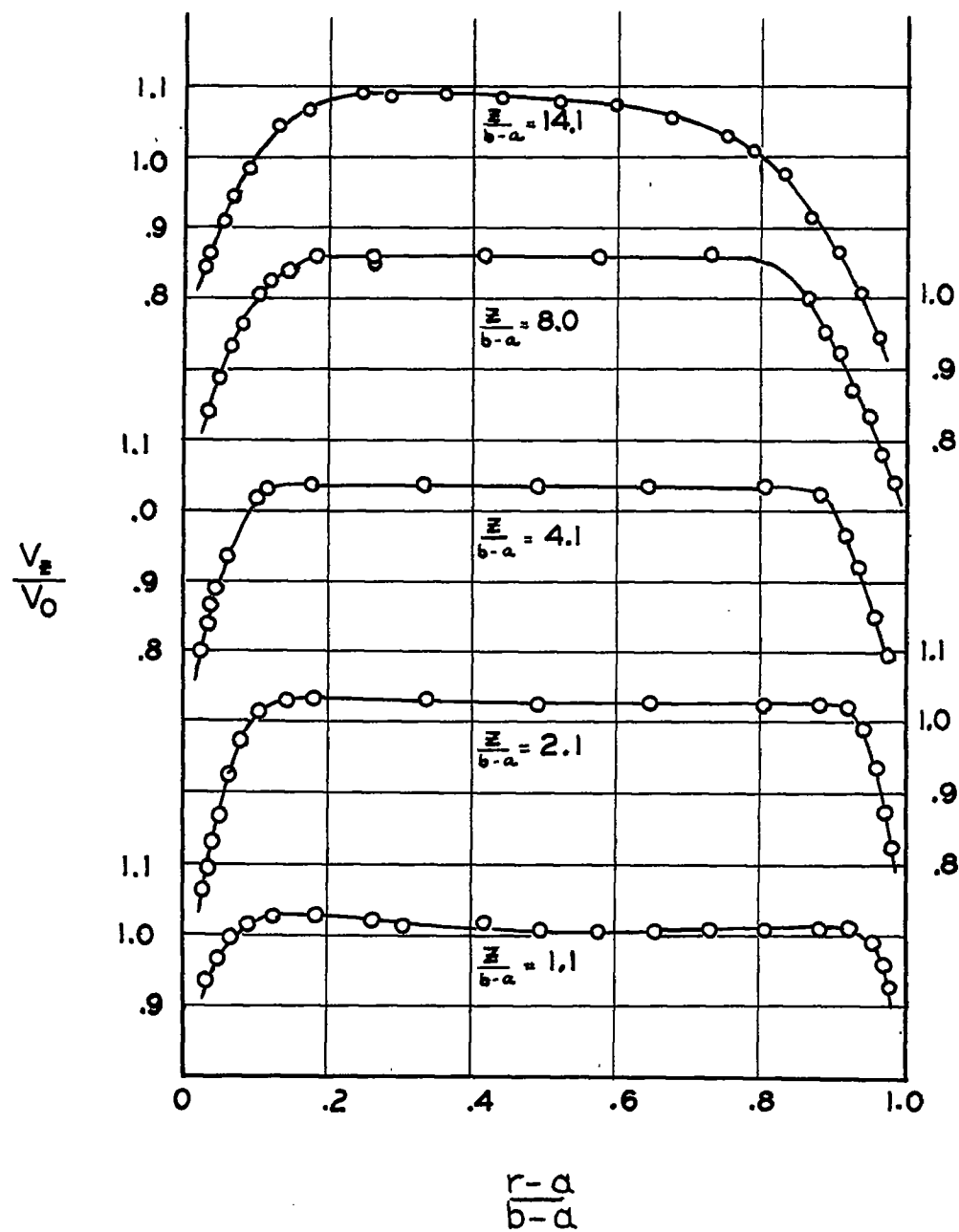
Figure 6.- Axial velocities without rotation.

$$\frac{r-a}{b-a}$$
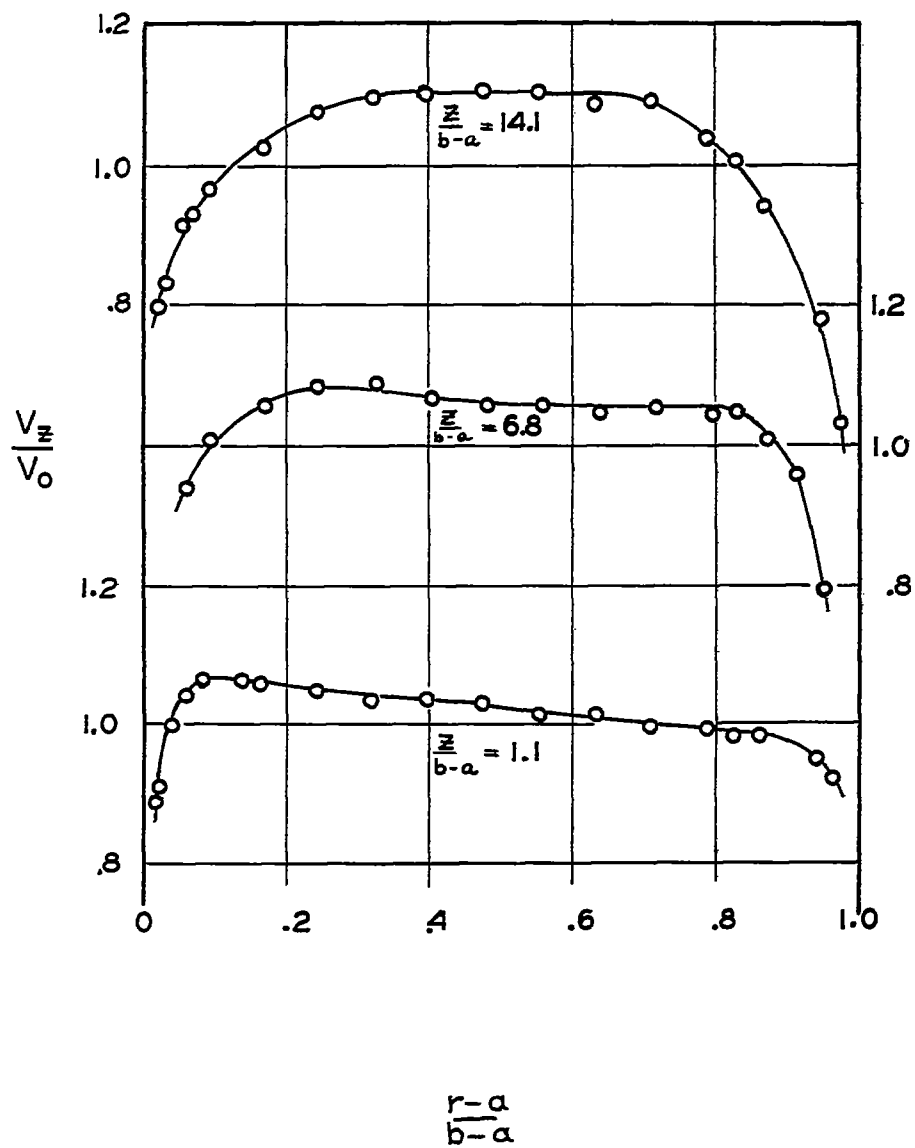
Figure 7.- Axial velocities with rotation.
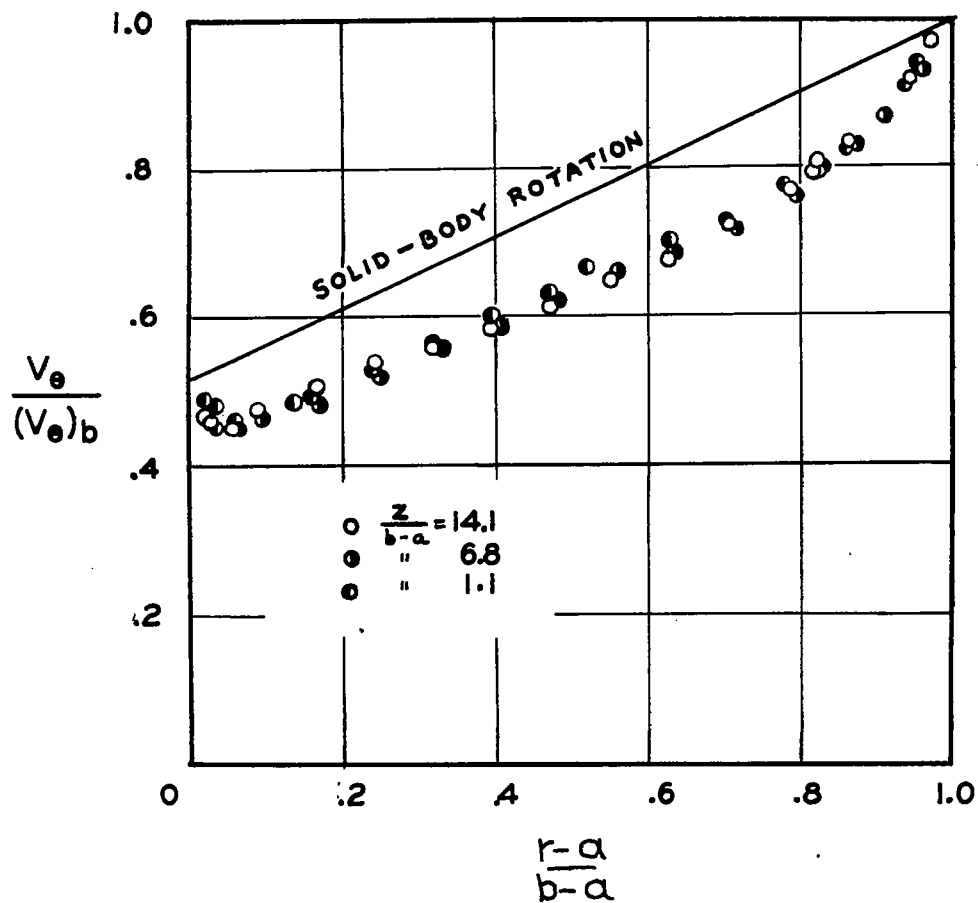
Figure 8.- Peripheral velocities.
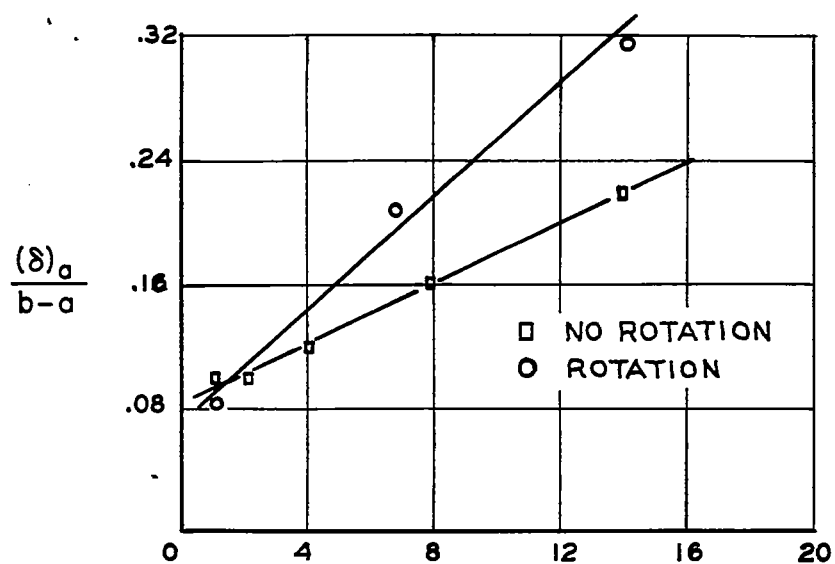
(a) Inside.
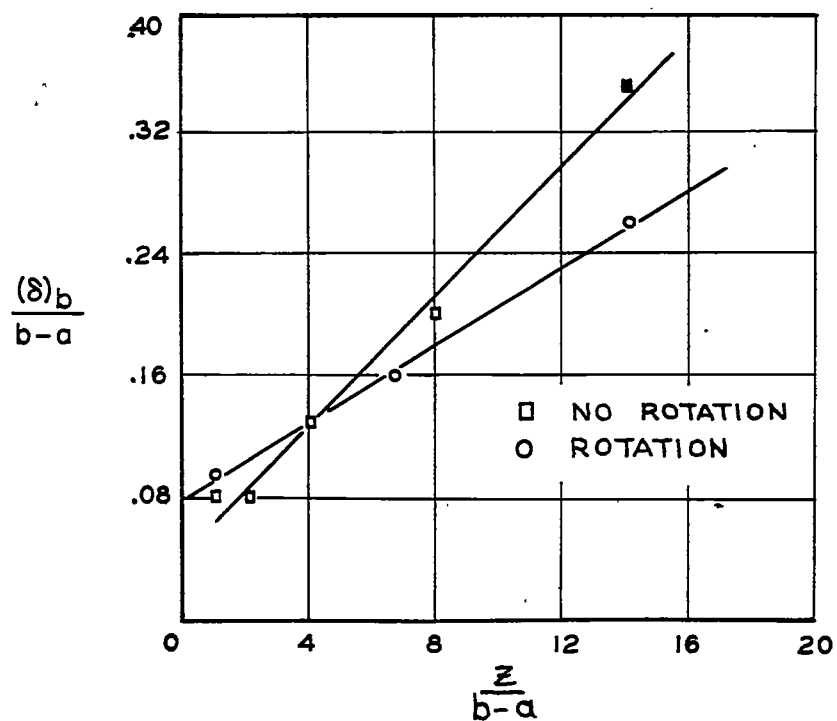
(b) Outside.

Figure 9.- Boundary-layer thicknesses.
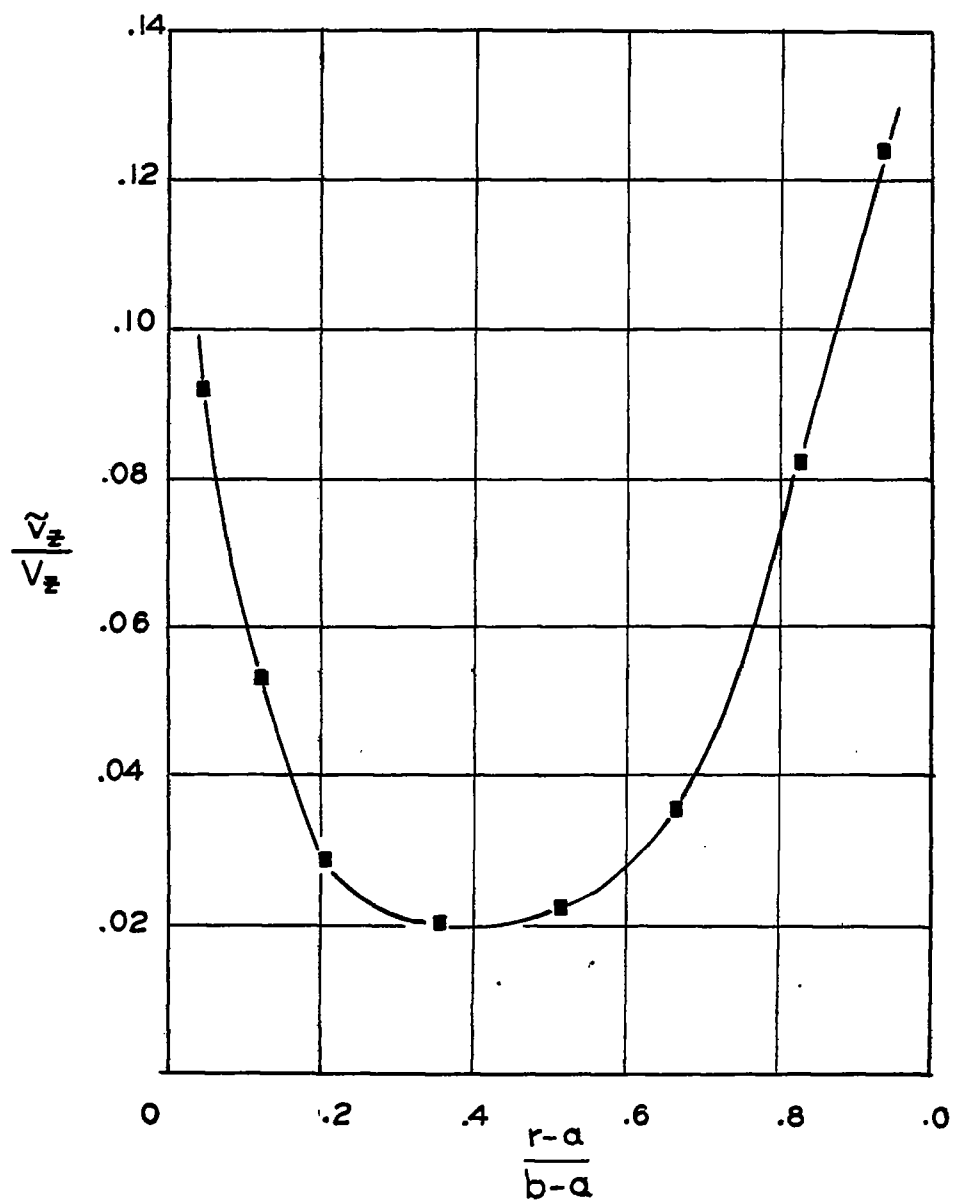
Figure 10.- Turbulence level far downstream, no rotation. $\dfrac{z}{b-a} = 14.1$.
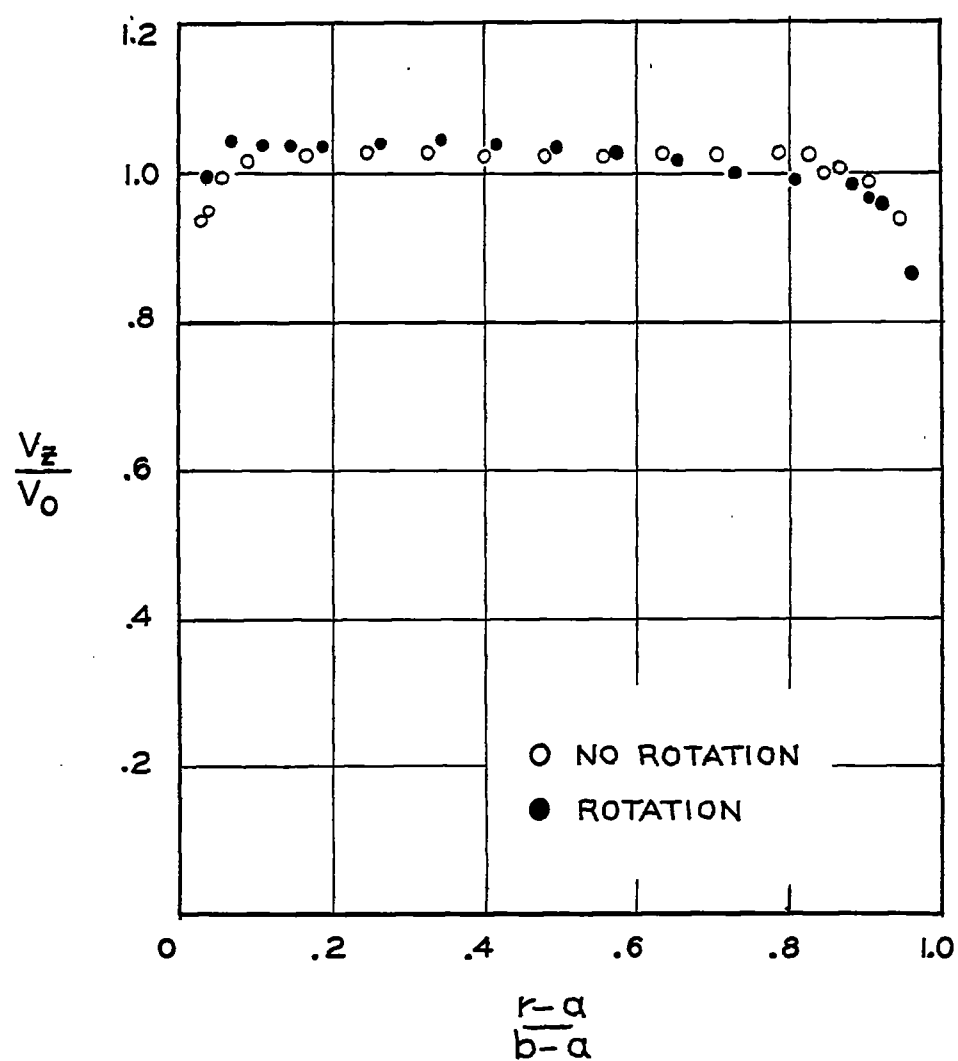
Figure 11.- Axial velocities with and without rotation. $\frac{\xi}{M} = 17.5$; $\frac{z}{b - a} = 7.1$.
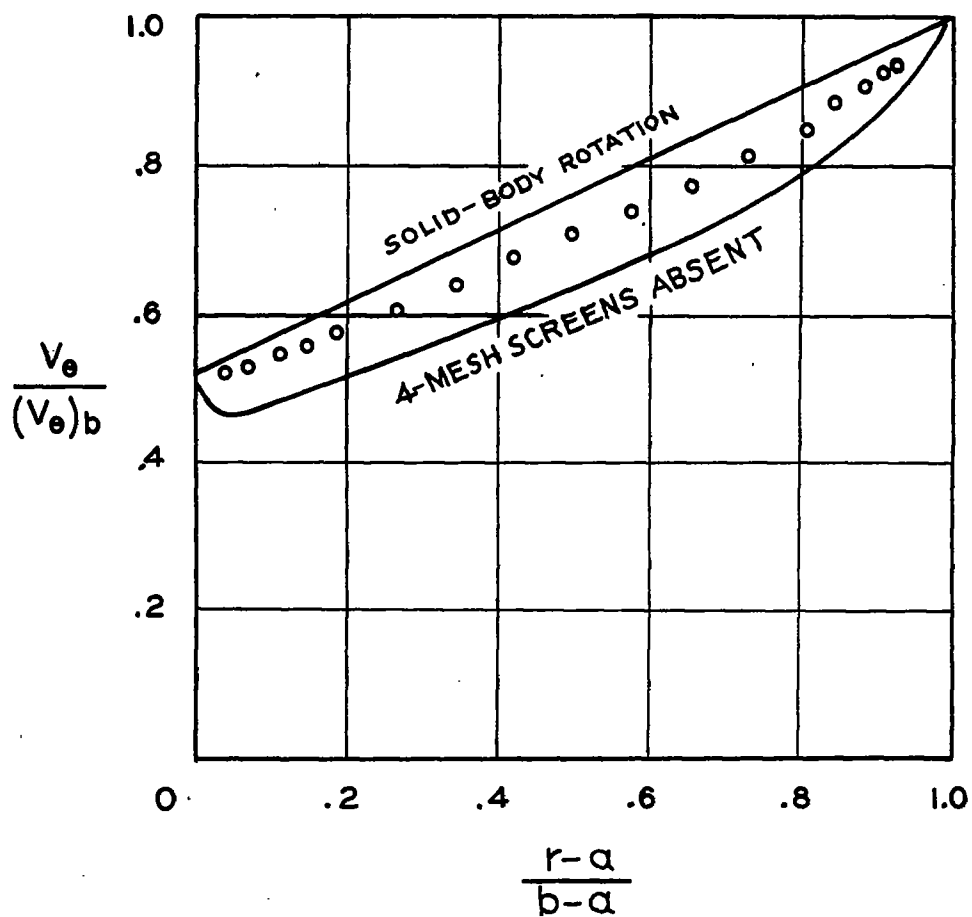
Figure 12.- Peripheral velocity with 4-mesh screens. $\frac{\xi}{M} = 17.5$; $\frac{z}{b-a} = 7.1$.
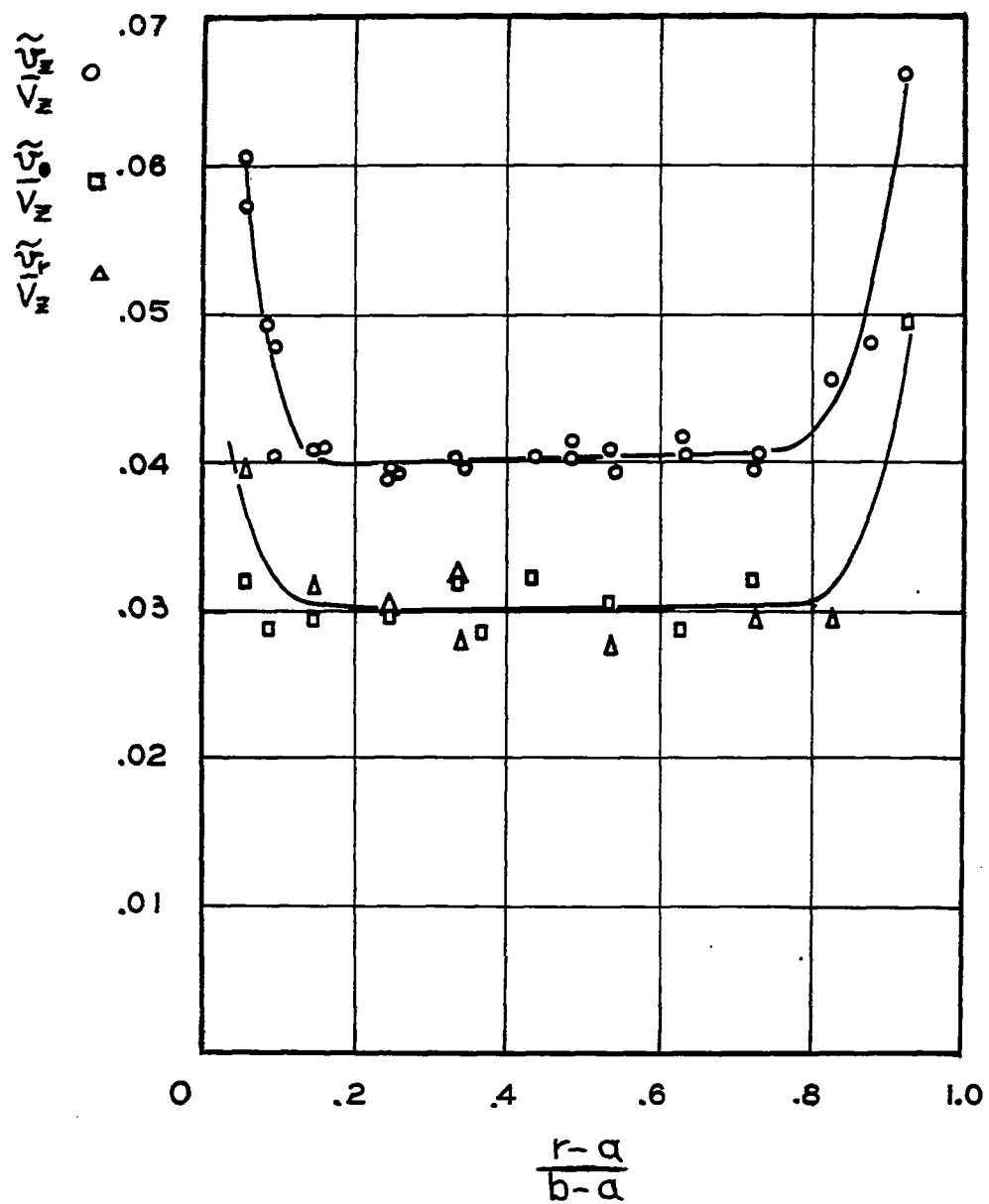
Figure 13.- Turbulence intensities without rotation. $\frac{\xi}{M} = 17.5$.
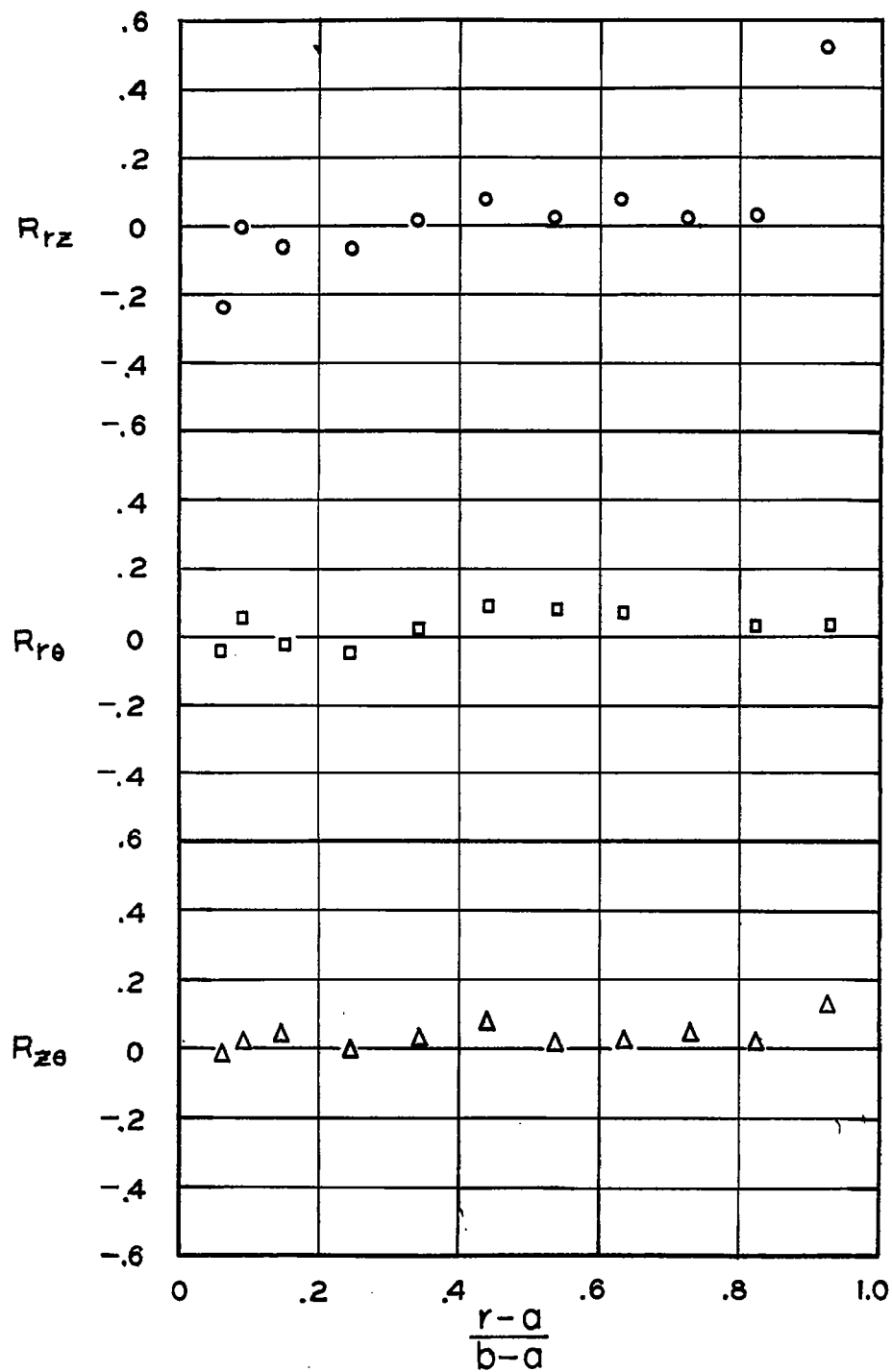
Figure 14.- Shear correlation coefficients without rotation. $\frac{\xi}{M} = 17.5$.
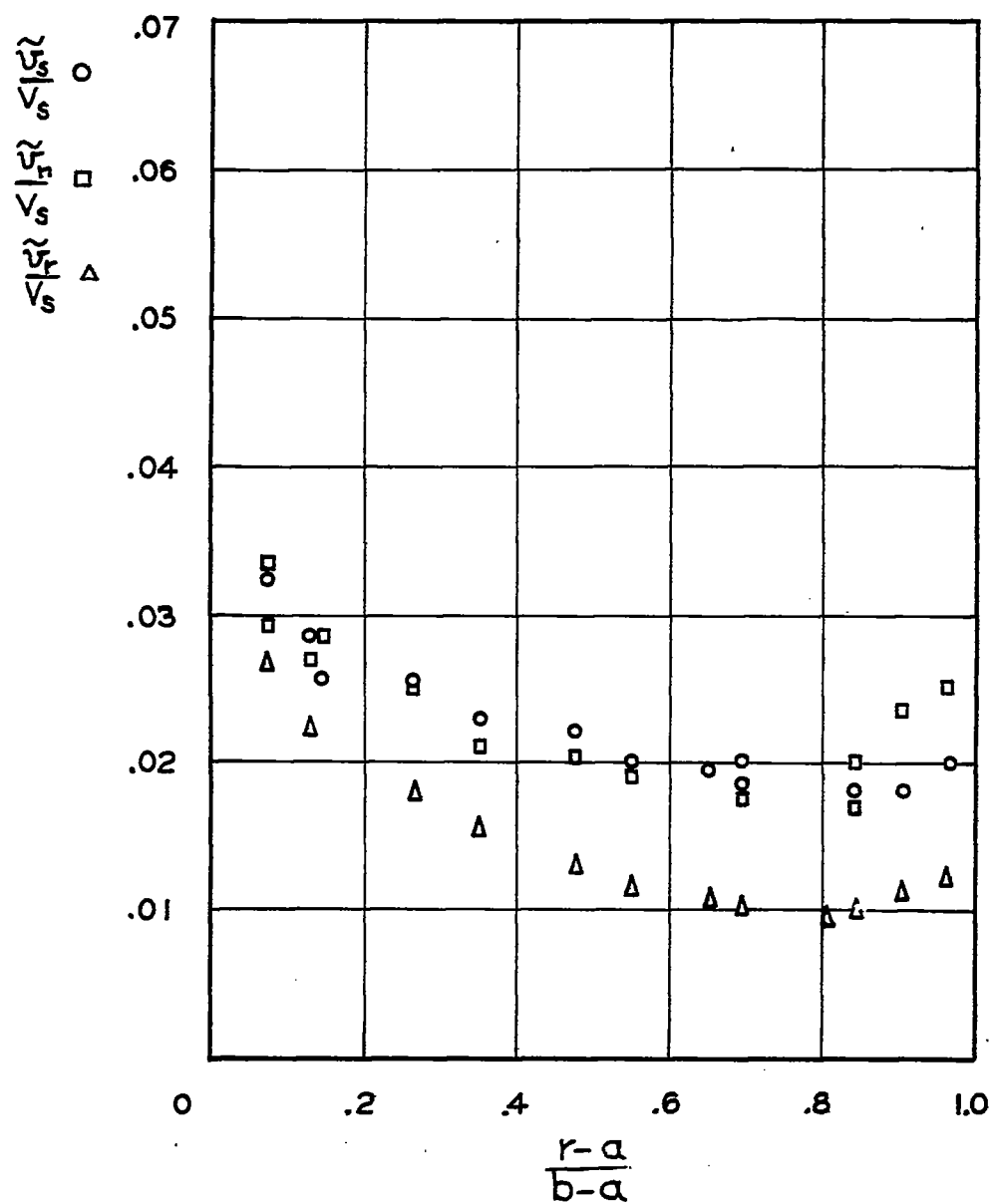
Figure 15.- Turbulence intensities with rotation. $\frac{\xi}{M} = 17.5$.
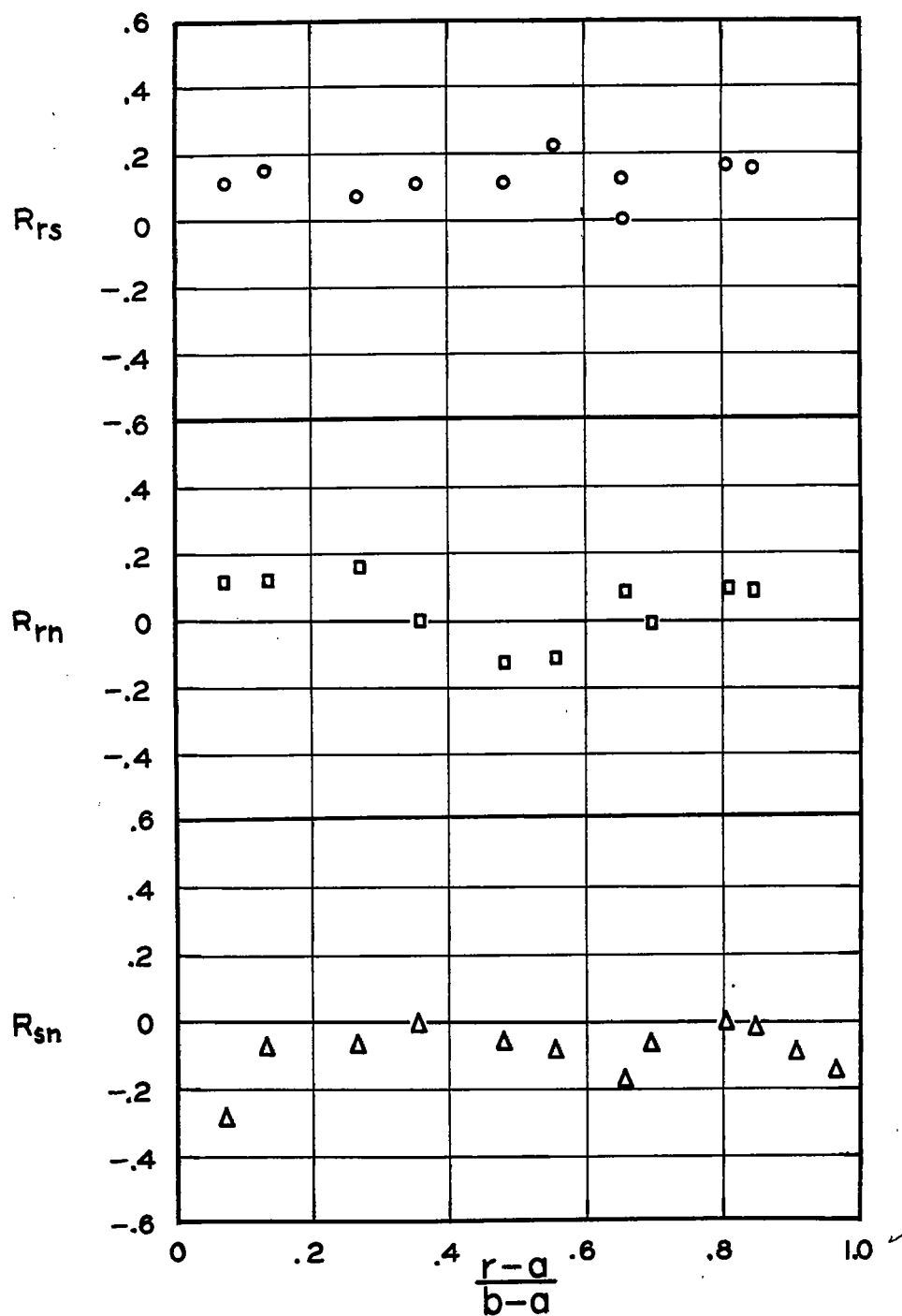
Figure 16.- Shear correlation coefficients with rotation. $\frac{\xi}{M} = 17.5$.
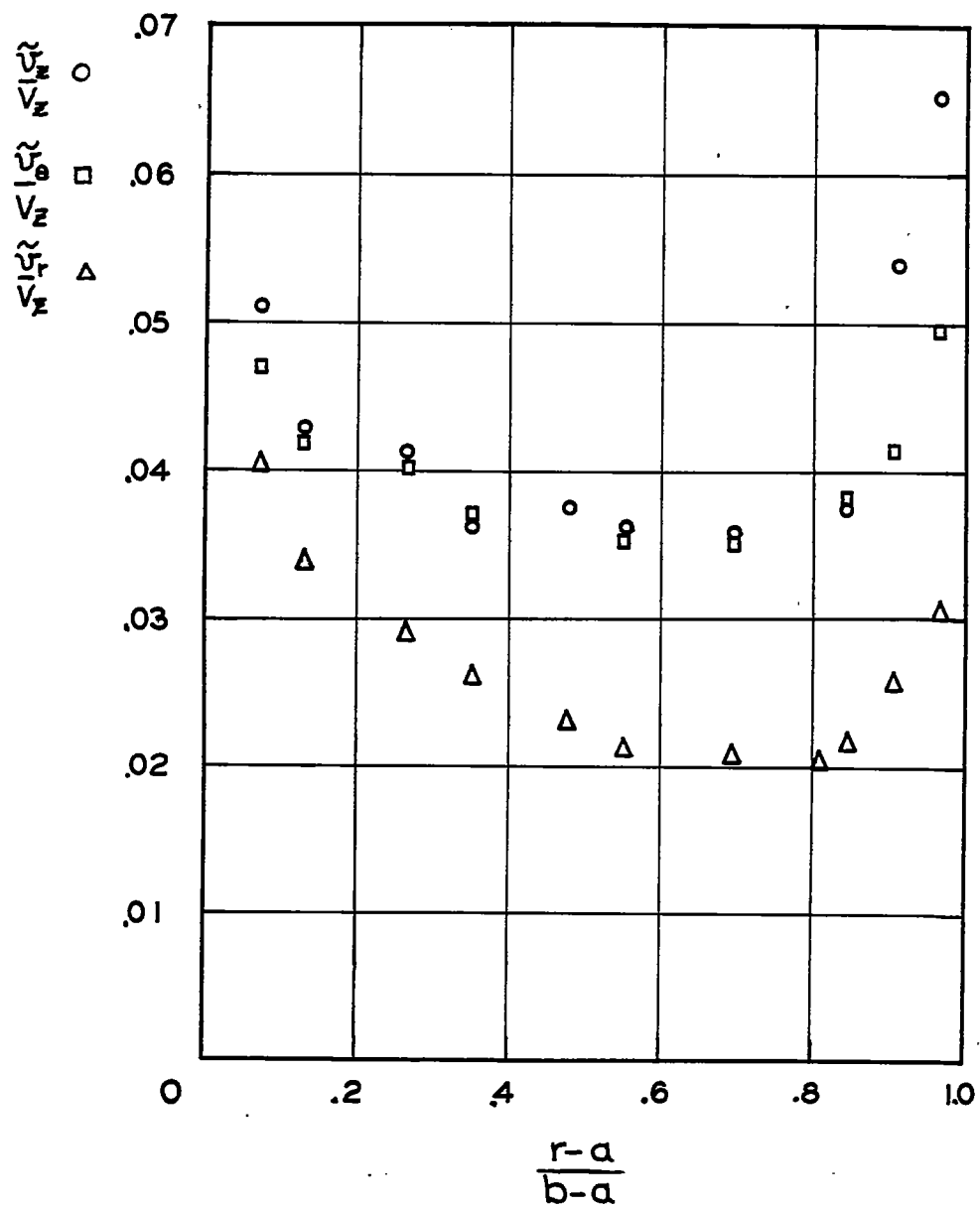
Figure 17.- Turbulence intensities with rotation. $\frac{\xi}{M} = 17.5$.
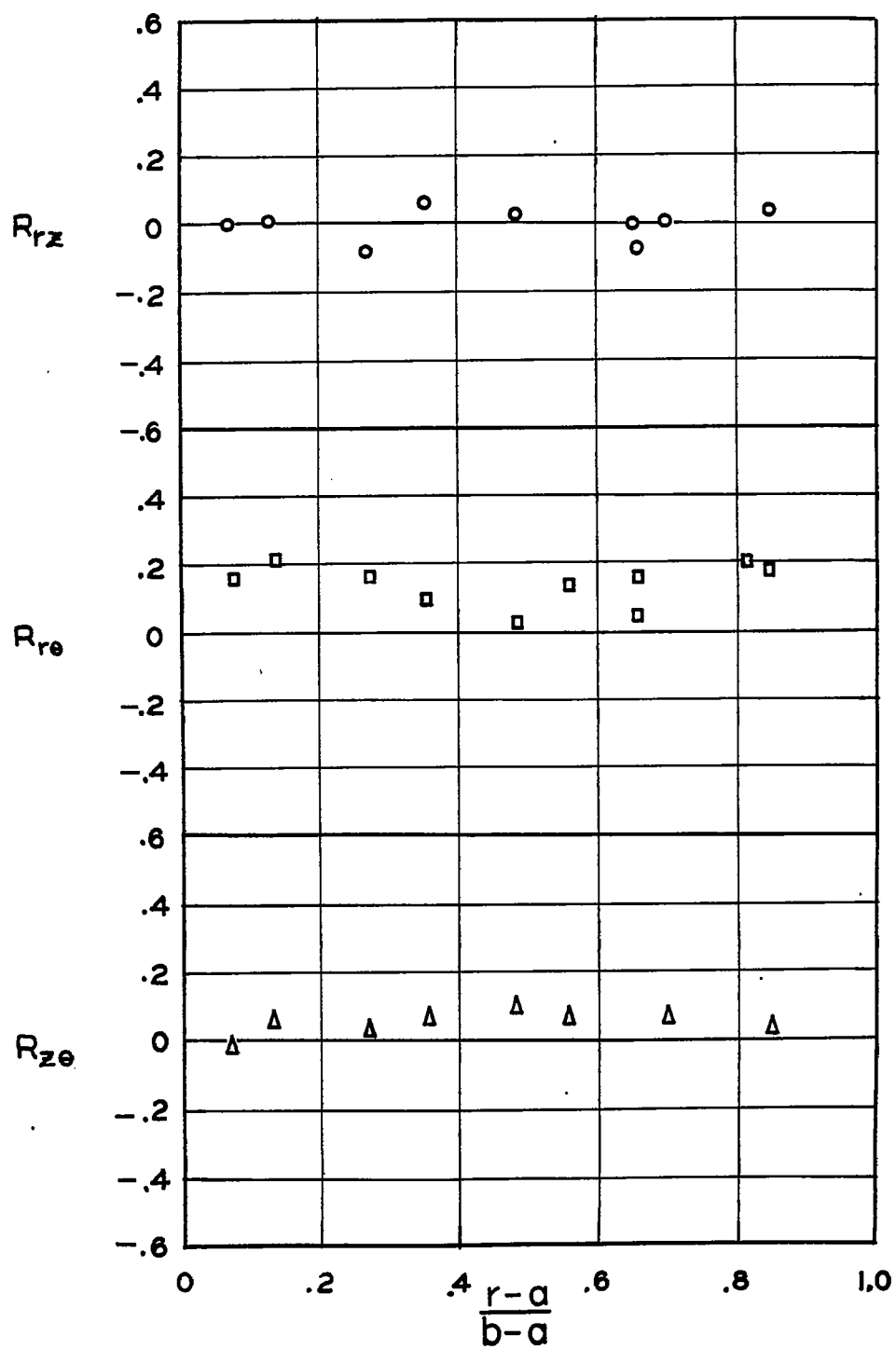
Figure 18.- Shear correlation coefficients with rotation. $\frac{\xi}{M} = 17.5$.
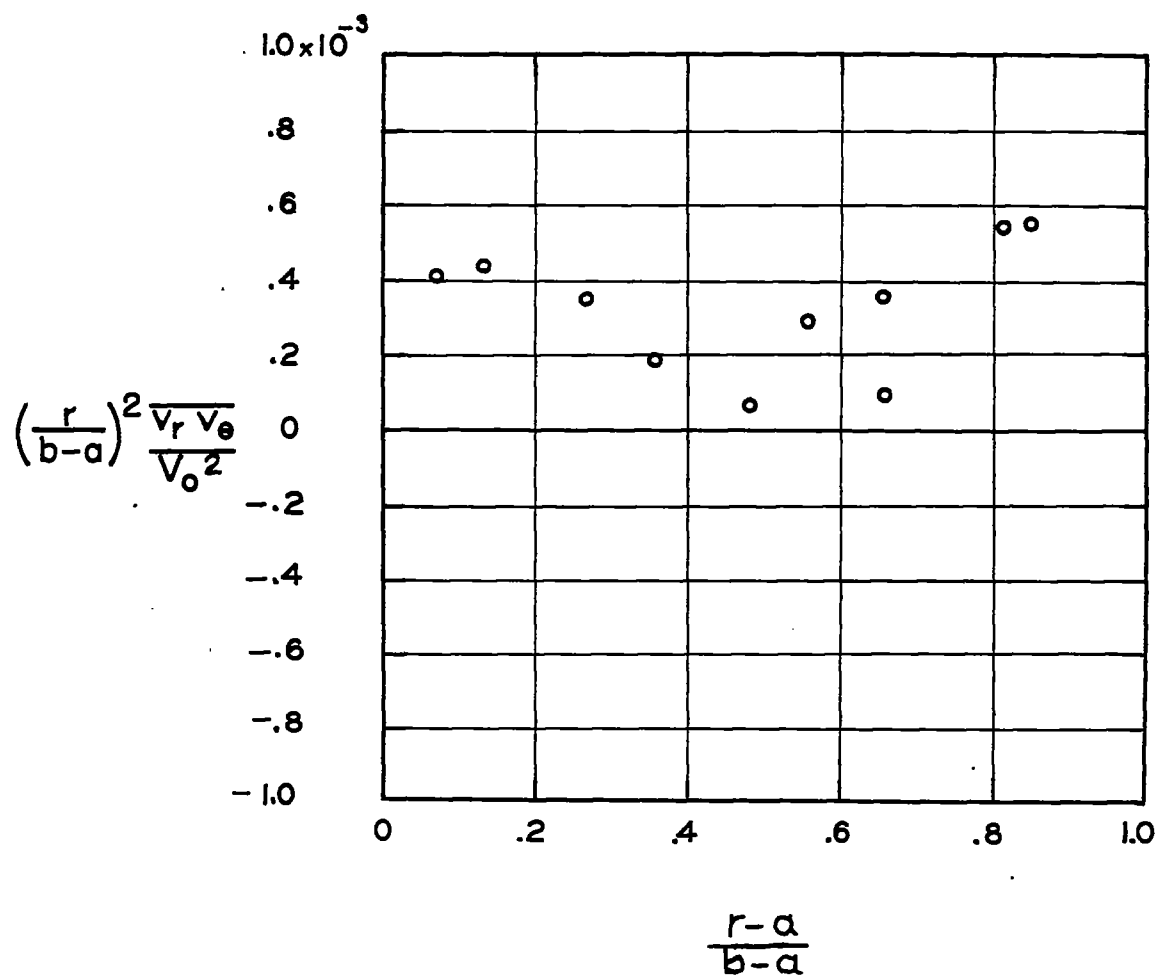
Figure 19.- Shear stress distribution with rotation. $\frac{\xi}{M} = 17.5$.
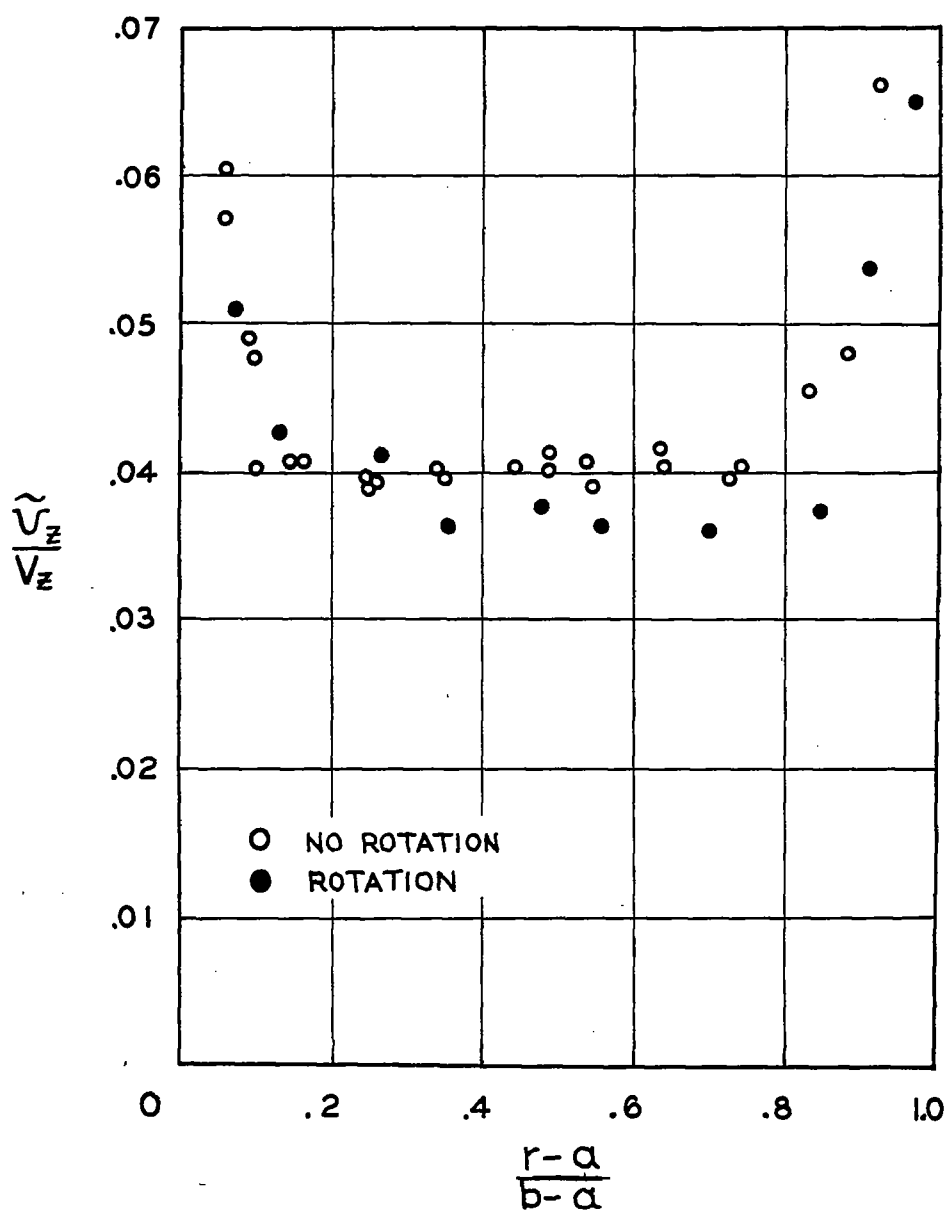
Figure 20.- Effect of rotation on $\dfrac{\tilde{v}_z}{V_z}$. $\dfrac{\xi}{M} = 17.5$.
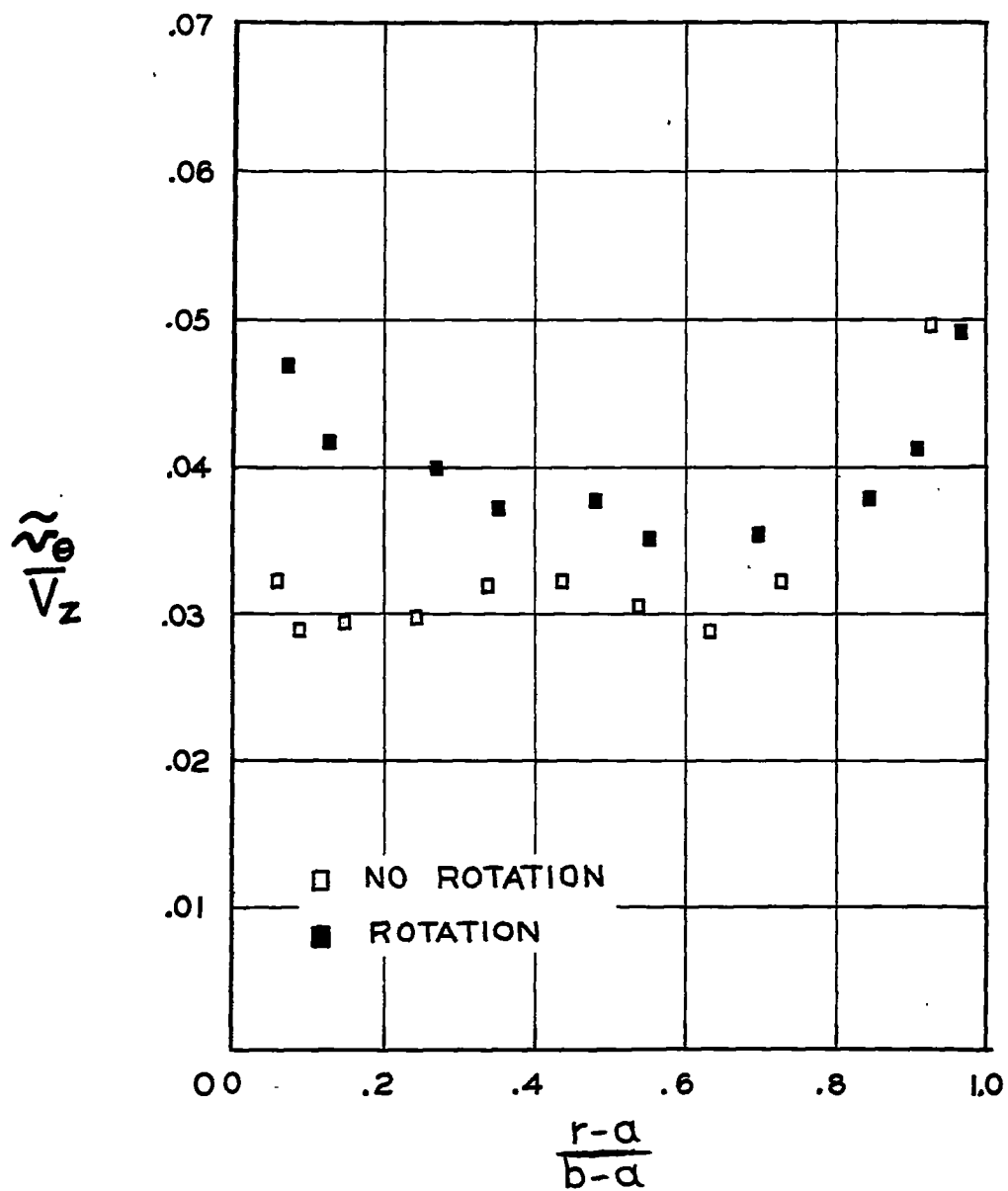
Figure 21.- Effect of rotation on $\dfrac{\tilde{v}_\theta}{V_z}$. $\dfrac{\xi}{M} = 17.5$.
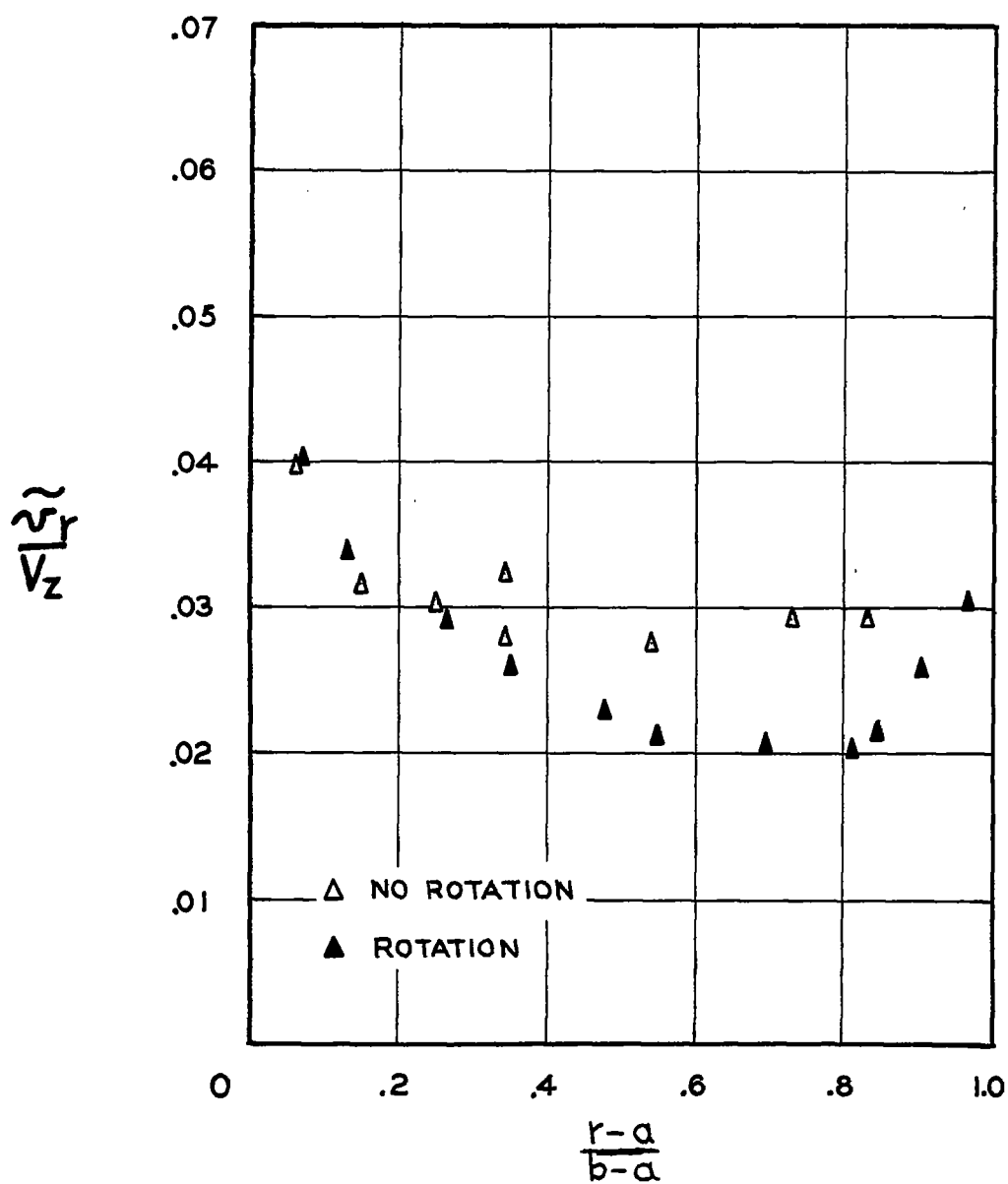
Figure 22.- Effect of rotation on $\dfrac{\tilde{v}_r}{V_z}$. $\dfrac{\xi}{M} = 17.5$.
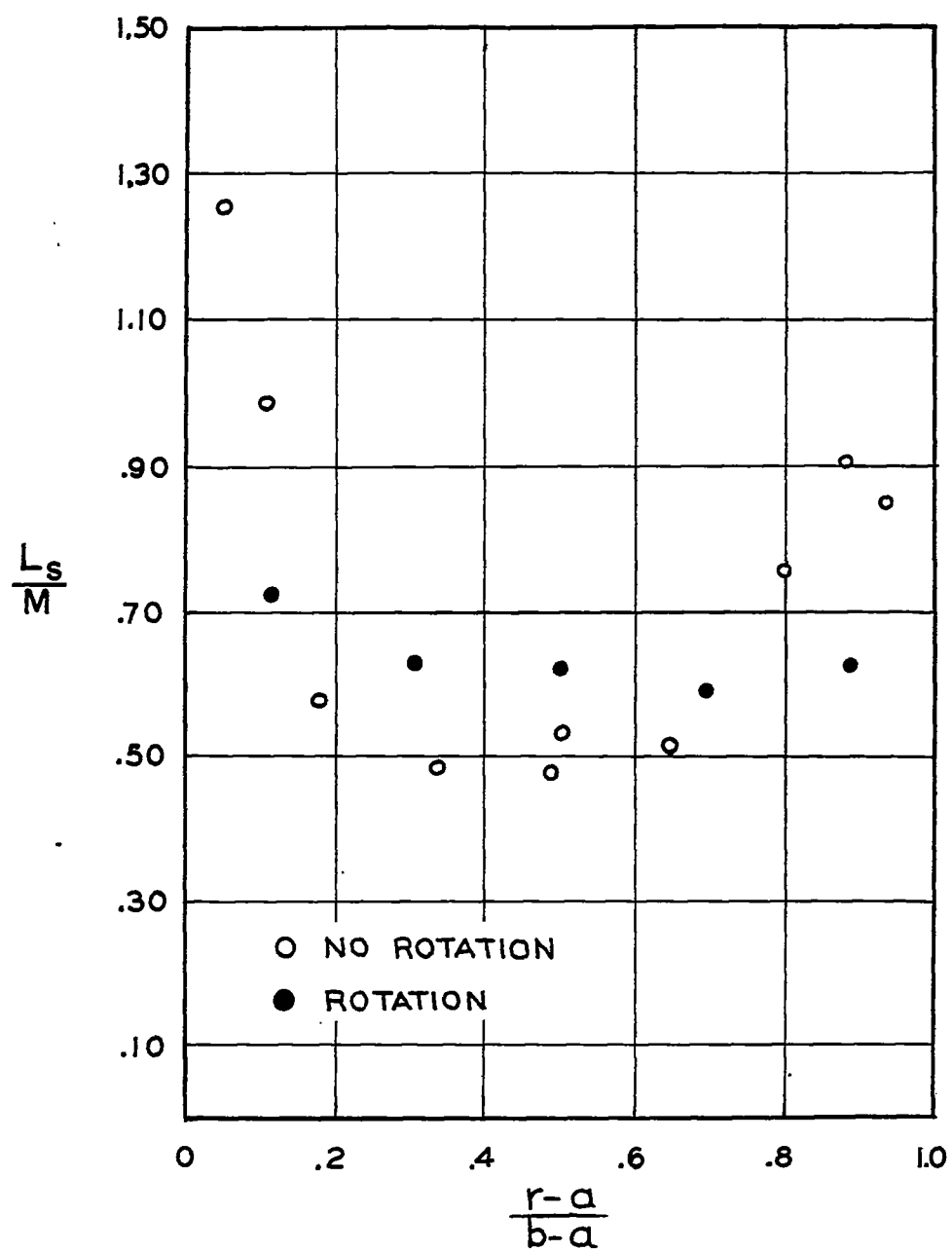
Figure 23.- Integral scale in mean flow direction. $\frac{\xi}{M} = 17.5$.
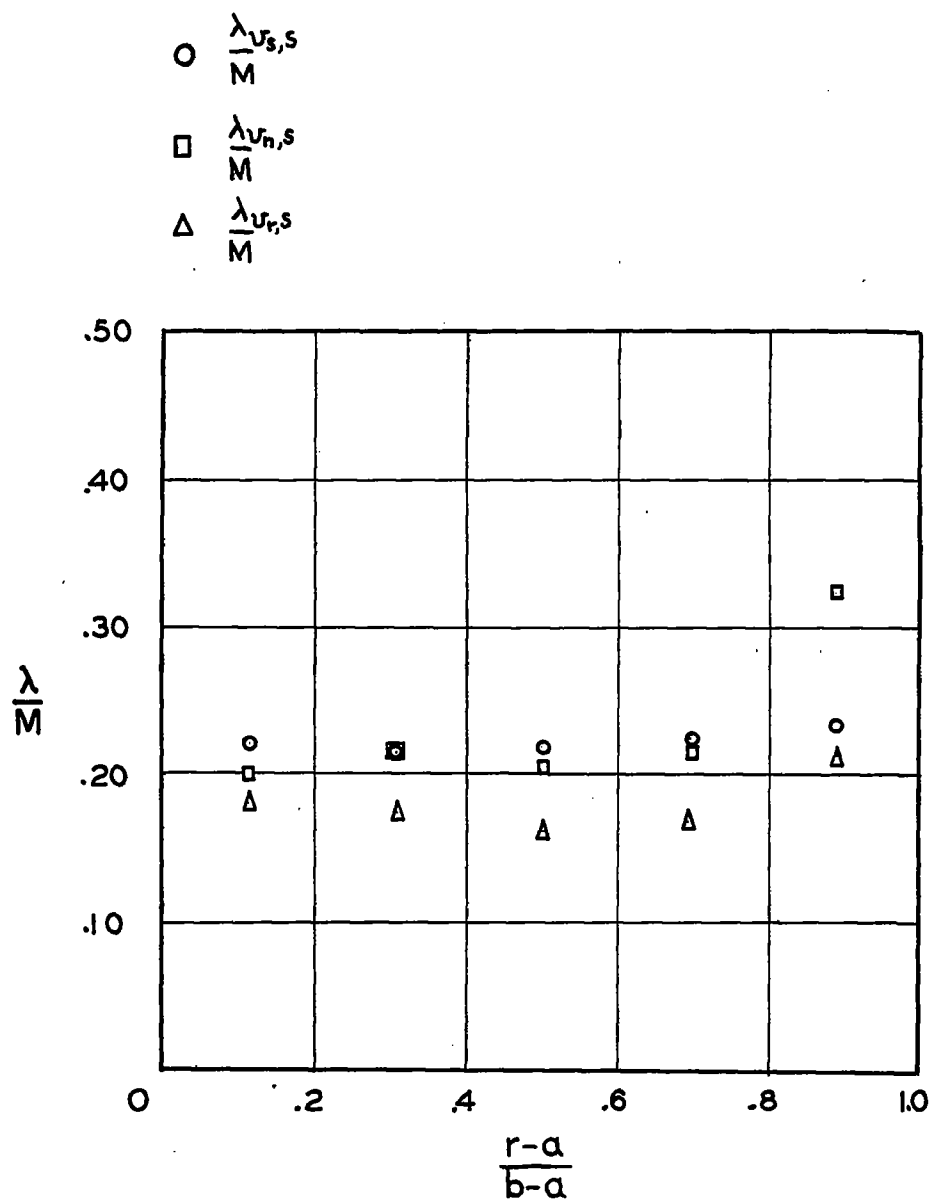
Figure 24.- Microscales with rotation. $\frac{\xi}{M} = 17.5$.
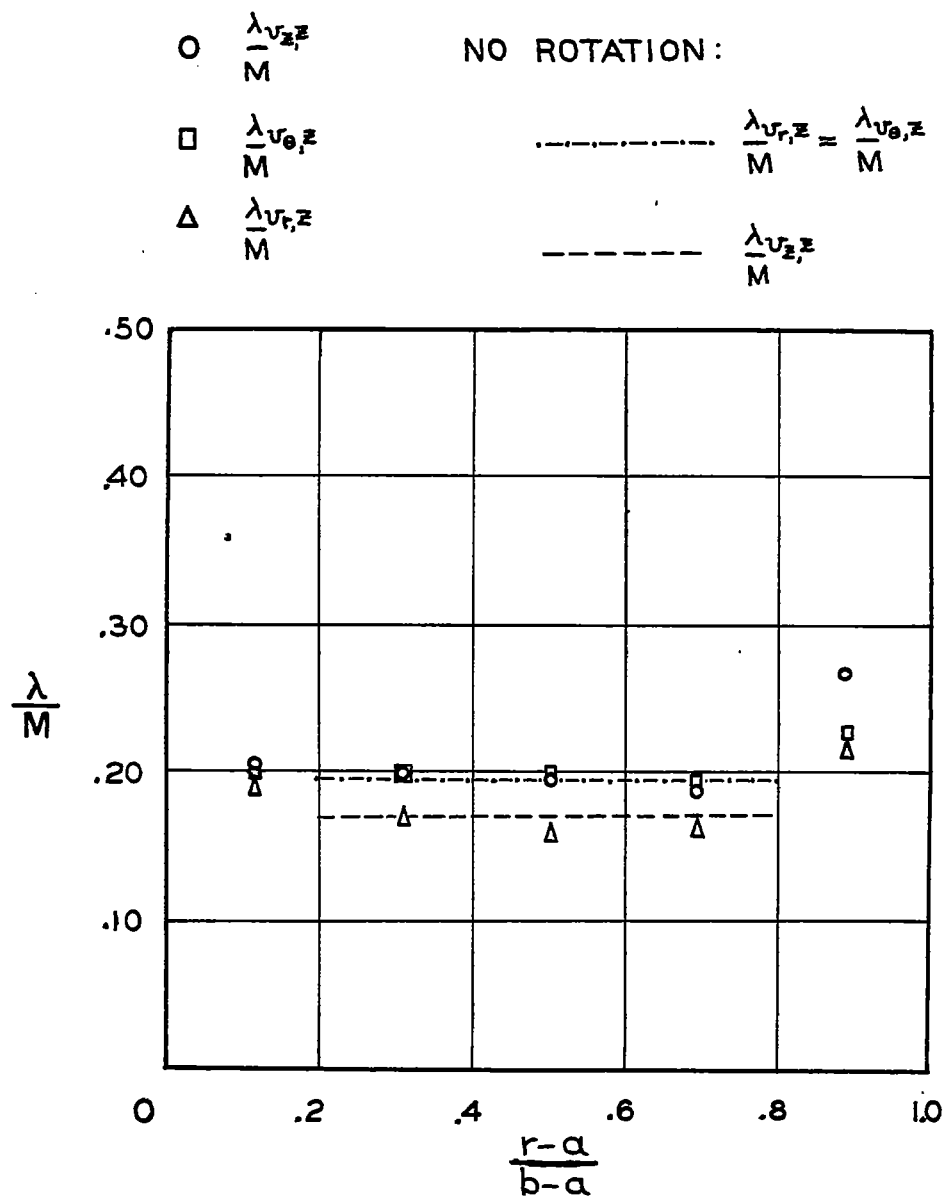
Figure 25.- Influence of rotation on microscales. $\frac{\xi}{M} = 17.5$.
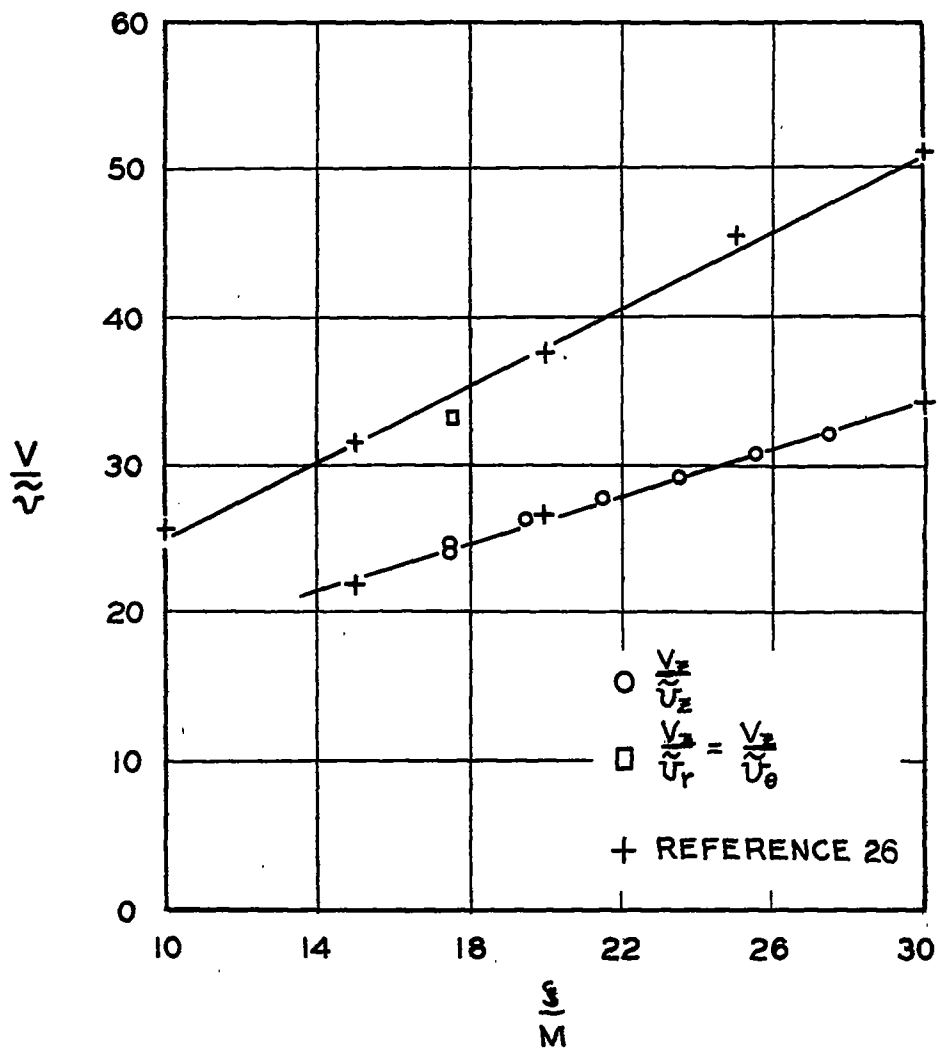
Figure 26.- Turbulence decay without rotation. $\dfrac{r - a}{b - a} = 0.5$.
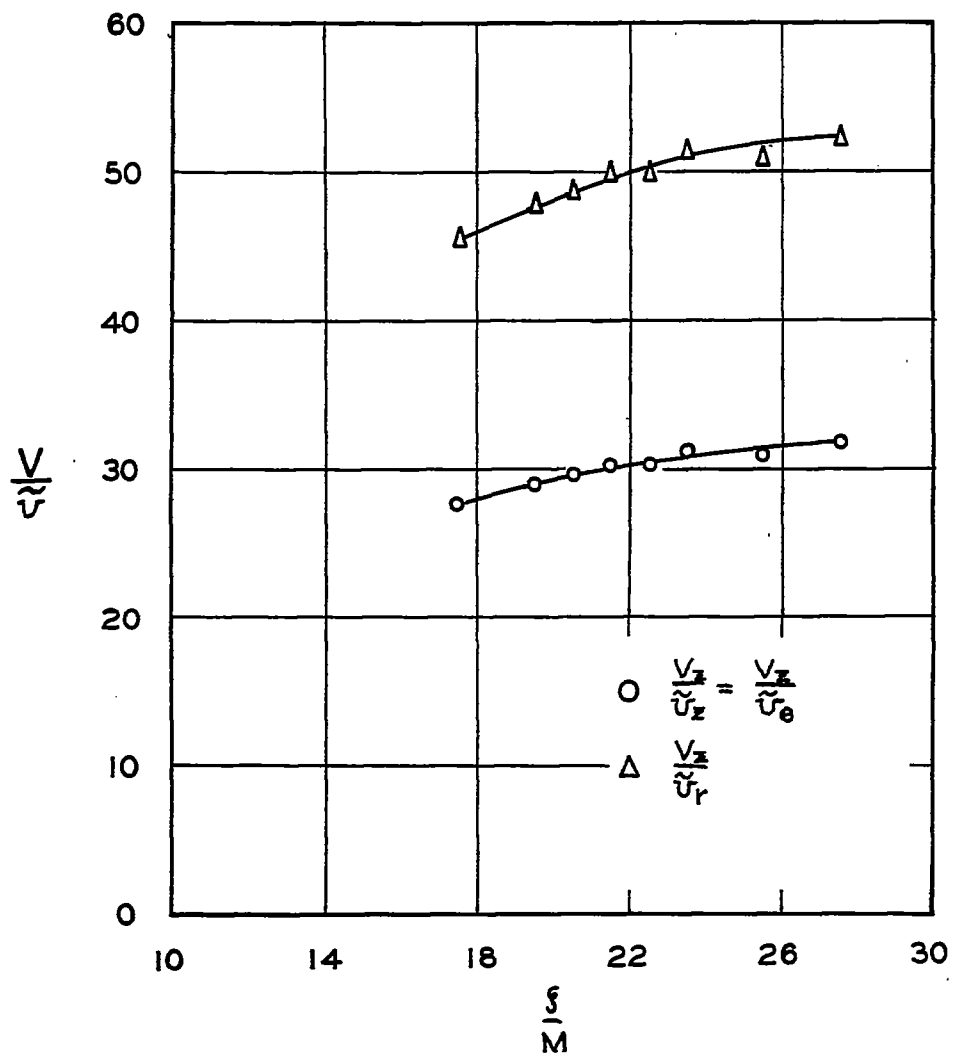
Figure 27.- Turbulence decay with rotation. $\dfrac{r - a}{b - a} = 0.5$.
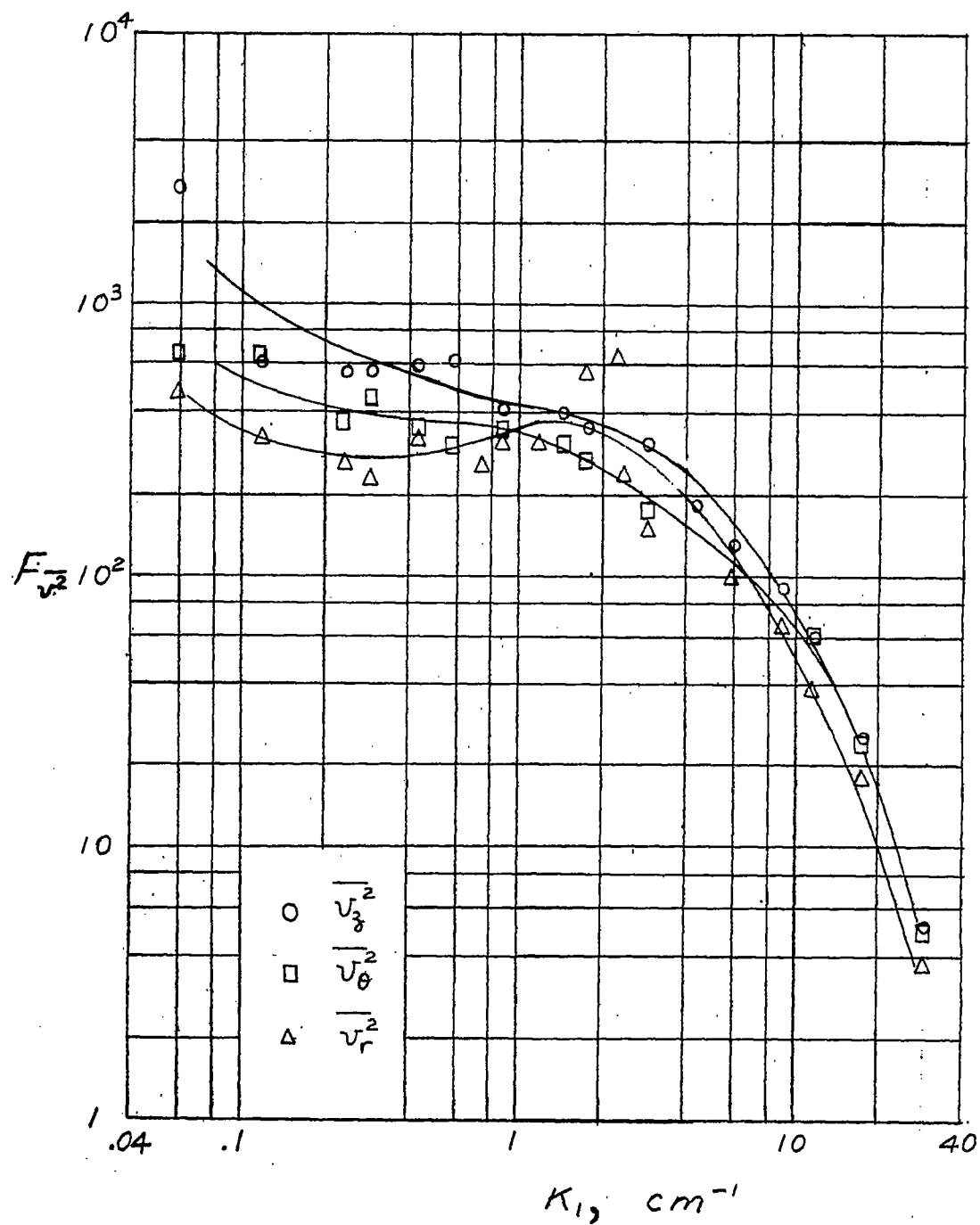
Figure 28.- One-dimensional spectra of turbulence intensities at
$\frac{r - a}{b - a} = 0.2.$
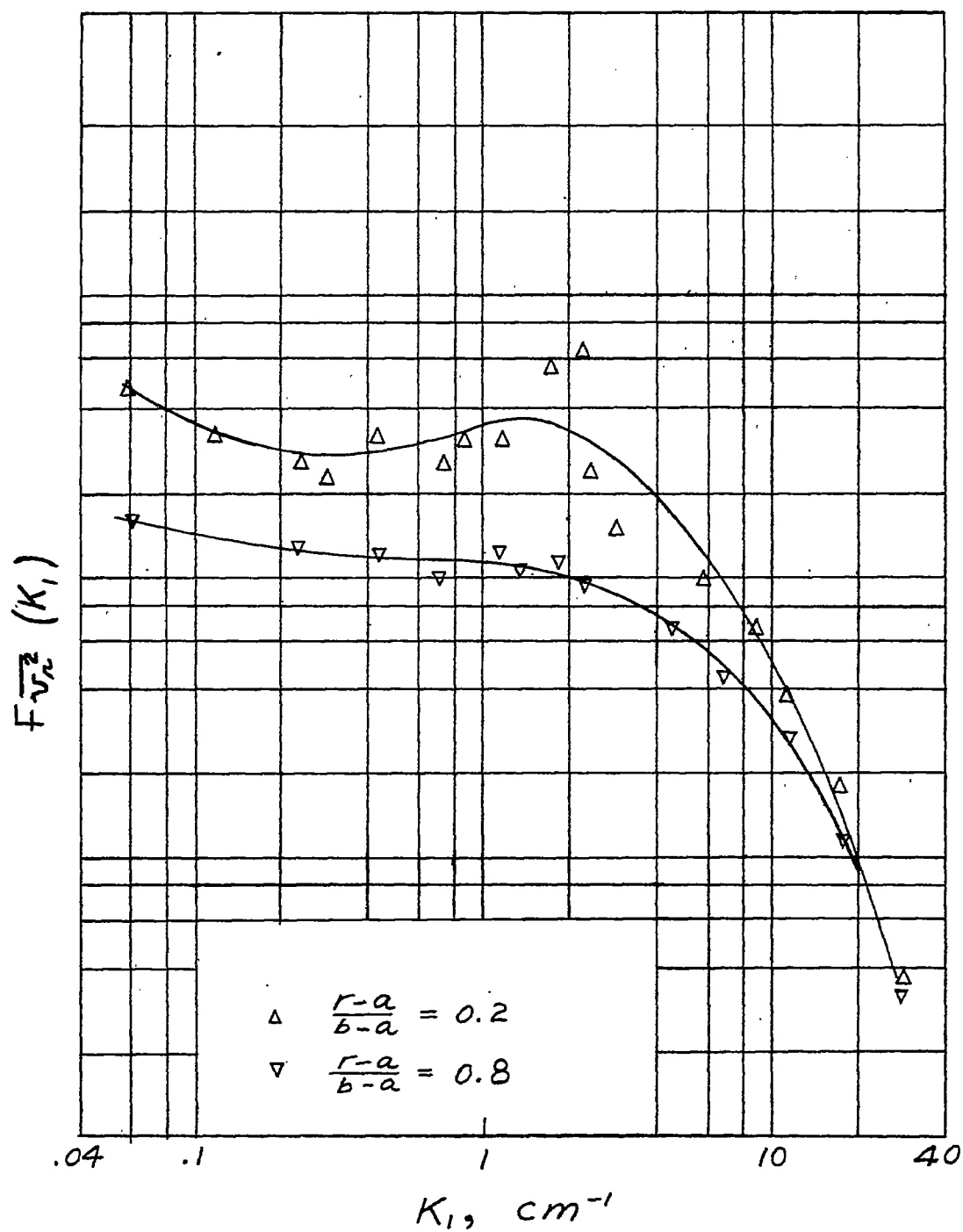
Figure 29.- One-dimensional spectra of $\overline{v_r^2}$.
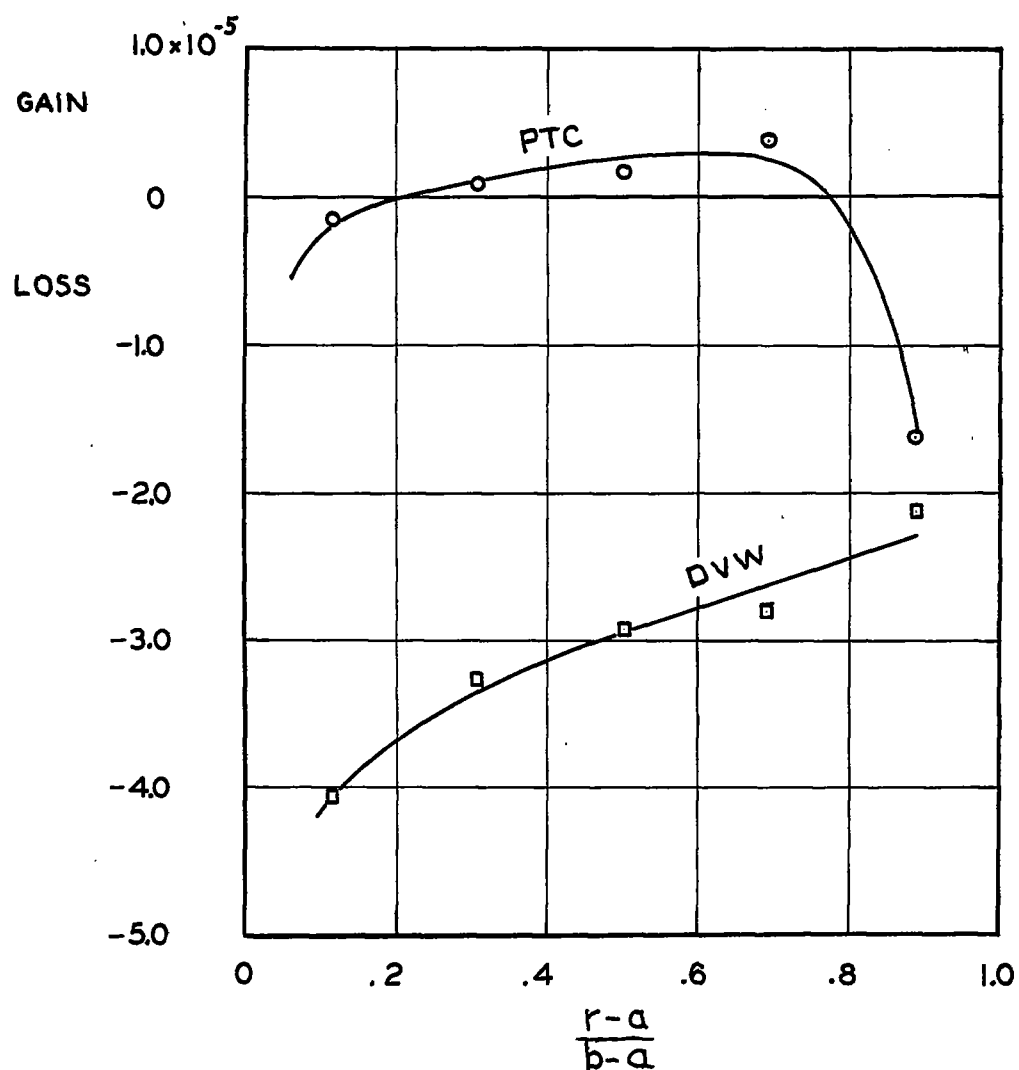
Figure 30.- Dimensionless energy balance on $\overline{v_z^2}$ with rotation. $\frac{\xi}{M} = 17.5$; PTC denotes the pressure-velocity and triple-velocity term; DVW denotes the term combining dissipation and viscous work.
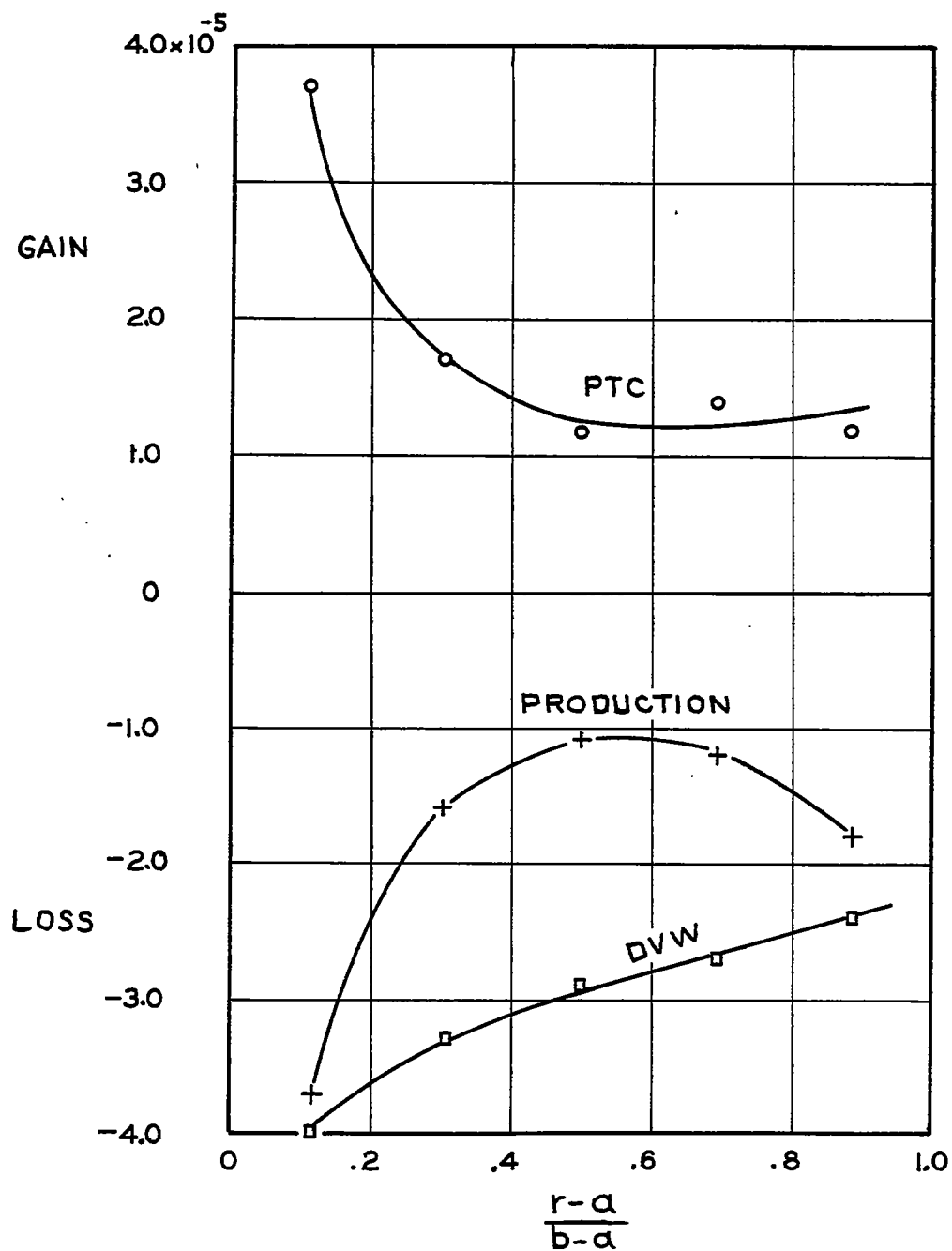
Figure 31.- Dimensionless energy balance on $\overline{v_\theta^2}$ with rotation. $\frac{\xi}{M}$ = 17.5; PTC denotes the pressure-velocity and triple-velocity term; DVW denotes the term combining dissipation and viscous work.
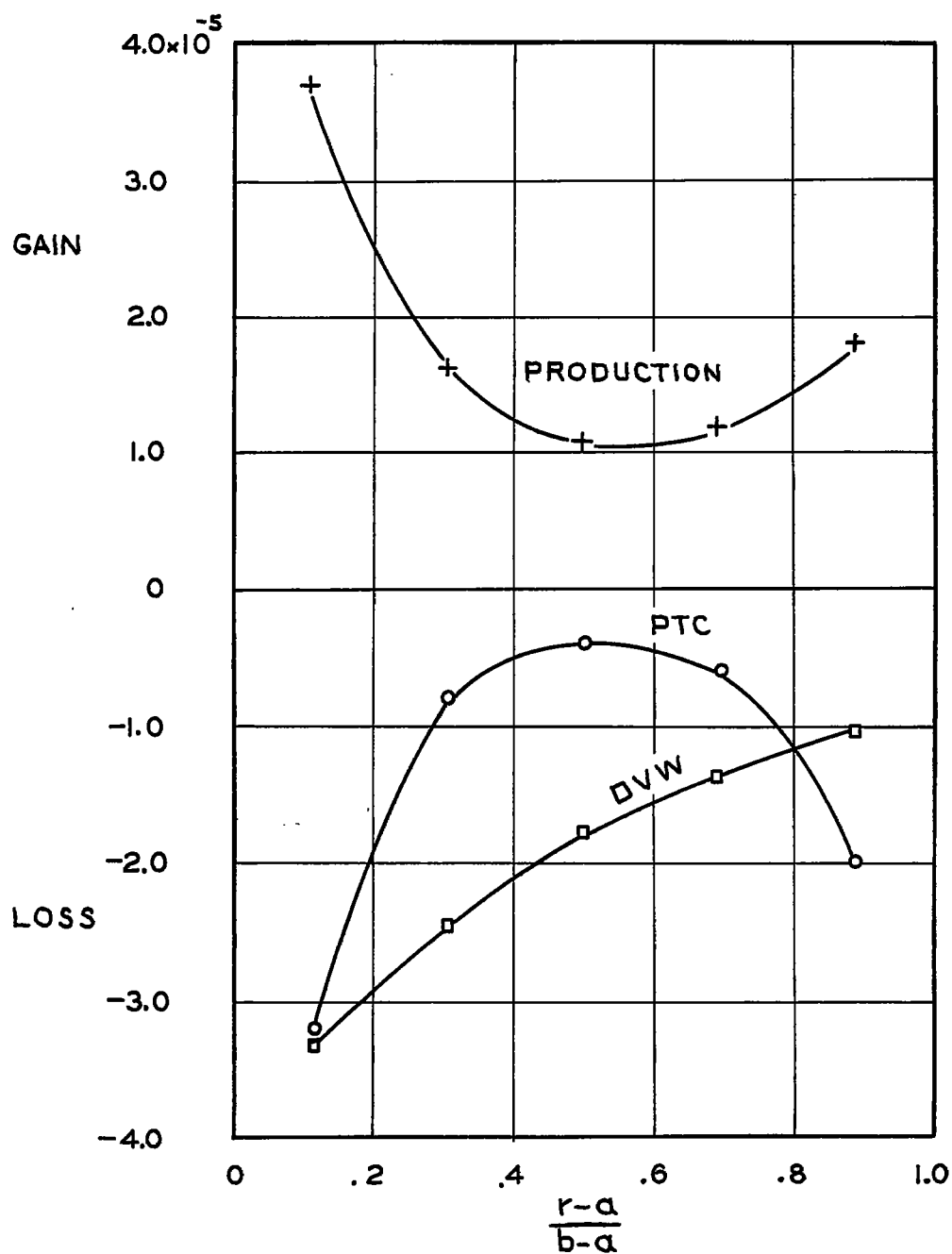
Figure 32.- Dimensionless energy balance on $\overline{v_r^2}$ with rotation. $\frac{\xi}{M}$ = 17.5; PTC denotes the pressure-velocity and triple-velocity term; DVW denotes the term combining dissipation and viscous work.
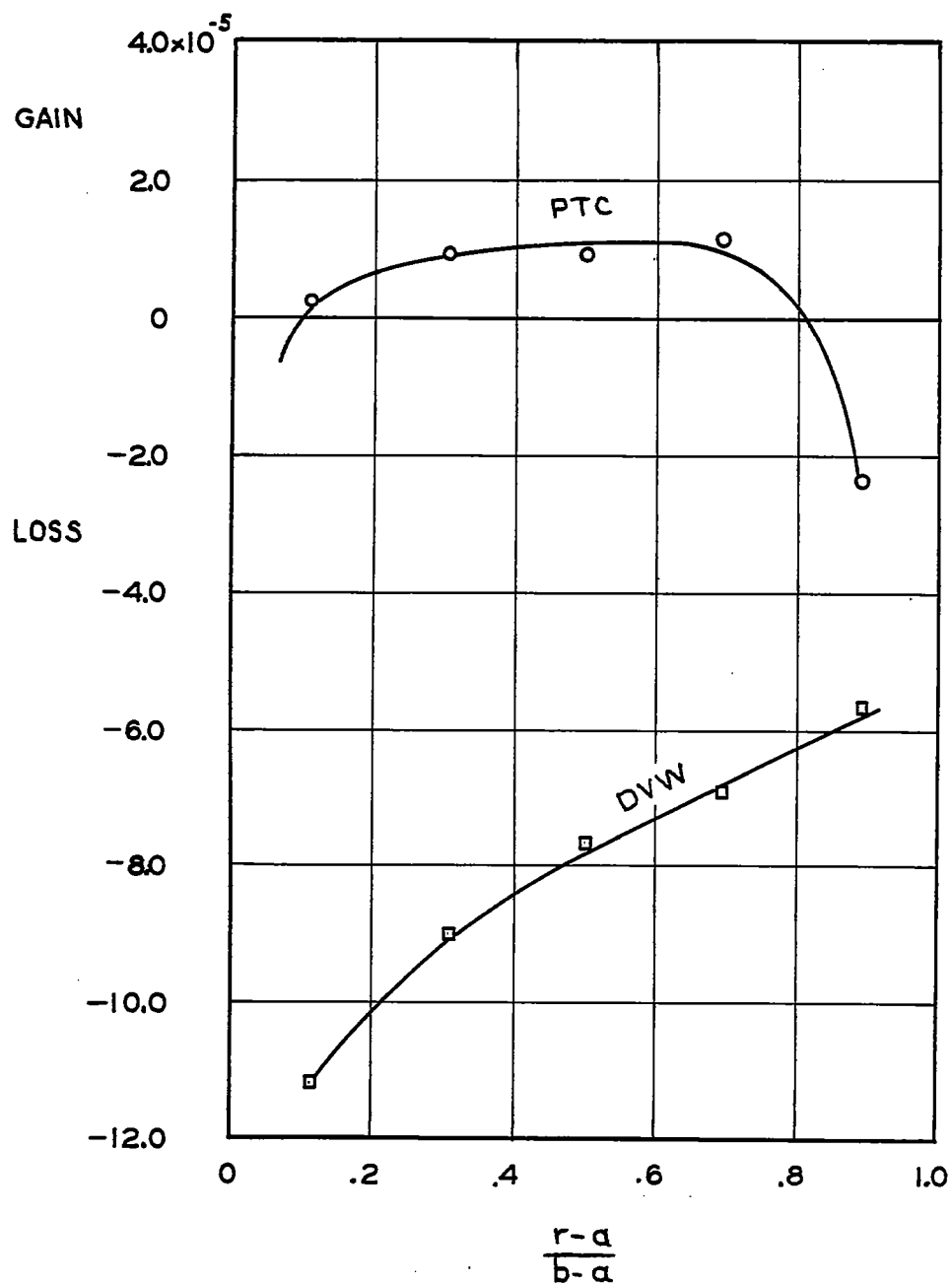
Figure 33.- Dimensionless energy balance on $\overline{q^2}$, with rotation. $\frac{\xi}{M} = 17.5$; PTC denotes the pressure-velocity and triple-velocity term; DVW denotes the term combining dissipation and viscous work.
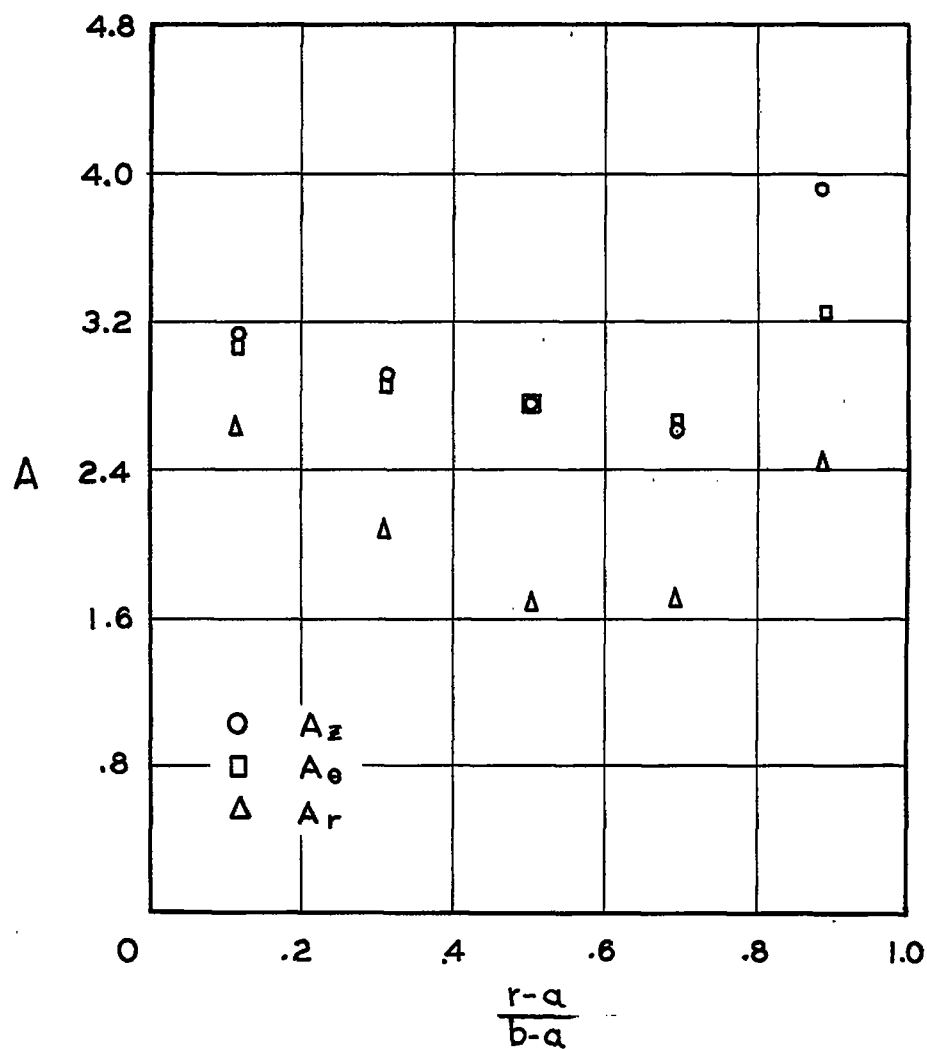
Figure 34.- Constant A in the relation $\dfrac{\lambda}{M} = \dfrac{A}{\sqrt{\dfrac{\hat{v}M}{v}}}$, with rotation.

$\dfrac{\xi}{M} = 17.5.$
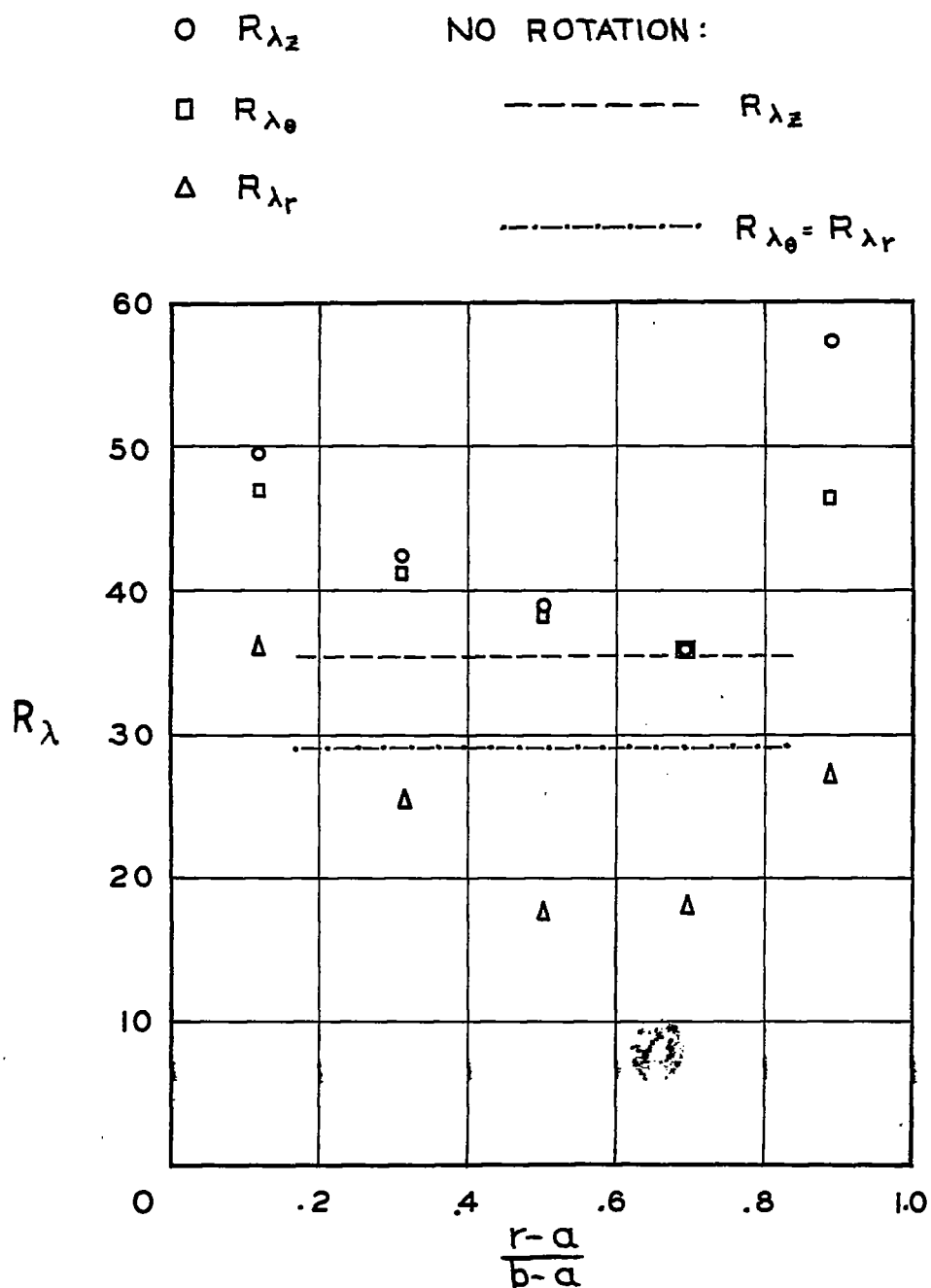
Figure 35.- Effect of rotation on turbulent Reynolds number. $\frac{\xi}{M}$ = 17.5.
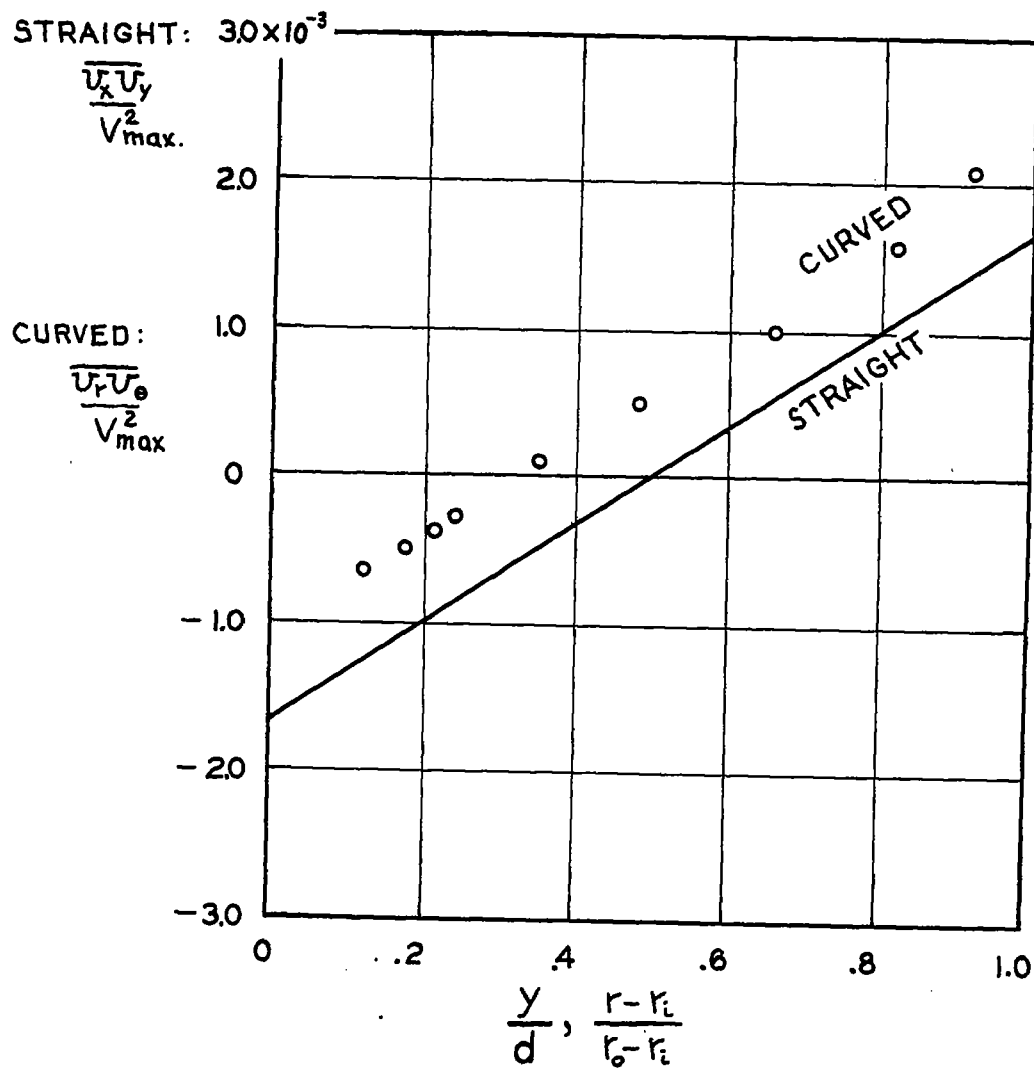
Figure 36.- Turbulent shear stress in a plane channel, from reference 14.

(a) Coordinate system.

$r, \theta, \mathfrak{z}$ cylindrical coordinates
 S direction of mean velocity V_s
 n normal to S in $\theta, \mathfrak{z}$ plane
 ϕ angle between S and $\mathfrak{z}$
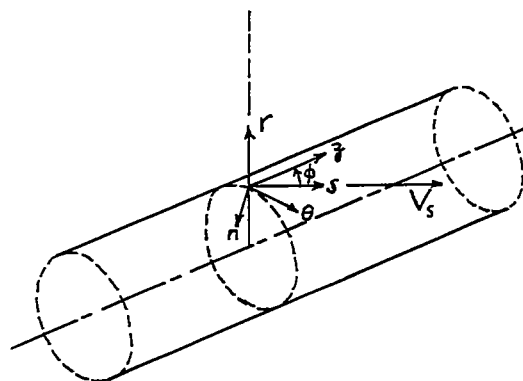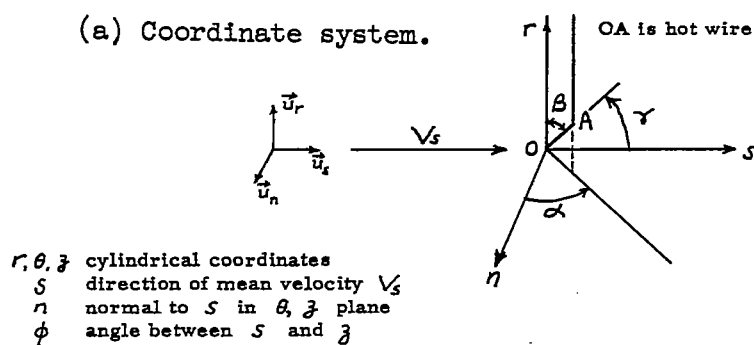
(b) Generalized position of wire.
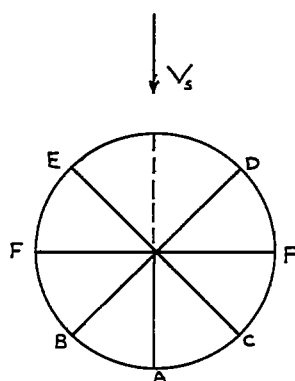
(c) Hot-wire measuring positions.

Figure 37.- Sketch illustrating quantities necessary to specify hot-wire position and orientation.
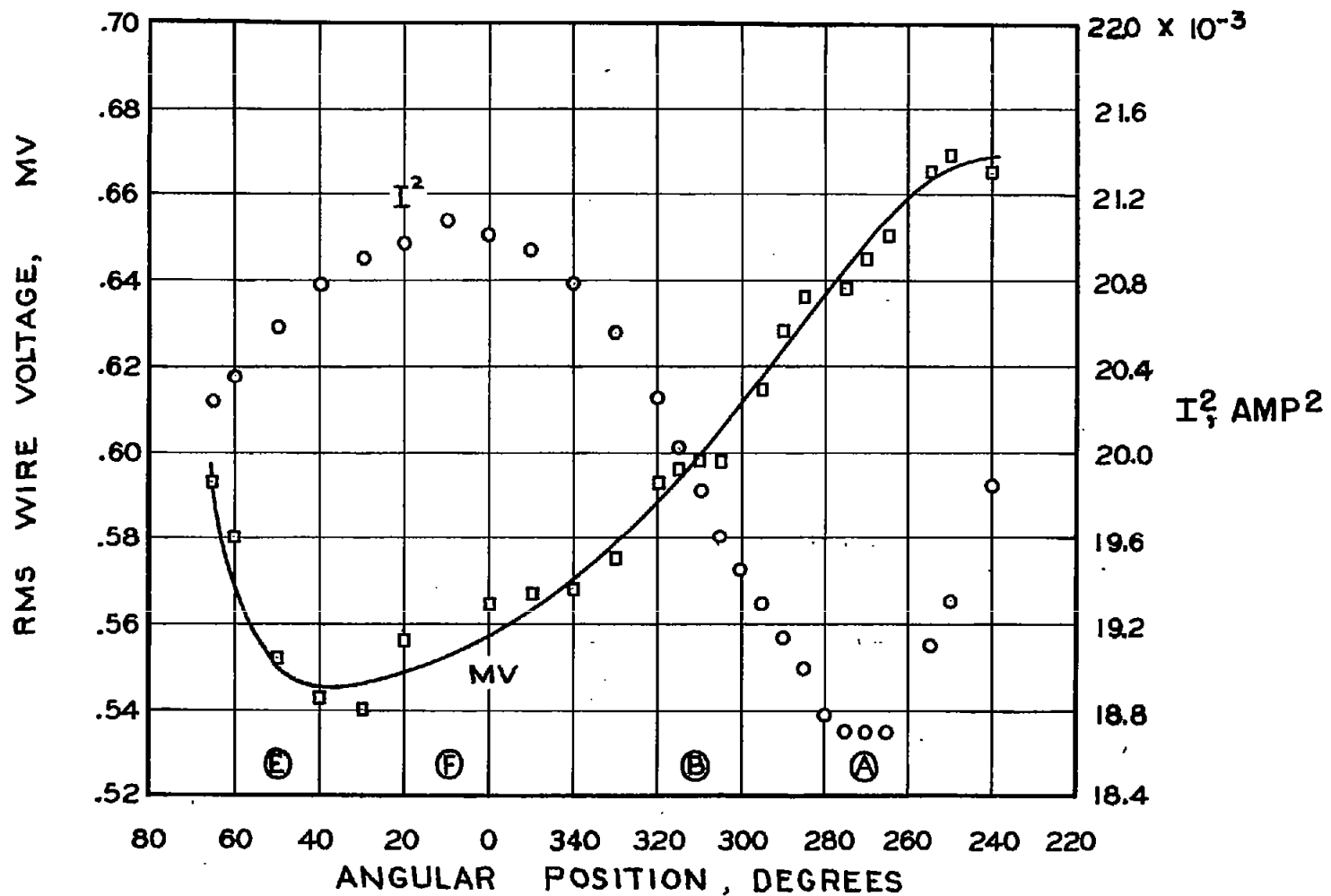
Figure 38.- Variation of wire signal with angular position.
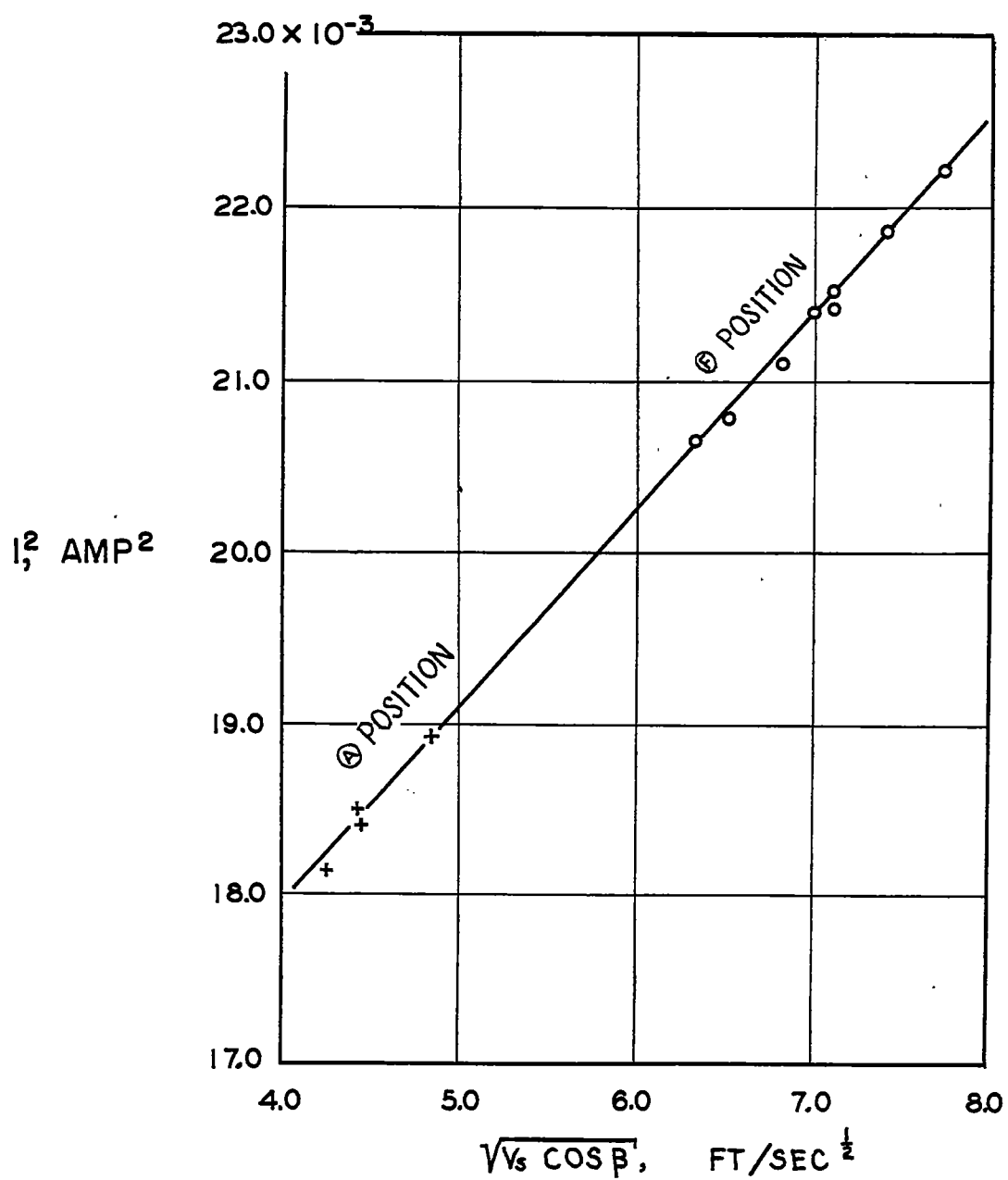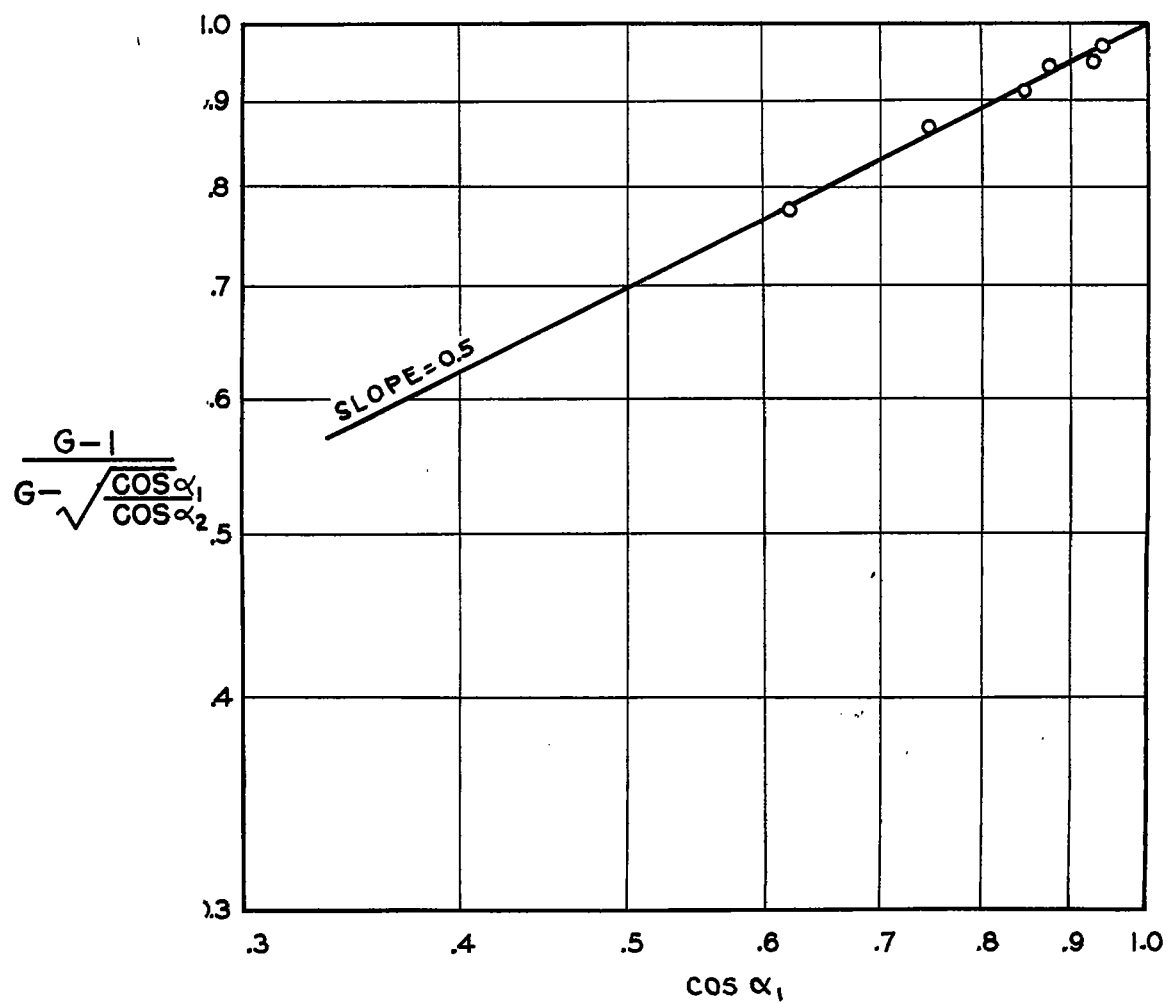
Figure 39.- Typical wire calibration.

Figure 40.- Determination of exponent η. $G = \dfrac{I_F{}^2 - I_{B_1}{}^2}{I_F{}^2 - I_{B_2}{}^2}$.
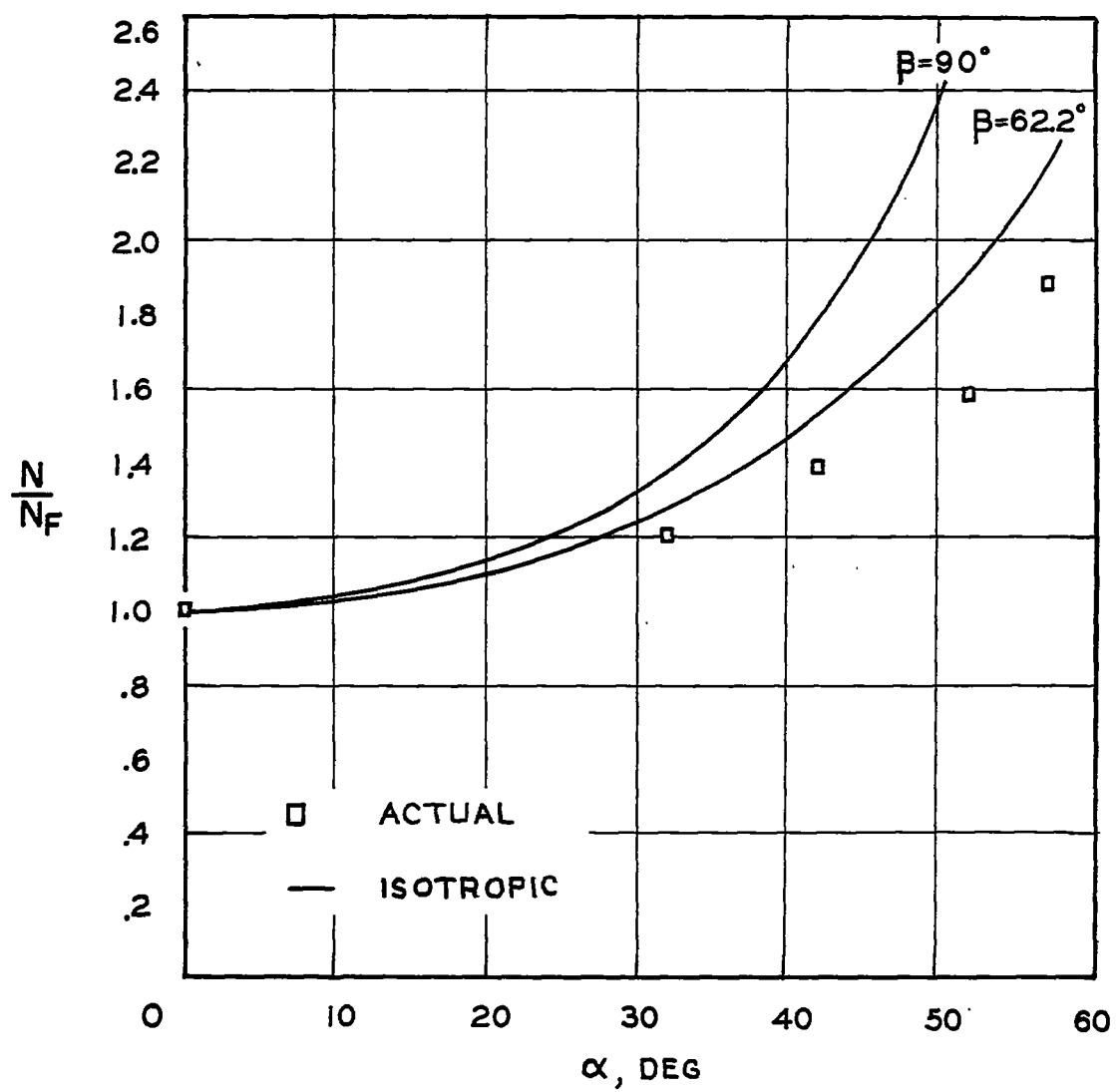
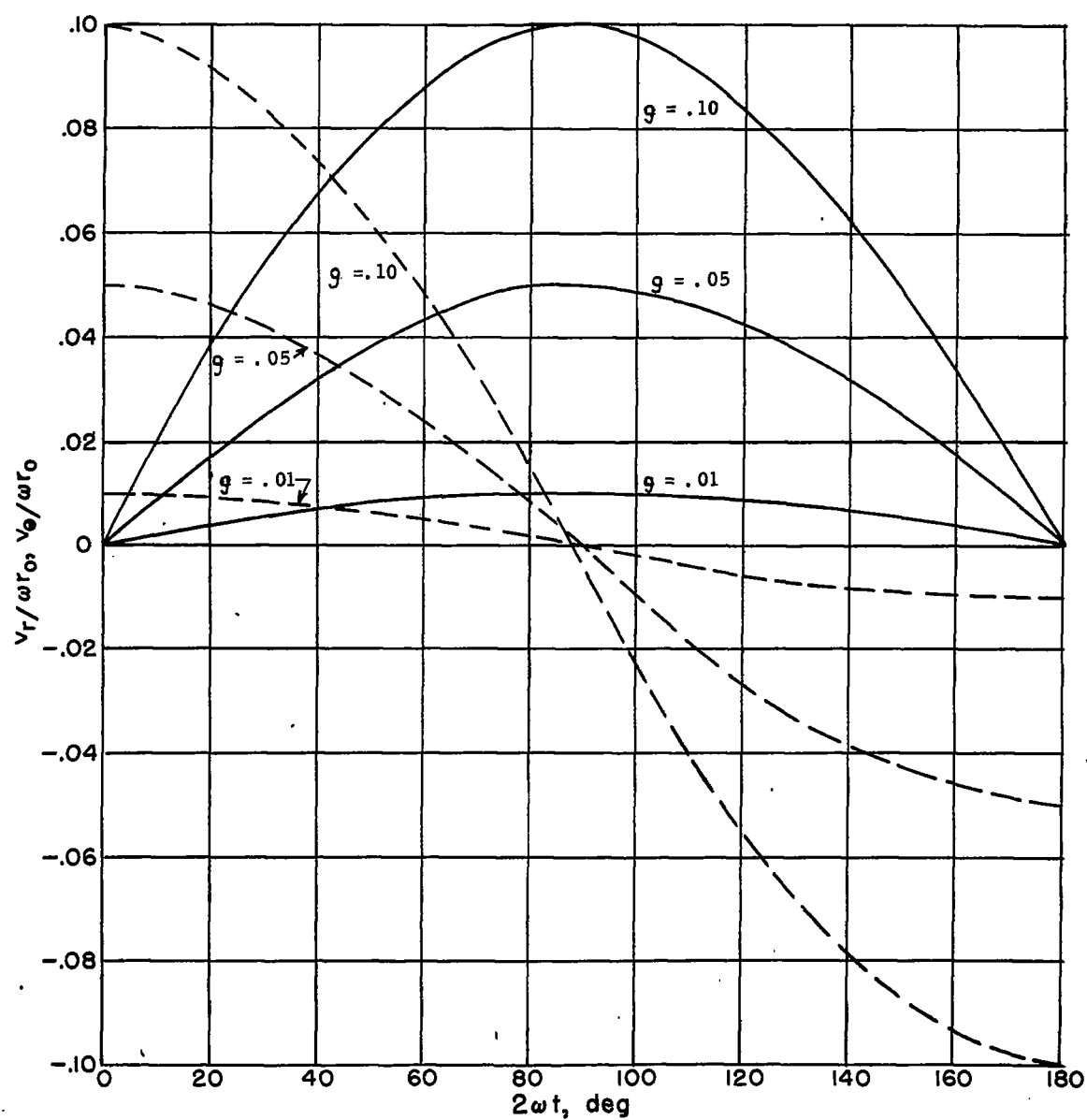Figure 41.- Variation of wire signal with wire turning angle.

Figure 42.- Variation of tangential and radial perturbing velocities with time in solid-body rotation of mean flow. Solid lines indicate $v_r/\omega r_o$; dashed lines indicate $v_\theta/\omega r_o$.